International Key Comparison of Thermal Neutron Fluence Measurements - CCRI(III)-K8

R. Nolte[1*], R. Böttger[1], J. Chen[2], H. Harano[3], D.J. Thomas[4]

[1] *Physikalisch-Technische Bundesanstalt (PTB), Braunschweig, Germany*
[2] *China Institute of Atomic Energy (CIAE), Beijing, P.R. China*
[3] *National Metrology Institute of Japan (NMIJ), Tsukuba, Japan*
[4] *National Physical Laboratory (NPL), Teddington, United Kingdom*

Abstract

After more than thirty years a new key comparison of thermal neutron fluence measurements was organized by section III of CCRI. The comparison was carried out by rotating four transfer instruments among the four participants (CIAE, PTB, NMIJ and NPL). The stability of the detectors was repeatedly verified by the pilot laboratory between the measurements. Each of the four transfer devices had a different dependence of the fluence response on the neutron energy. Hence the comparison was also sensitive to the knowledge of the spectral distributions of the facilities used by the participants for their measurements. The results of the comparison showed signs of inconsistencies which could not be resolved during the analysis. Therefore the arithmetic mean of the results was used to calculate the key comparison reference value.

1. Introduction

The first comparison of thermal neutron fluence measurements [AXT70] was finished in 1969 and comprised mainly so-called thermal standards. In these devices thermal neutrons are produced by moderation of fast neutrons from a radionuclide source, or sources, inserted in a graphite pile. The neutron fluence was always measured using the activation of gold foils. Cadmium covers were used to subtract most of the activity produced by epithermal neutrons.

Since then, no further comparison was carried out until 2005 when a new comparison was initiated by the Comité Consultatif de Rayonnements Ionisants (CCRI(III)) of the Bureau International de Poids et Mésure (BIPM). The kind of facilities participating in the new comparison was more diverse, ranging from conventional thermal standards to accelerator-based facilities, thermal columns and neutron guides installed at research reactors. Hence, the spectral and angular distributions of the neutrons were expected to vary considerably. In general, the spectral distributions present in the facilities deviated from a Maxwellian characterised by a reference temperature $kT = 25.3$ meV and different corrections have to be applied at each facility to account for such deviations.

It was therefore necessary that the comparison was also sensitive to the correct characterisation of the neutron fields. This could only be achieved by sending around a transfer device instead of each participant performing measurements at one reference facility, as in the recent comparison of fast neutron fluence measurements [CHE07]. To enhance the sensitivity to the spectral distribution even more, it was decided to actually use four transfer devices with different energy dependences of the fluence response. Two of the instruments had a rising and two a decreasing sensitivity with neutron energy. Hence, under ideal conditions, the ratio of the results obtained using the instruments without and with a moderator sphere would allow the temperature of the neutron energy distribution to be determined.

[*] corresponding author: ralf.nolte@ptb.de

The fluence measurements at the participating facilities were all traceable to the activation of thin gold foils, i.e. measurement of the ^{198}Au activity resulting from the ^{197}Au(n,γ)^{198}Au reaction. The activity measurements were carried out using the 4πβ or the 4πβ−γ counting technique. In some cases, however, additional local transfer instruments were used for the actual fluence measurement and the fluence response of these instruments was determined using the activation of gold foils in a separate step. This included, for example, the use of a ^{6}Li glass scintillation detector for the fluence measurement or of calibrated β- or γ-counters for the determination of the ^{198}Au activity.

Although a larger number of national metrology institutes (NMIs) or designated institutes (DIs) expressed their interest to participate in the comparison, the exercise was finally carried out by only four NMIs or DIs: the China Institute of Atomic Energy (CIAE), the National Metrology Institute of Japan (NMIJ), the National Physical Laboratory (NPL) of the United Kingdom and the Physikalisch-Technische Bundesanstalt (PTB) of Germany.

In addition, measurements were also carried out at the D.I. Mendeleyev Institute for Metrology (VNIIM) in Russia. Unfortunately, the VNIIM was finally not able to deliver results. These difficulties were at least partly related to customs problems with the shipping of the circulating transfer instruments. The National Institute of Standards and Technology (NIST) of the United States of America received the transfer instruments, but was not able to carry out measurements due to technical problems with the thermal column of the NIST reactor.

The comparison was organised by the PTB, but the co-ordinator was not involved in the PTB measurements. The PTB results were delivered to the BIPM before the results of the measurements of the other participants were received by the co-ordinator. The transfer instruments were circulated among the participants from October 2006 until July 2010. The last report with results was received in June 2010. Since the time of the measurements, at least two of the facilities used for the comparison went out of service or were no longer available for metrological use. This applies to the FRG-1 reactor at the GKSS research centre used by the PTB and to the thermal column of the Chinese reactor used by the CIAE.

2. The Transfer Instruments

The co-ordinating laboratory provided two spherical proportional counters filled with ^{3}He as transfer instruments. The counters were of the CENTRONIC SP9 type and had nominal ^{3}He pressures of 20 kPa (E-detector) and 200 kPa (G-detector), respectively. In addition, a spherical polyethylene (PE) moderator, 7.62 cm (3") in diameter, was provided to modify the energy dependence of the response of the 20 kPa counter and the 200 kPa counter. Therefore four transfer devices were available for the comparison exercise. The selection of the most appropriate bare counter was made by the participants based on count rate considerations. If possible, all four instruments were used.

The relative response $r(E) = R(E)/R(E_{\mathrm{ref}})$ for $E_{\mathrm{ref}} = 25.199$ meV, as calculated using MCNPX [X-587], is shown in fig. 1 for the two bare counters and the counters in the 3" PE moderator. The responses $R(E_{\mathrm{ref}})$ for the bare 200 kPa counter, the bare 20 kPa counter, the 200 kPa in the PE sphere and the 20 kPa counter in the PE sphere were about 3 cm^2, 0.4 cm^2, 1 cm^2 and 0.2 cm^2, respectively.

The signals provided by the counters were processed by an electronic module (AIOSAP) [ALE06] which comprised a high-voltage supply, a pre-amplifier, a shaping amplifier and two discriminators. This module was also provided by the co-ordinating laboratory. One discriminator (D1) was used to separate events resulting from the ^{3}He(n,p)^{3}H reaction from those due to photons and electronic noise. The number N of the TTL output pulses of D1 had to be counted by the participants to determine the response R in their neutron field or beam. For this purpose, a counting module had to be provided by the participants. The proper setting of D1 had to be checked individually using a multichannel analyser (MCA) provided by the participants.

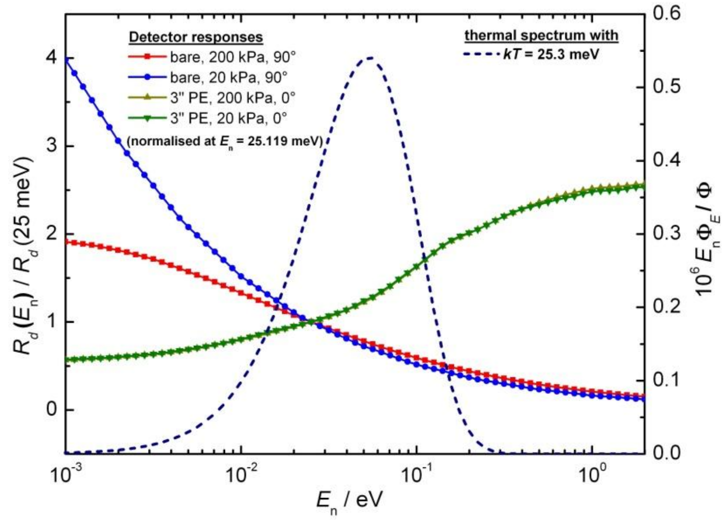

Fig. 1 Relative response $r(E) = R(E)/R(E_{ref})$ for the four transfer instruments as calculated with MCNP (left axis) for E_{ref} = 25.119 meV. Also shown is a relative Maxwellian spectral fluence distribution for kT = 25.3 meV (right axis). The responses for the bare counters and the counters in moderator sphere were calculated using MCNP for a parallel beam incident perpendicular (90°) and parallel to the symmetry axis (0°), respectively. The relative responses of the two detectors inside the 3″ polyethylene (PE) sphere were almost identical.

The dead-time τ introduced by D1 was measured using the pulse interval method. The effective dead-time resulting from the interval distribution shown in fig. 2 was $\tau = (7.2 \pm 0.9)$ µs. The interval distribution was in general compliance with the assumption of a non-extending dead-time although the measured interval distribution showed slight deviation from the theoretical distribution around the edge.

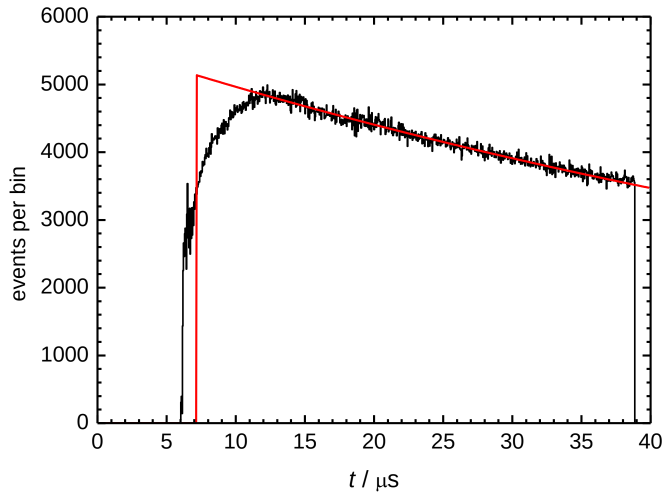

Fig. 2 Distribution of the time intervals between successive pulses of the discriminator D1 (black histogram). The red solid line shows the fitted interval distribution $N(t) = N_0 \cdot \exp(-\rho(t-\tau_{eff}))$ with an effective non-extending dead-time $\tau_{eff} = (7.2 \pm 0.9)$ µs. The count rate $\rho = dN/dt$ was 1.2×10^4 s^{-1}.

The dead-time correction was also checked in 2008 during an experiment at the thermal neutron beam facility used by the PTB (see below). The count rate of the detector was varied between about $9 \times 10^2\ s^{-1}$ and $2 \times 10^4\ s^{-1}$. The beam was monitored using a ^3He ionisation chamber. The dead-time of the monitor was about 1 µs. Due to the low count rate, the dead-time correction for the monitor was smaller than 0.3 %. The correction of the SP-9 count rate was carried out assuming a non-extending dead-time τ of 7.2 µs. The dead-time correction ranged between 0.5 % and 14 %. Fig. 3 shows the ratio of the corrected SP9 count rate R_{cor} to the count rate M of the ^3He monitor. The data are normalised to the mean value $<R_{cor}/M> = 10.418 \pm 0.016$. With the exception of two data points, the error bars overlap with the mean value within its uncertainty which confirms the dead-time of 7.2 µs specified in the protocol, although there seems to be a slight systematic trend depending on the corrected rate of the SP9 counter. However, the maximum deviation from the mean amounts to only 1.5 %.

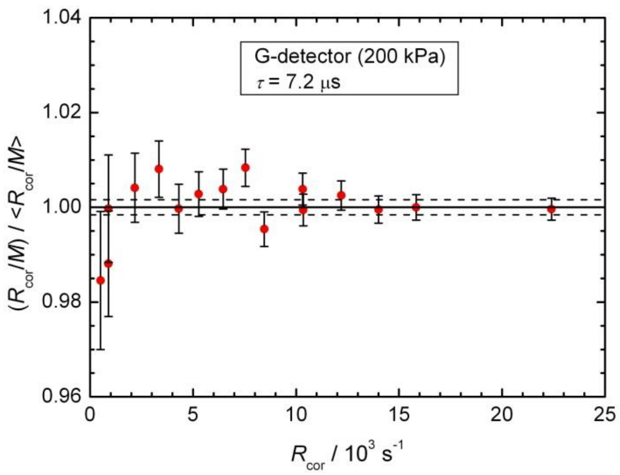

Fig. 3 Ratio of the corrected count rate $R_{cor} = k_2 \cdot (dN/dt)$ of the 200 kPa SP9 counter to the monitor count rate M in a thermal neutron beam. The SP9 count rate was corrected using a non-extendable dead-time τ of 7.2 µs (cf. eq. (3) below). The dead time correction applied to the monitor count rate was smaller than 0.3 % at maximum.

The stability of the two ^3He counters was monitored at the PTB prior to sending the instruments to the participants and after receiving them. This stability check was carried out by inserting the counters into the test device HANNA which consists of a paraffin moderator equipped with an AmBe radionuclide neutron source at a distance of 20 cm from the centre of the counter. Fig. 4 shows the relative deviation of counts rates after correction for the decay of ^{241}Am as a function of the measurement date. The relative type-A uncertainties of the individual measurements are about 0.15 % and 0.06 % and the standard deviations of all measurements are 0.46 % and 0.43 % for the 20 kPa and the 200 kPa counter, respectively.

Two tightly fitting cylindrical cadmium shields 1 mm in thickness were provided for measuring the effect of epithermal neutrons above the cadmium threshold on the bare counters and the counters inside the 3" PE moderator, respectively. For a cadmium foil, 1 mm in thickness, covering a $1/v$-absorber, the cadmium cutoff energy E_{Cd} is 0.68 eV for a D_2O moderator [BEC64]. This value was used as a reference below.

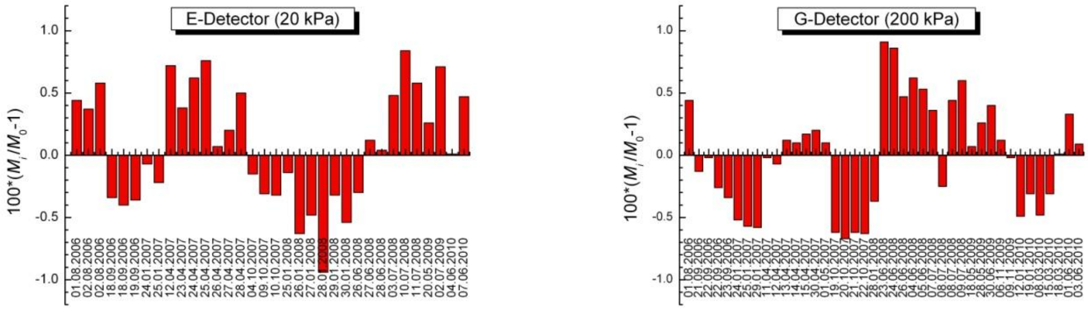

Fig. 4 Relative deviation of the count rate of the two ^{3}He counters from a reference value. The count rates were corrected for the decay of ^{241}Am as a function of the measurement date.

3. Quantity to be Determined as the Key Comparison Reference Value

The participants were asked to determine the response R_{ref} of the counters for a homogeneous unidirectional irradiation with neutrons which have a Maxwellian fluence distribution $\Phi_E^{(\text{ref})}$ characterised by a temperature kT = 25.3 meV.

$$\frac{\Phi_E^{(\text{ref})}\,\mathrm{d}E}{\Phi^{(\text{ref})}} = \left(\frac{E}{kT}\right)\exp\left(-\frac{E}{kT}\right)\frac{\mathrm{d}E}{kT} \tag{1}$$

This required the relative spectral fluence (Φ_E/Φ) and the fluence

$$\Phi = \int_0^{E_{\text{Cd}}} \Phi_E\,\mathrm{d}E \tag{2}$$

below the nominal cadmium threshold E_{Cd} to be determined in the neutron beam at the same location and under the same conditions as for the measurement with the counter.

Appropriate correction factors had to be determined if the actual irradiation conditions deviated from the reference conditions. Most important, the spectral distribution of the actual neutron field could have deviated from a Maxwellian with the reference temperature parameter. The relative responses shown in fig. 1 were provided in numerical form for the calculation of correction factors. The correction factor k_1 for the spectral distribution is given by

$$k_1 = \frac{\int_0^{\infty}\left(\Phi_E^{(\text{ref})}/\Phi^{(\text{ref})}\right) r(E)\,\mathrm{d}E}{\int_0^{E_{\text{Cd}}}\left(\Phi_E/\Phi\right) r(E)\,\mathrm{d}E} \tag{3}$$

where the integration over the relative spectral fluence (Φ_E/Φ) of the neutron field or beam is extended up to the nominal cadmium threshold energy E_{Cd} at 0.68 eV. Also dead-time losses had to be corrected for. The dead-time correction k_2 is

$$k_2 = \frac{1}{1-\tau\rho}, \quad \rho = \mathrm{d}N/\mathrm{d}t \tag{4}$$

for a non-extending dead-time τ.

Other correction factors could, for example, account for an inhomogeneous fluence distribution over the sensitive area of the counter. This effect could either be corrected for experimentally by using a scanning procedure or calculated using the Monte Carlo method. Also the angular distribution of the spectral fluence could have required corrections if fields were used which were not unidirectional. An MCNP model of the detector for the calculation of correction factors was made available by the pilot laboratory on request. Correction factors were also required if the fluence was not measured at the same position as the counter or, in the case of inhomogeneous fields, the sensitive area of the instrument used for the fluence measurement was different from that of the counter. In fields or beams produced by the moderation of fast neutrons, the slowing-down part of the spectral distribution extends below the cadmium threshold. Hence, a correction for the count rate produced by these epithermal sub-cadmium neutrons had to be applied.

With these correction factors k_i and the number of monitor counts M_Φ , M_N and $M_N^{(\mathrm{Cd})}$ for the measurement with the instrument used for the fluence measurement, the counter without cadmium cover and with cadmium cover, the response at reference conditions is given by

$$R = \prod_{i=1}^{n} k_i \cdot \frac{\left(N / M_N - k^{(\mathrm{Cd})} N^{(\mathrm{Cd})} / M_N^{(\mathrm{Cd})}\right)}{\left(\Phi / M_\Phi\right)} \qquad (5)$$

Here $n \geq 2$ denotes the number of correction factors k_i. The correction factor $k^{(\mathrm{Cd})}$ accounts for the absorption of epithermal neutrons in the Cd shield (1 mm Cd + 1 mm Al) and had to be calculated by the participants if this correction could not be neglected.

4. Summary of the Measurements and Analysis Procedures used by the Participating Institutes

4.1. General Remarks

As mentioned in the introduction, the measurement and analysis procedures used by the different participants were very diverse. This diversity made the reporting of the uncertainty budgets more complicated than for a single step approach. This is why a complete documentation of the uncertainty budgets is left to the individual reports of the participating institutes which are attached to this report. Instead, this section aims only at summarising the most important steps of each approach.

4.2. China Institute of Atomic Energy (CIAE)

The CIAE used a collimated thermal neutron beam which was extracted from a thermal column of a 2 MW research reactor. The extraction channel had a diameter of 30 mm. The neutron fluence at the point of reference was measured using the activation of gold foils, 20 µm and 40 µm in thickness. The contribution of epithermal neutrons was investigated using the simultaneous irradiation of a 5 µm gold foil on top of a 20 µm gold foil. The specific activities of the two foils agreed within 1 % despite the expected shielding effect of the thinner foil, in particular in the energy region around the strong resonance at 4.9 eV. Therefore it was concluded that the epithermal contribution could be neglected. The cadmium ratio for the ^{197}Au(n,γ) reaction was determined in a separate measurement to be about 479 for a cadmium cover 1 mm in thickness.

The determination of the ^{198}Au activities was carried out in a NaI borehole detector. The detection efficiency of this detector was calibrated using a 5 µm gold foil which had been activated in the reactor core. The ^{198}Au activity in this foil was measured using the 4π β–γ coincidence counting technique.

The relative spectral fluence distribution was characterised using the time-of-flight (TOF) method with a rotating chopper and a ^{3}He detector. For these measurements a lead collimator with an opening 3 mm in diameter was inserted into the extraction channel. MCNP calculations were carried out to verify that the spectral distribution was not changed by the different ‘cuts’ in momentum space introduced by the extraction channel and the narrow collimator. The spectral distribution measured at the CIAE facility is shown in fig. 5 together with a fitted Maxwellian distribution. The temperature kT of this Maxwellian distribution is 25.15 meV, i.e. $T = 280.3$ K, but the high-energy tail of the Maxwellian exceeds the measured distribution considerably. There was no further information on how such a non-equilibrium distribution could have been produced by a thermal column operated at or slightly above room temperature. The measured spectral distribution was used to calculate the spectrum-averaged cross section $\bar{\sigma}$ using the ENDF/B-VII cross section data for the ^{197}Au(n,γ) reaction.

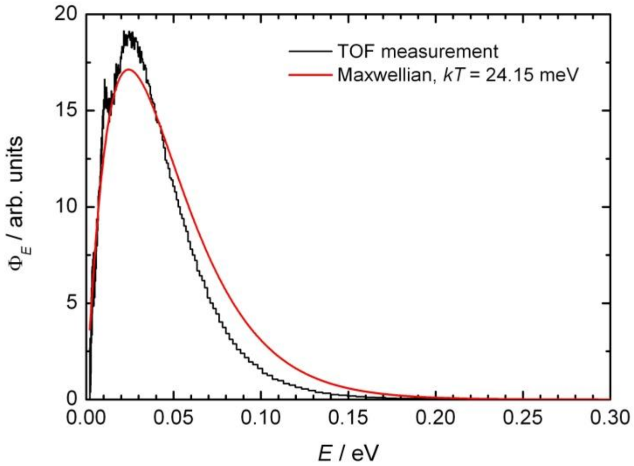

Fig. 5 Spectral distribution (black histogram) measured at the CIAE facility using the narrow beam produced by the lead collimator insert for the extraction channel. The red solid line shows a Maxwellian fit to this distribution. The temperature of this distribution is smaller than that of the reference Maxwellian.

The irradiation of the transfer devices was also carried out using the collimated beam. A scanning device was employed to simulate a homogeneous irradiation. The measurements with the cadmium shields were, however, only carried out for instruments positioned with their centres at the reference point. The measurements with the broad beam from the extraction channel and the narrow collimated beam were related by additional measurements using a ^{235}U fission ionisation chamber. The ^{235}U deposit had a diameter of about 20 mm, i.e. it was suitable for a measurement of the neutron fluence in broad beam and of the total neutron rate in the collimated beam.

4.3. National Metrology Institute of Japan (NMIJ)

In contrast to the other facilities, the NMIJ calibrated the transfer instruments inside a thermal standard. Hence, to first order, the angular neutron distribution was an isotropic field in a scattering medium, in contrast to the beam-like unidirectional distributions used by the other participants. The thermal pile of the NMIJ consists of a large graphite block with a central cavity for a high emission rate AmBe neutron source. A second channel for the transfer instruments was created by removing graphite bricks. The instruments were positioned at a distance of about 90 cm from the neutron source.

The spectral distribution at the irradiation position was calculated using MCNPX. It can be described by a Maxwellian distribution with temperature $kT = 26.2$ meV and a $1/E$ slowing-down contribution.

$$\Phi_E(E) = \Phi_{\mathrm{th}} \frac{E}{(kT)^2} \exp\left(-\frac{E}{kT}\right) + \Phi_{\mathrm{nth}} \frac{\Delta(E)}{E} \tag{6}$$

where Φ_t and Φ_{nth} denote thermal and the non-thermal slowing-down fluence, respectively. No details were given about the joining function $\Delta(E)$, in particular on the lower cut-off energy. It should be noted, however, that Φ_{nth} denotes the total non-thermal fluence extending to about the 10 MeV region. The relative non-thermal fluence $\Phi_{nth}/(\Phi_{th} + \Phi_{nth})$ was 1.7×10^{-3}.

The thermal neutron fluence rate was measured using the activation of gold foils, 2 cm in diameter and 25 µm in thickness. The foils were encapsulated in aluminium and cadmium covers, 1 mm in thickness, and the cadmium difference method was applied to subtract the activity resulting from the non-thermal fluence above the cadmium threshold. The activity of ^{198}Au was measured by 4π γ-counting in a NaI(Tl) borehole detector. The detection efficiency of this detector was determined earlier by a comparison with a measurement of the ^{198}Au activity using the 4π β–γ coincidence counting technique. The quantity specified by the gold foil measurements is the sub-cadmium fluence Φ, i.e. the thermal fluence Φ_{th} plus the non-thermal fluence below the nominal cadmium threshold $E_{Cd} = 0.68$ eV. The relation between the measured saturated ^{198}Au activity and Φ was established using MCNPX, thereby including all corrections for self-shielding, flux depression etc. No information was given on the particular evaluation used for the ^{197}Au(n,γ) cross section. The relative uncertainty of the calibration factor η relating the saturated ^{198}Au activity to the sub-cadmium neutron fluence Φ is only 0.54 %.

Measurements using the transfer devices were carried out using the cadmium difference method to determine the response of all four possible combinations of counters and moderator sphere. The pulse-height spectra of the counters showed a strong distortion from γ-radiation from neutron capture in cadmium when the counters were covered with the cadmium shields. Hence higher pulse-height thresholds had to be used. The missing events were corrected for using the shape of the undistorted spectra from the bare counters.

The measurements were analysed using MCNPX simulations of the full set-up, including a model of the SP9 counters filled with ^{3}He. From these calculations corrections factors were derived to account for the distortions of the neutron field resulting from the presence of the counters, i.e. self-shielding and flux depression. In addition, the residual spatial variation of the neutron field over the volume of the counters was corrected for. As expected, the corrections were largest for the 200 kPa counter inside the moderator sphere. For this condition, a total correction for these effects of about 4.5 % was obtained.

Finally, MCNPX was used to calculate the correction factors for the difference of the calibration field and the reference neutron field with respect to the angular and spectral distributions. The product of the correction factors corresponds to the correction factor k_1 defined in the protocol. For the bare counters a correction of about 4.7 % was found, while the correction was only 0.5 % for the counters inside the moderator sphere.

4.4. National Physical Laboratory (NPL)

At the NPL, thermal neutrons were produced in a so-called thermal pile. This device consists of a large graphite block in which neutrons are produced by bombarding two beryllium targets with a deuteron beam from the 3.5 MV Van de Graaff accelerator of the NPL. The irradiation position was situated above a hole in the graphite moderator, the so-called ‘thermal column’, which is located roughly above one of the beryllium targets.

The neutron distribution at the irradiation position consists of a Maxwellian with temperature parameter kT and a slowing-down component. This slowing down component has a spectral distribution proportional to $1/E$ and a lower cut-off energy $E_\Delta = \mu kT$ with $\mu = 3.68$. The parameters of the spectral distribution were determined earlier using activation foil measurements. The following results were obtained: relative thermal fluence $\Phi_{th}/\Phi = 0.9676$, $kT = 27.2$ meV and relative epithermal fluence below E_{Cd} $\Phi'_{nth}/\Phi = 0.0324$. Here Φ denotes the total fluence below the cadmium cut-off and a cadmium cut-off energy E_{Cd} of 0.5 eV was used, instead of 0.68 eV, as specified in the protocol.

$$\frac{\Phi_E \mathrm{d}E}{\Phi} = \left(\frac{\Phi_{th}}{\Phi}\right)\left(\frac{E}{kT}\right)\exp\left(-\frac{E}{kT}\right)\frac{\mathrm{d}E}{kT} + \left(\frac{\Phi'_{nth}}{\Phi}\right)\frac{1}{\ln\left(E_{Cd}/E_\Delta\right)}\frac{\mathrm{d}E}{E}\Delta\left(E_\Delta, E_{Cd}\right) \qquad (7)$$

Here $\Delta(E_\Delta,E_{Cd})$ denotes a rectangular joining function which is equal to one for $E_\Delta \leq E \leq E_{Cd}$ and vanishes outside. These distributions were also used to calculate the correction factor k_1 for the effect of the deviation of the actual spectral distribution from the reference distribution.

The fluence rate at the irradiation position is held constant using an accelerator feedback system which includes several ionisation chambers positioned in the pile underneath and below the targets. Two ^{235}U fission ionisation chambers located in the moderator closer to the thermal column were available as additional monitors.

The monitors were calibrated by activation of two gold foils, 50 µm in thickness, one bare and one covered with cadmium 1 mm in thickness, to subtract the activity induced by neutrons above the cadmium cut-off energy. The fluence rate during the activation of the foil was about an order of magnitude higher than that for the calibration of the transfer instruments. The activity induced in the foils was measured by $4\pi\beta$ counting. The counting efficiency of the foils was determined earlier using $4\pi\ \beta-\gamma$ coincidence counting of foils activated in a thermal reactor. A correction for the different spectral distributions in the reactor and the thermal pile was applied to the bare foils. No correction was required for the foils covered with cadmium. The ^{197}Au(n,γ) cross section was taken from the ENDF/B-VI standards evaluation.

The ratios of the monitor readings were carefully investigated for different fluence rate levels ranging up to that of the gold activation runs. Except for the two lowest fluence rate levels, the ratios were independent of the fluence rate within the uncertainties. The measurements at the lowest fluence rate level were therefore not used for the analysis and the monitor readings of the ^{235}U fission chambers for the second but lowest fluence rate levels were increased by 1 % to account for the observed nonlinearity.

The transfer instruments were irradiated with and without the cadmium shields, with and without the PE moderator and parallel and perpendicular to their symmetry axis. However, only the four combinations requested in the protocol are analysed here. For the bare 200 kPa counter with irradiation along the axis, a large number of measurements at different fluence rate levels were carried out. The count rate of the counter was corrected according to eq. (3) using a non-extendable dead-time $\tau = 7.2$ µs. The ratio of the count rate corrected for dead-time to the monitor rate from one of the fission chamber monitors and to one of the control ionisation chambers is shown in fig. 6.

A residual dependence on the count rate is clearly visible, in contrast to the results shown in fig. 3. A possible reason for this discrepancy could be the combination of the AIOSAP module and a gate and delay generator used for interfacing to the NPL scaler cards. Fortunately, the measurements used for deriving the final results were carried out at count rates below 10^3 s^{-1}, where the discrepancy amounts to about 2 %. To account for it, a variable dead-time correction according to

$$k_2 = \frac{1}{\left(1 - R\cdot\left(1+\rho/\rho_0\right)\cdot\tau\right)}, \quad \rho = \mathrm{d}N/\mathrm{d}t, \quad \rho_0 = 1.6\times10^4\,\mathrm{s}^{-1} \tag{8}$$

was employed to calculate the dead-time correction factor k_2.

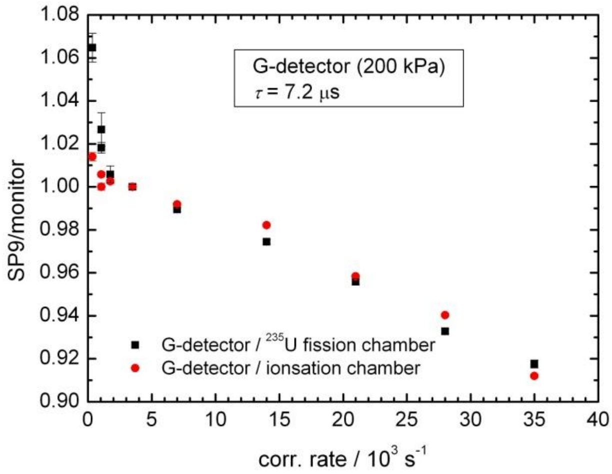

Fig. 6 Monitor ratios for the 200 kPa counter as a function of the corrected count rate measured at the NPL thermal pile. The dead-time correction was carried out using a non-extendable dead-time of 7.2 µs (cf. eq. (3) above).

4.5. Physikalisch-Technische Bundesanstalt (PTB)

The PTB used a thermal neutron beam at the research reactor FRG-1 of the GKSS research centre in Geesthacht (Germany). The thermal neutron beam facility was installed at the exit of a bent thermal neutron guide which made the beam virtually free of photons and epithermal neutrons. The cadmium ratio for the activation of gold was about 3.3×10^4. The facility was equipped with a rotating beam chopper which enabled the relative spectral fluence distribution to be measured using the time-of-flight (TOF) method and a ^{6}Li glass scintillation detector. A ^{3}He ionisation chamber was placed permanently in the beam and served as a transmission monitor for the neutron rate J.

The neutron beam was defined by two quadratic apertures. The small aperture with an area of less than 9 mm^2 was located close to the exit of the beam guide. The large aperture was positioned in a distance of about 4.6 m from the small aperture and had an area of 100 mm^2. The small aperture was varied in size to adjust the neutron rate and control the dead-time corrections required for the transfer instruments. The large aperture was kept constant during all measurements because its size influences the spectral distribution of the neutrons. The spectral distribution was measured using the TOF method. It could be fitted with a Maxwellian fluence distribution with $kT = 23$ meV, but the experimental distribution was used for the calculation of all correction factors.

The area of the neutron beam at the position of the transfer devices was 13 mm × 13 mm. Due to the influence of the neutron guide, the spatial distribution of the neutron fluence was inhomogeneous. Hence, the transfer instrument had to be scanned step-by-step over a larger scanning area to simulate an homogeneous irradiation.

Prior to the measurements with the transfer instruments, the neutron rate J in the beam was measured using the ^{6}Li Glass detector. This detector had a diameter of 76 mm to accommodate the full neutron beam. The dead-time of the detector and the associated electronic modules amounted to (3.6 ± 0.6) μs. The energy-dependent efficiency ε was calculated according to

$$\varepsilon = 1 - \exp\left(-23.17\mathrm{nm}^{-1} \cdot \lambda\right), \quad \lambda = \frac{hc}{\sqrt{2E\, m_\mathrm{n} c^2}} \tag{9}$$

where λ, E and m_n denote the wavelength, energy and mass of the neutron, respectively. For the measured spectral distribution, the correction for the detection inefficiency of the ^{6}Li glass detector amounted to 1.045 ± 0.012, i.e. the detector was almost 'black'.

Directly before the measurements carried out for the key comparison, the neutron number per event in the ^{3}He transmission monitor was measured using the ^{6}Li glass detector and the activation of a gold foil. The activity of the gold foil was measured using the 4πβ-γ coincidence method. The ratio of measured neutron rate values $J_\mathrm{Au}/J_\mathrm{LiG}$ was 1.001 ± 0.029 which made the measurements using the ^{6}Li glass detector traceable to the primary standard.

The measurement of the neutron rate with the ^{6}Li glass detector was used to determine the calibration factor f = 386.5 ± 7.8 of the ^{3}He transmission monitor. Using this calibration factor, the neutron fluence was calculated from the number of monitor events and the scanning area. In view of the large cadmium ratio no separate measurements with the transfer instruments covered by the cadmium shields were carried out.

Corrections were applied for the deviation of the relative spectral distribution from the Maxwellian reference distribution with kT = 25.3 meV (k_1) and for dead-time losses (k_2). As mentioned above, the experimental spectral distribution was used to calculate k_1. Thus, this correction includes any contribution from epithermal neutrons. The correction k_2 was calculated using an average of the dead-time corrections for the individual steps of the scanning procedure.

The relative uncertainty of the correction factor Li_korr for the detection inefficiency of the ^{6}Li glass detector is 0.007, which is smaller than the uncertainty of the neutron rate ratio $J_\mathrm{Au}/J_\mathrm{LiG}$. From the data given in [BOE04], the relative uncertainty of this ratio is calculated to be about 0.022. Hence, it has to be concluded that the uncertainty of this ratio has to be added quadratically to the relative uncertainties of all fluence response values R measured for the transfer devices to make the calibration traceable to the ^{197}Au(n,γ) reference cross section.

5. Results

5.1. General remarks

The goal of a key comparison is to evaluate the performance of the participants by the degree of equivalence (DOE), i.e. the deviation of their results from the key comparison reference value (KCRV). In contrast to other comparison [CHE07] several transfer devices are used in CCRI(III)-K8. In this chapter the results obtained by the participants are reported in detail. To arrive at a single final results for each participant and a single value for the KCRV, the relative measured response values for the four combinations of detectors and moderator were averaged for each participant. This procedure was already used in the key comparison CCRI(III)-K1 of 24 keV neutron fluence measurements [THO10].

In key comparison usually the weighted mean is used to average results and to calculate the KCRV. As outlined below, however, the results of the present key comparison show a considerable spread. Procedures for the treatment of 'outliers' are available from the literature [COX07]. Nevertheless, in view of the small number of only four participants, it was not considered to be reasonable to discard two out of four results to formally obtain a largest consistent subset (LCS) which can be used to calculate a KCRV.

Because smaller uncertainties were reported by the NMIJ than by the other participants, the use the weighted mean would produce a bias towards the result with the smallest uncertainty.

For each detector-moderator combination j (j = 1, 4), the arithmetic mean $\overline{R}_j$ and its standard uncertainty $u_{\overline{R}_j}$ (k = 1) was calculated from the results $R_{i,j}$ of the n = 4 participants i (i = 1, n).

$$\overline{R}_j = \frac{1}{n}\sum_{i=1}^{n} R_{i,j} \quad \text{and} \quad u_{\overline{R}_j} = \sqrt{\frac{1}{n(n-1)}\sum_{i=1}^{n}(R_{i,j}-\overline{R}_j)^2} \tag{10}$$

The uncertainties $u_{\delta R_{i,j}}$ (k = 1) of the deviations $\delta R_{i,j} = R_{i,j} - \overline{R}_j$ were calculated from the uncertainties $u_{i,j}$ of the results [RAT05].

$$u^2_{\delta R_{i,j}} = \left(1-\frac{2}{n}\right)u^2_{i,j} + \frac{1}{n^2}\sum_{i=1}^{n} u^2_{i,j} \tag{11}$$

The 'quality' of the data can be judged from a comparison of the experimental χ^2

$$\chi^2_j = \sum_{i=1}^{n}\frac{(R_{i,j}-\overline{R}_j)^2}{u^2_{i,j}} \tag{12}$$

with $\left(\chi^2\right)^{-1}(n-1, 0.05)$, i.e. the argument at which the χ^2 distribution function for n-1 degrees of freedom is equal to 0.95. For n = 4, $\left(\chi^2\right)^{-1}(3, 0.05) = 7.81$.

As usual for key comparisons, the deviations $\delta R_{i,j}$ are reported together with the expanded uncertainties $U_{\delta R_{i,j}}$ (k = 2).

$$U_{\delta R_{i,j}} = 2u_{\delta R_{i,j}} \tag{13}$$

The relative response values $x_{i,j} = R_{i,j} / \overline{R}_j$ and their uncertainties $u_{x_{i,j}} = u_{i,j} / \overline{R}_j$ were averaged over all detector-moderator combination using the unweighted mean. This procedure accounts for the fact, that the results for the different moderator-detector combinations have a considerable degree of correlation. The mean relative response and its uncertainty (k = 1),

$$\overline{x}_i = \frac{1}{4}\sum_{j=1}^{4} x_{i,j} \text{ and } u_{\overline{x}_i} = \frac{1}{4}\sum_{j=1}^{4} u_{x_{i,j}}\ , \tag{14}$$

is the final results for each participant i.

The KCRV is then defined as 1 cm^2/cm^2. The deviation D_i of participant i from the KCRV and its expanded uncertainty (k = 2) is

$$D_i = \overline{x}_i - 1 \text{ and } U_{D_i} = 2u_{\overline{x}_i} \tag{15}$$

The degrees of equivalence (DOEs) $D_{ij} = \bar{x}_i - \bar{x}_j$ between participants i and j and their expanded uncertainties (k = 2)

$$U_{D_{ij}} = 2\sqrt{u_{\bar{x}_i}^2 + u_{\bar{x}_j}^2} \qquad (16)$$

are reported as well.

5.2. Evaluation of the results

Tables 1.1 –1.4 contain the numerical results of the participants for the response $R_{i,j}$ of the transfer instruments at reference conditions together with the arithmetic means $\bar{R}_j$, the relative response values $x_{i,j}$ and the experimental χ_j^2 for all four combinations of detectors and the moderator sphere. The uncertainty indicated for $\bar{R}_j$ is the standard measurement uncertainty (k = 1).

Table 1.1 Results for the E-Detector (20 kPa)

E-Detector (20 kPa): j = 1							
	$R_{i,j}$ / cm^2	$u_{i,j}$ / cm^2	$u_{i,j}$ / $R_{i,j}$	$\delta R_{i,j}$ /cm^2	$U_{\delta R_{i,j}}$ /cm^2	$x_{i,j}$	$u_{x_{i,j}}$
CIAE	0.394	0.009	0.024	0.022	0.017	1.060	0.025
NMIJ	0.370	0.005	0.014	-0.001	0.013	0.997	0.014
NPL	0.347	0.010	0.029	-0.025	0.017	0.934	0.027
PTB	0.375	0.014	0.038	0.003	0.023	1.009	0.009
$\bar{R}_j$	0.372	0.010	0.026				
χ_j^2	11.86						

Table 1.2 Results for the G-Detector (200 kPa)

G-Detector (200 kPa): j = 2							
	$R_{i,j}$ / cm^2	$u_{i,j}$ / cm^2	$u_{i,j}$ / $R_{i,j}$	$\delta R_{i,j}$ /cm^2	$U_{\delta R_{i,j}}$ /cm^2	$x_{i,j}$	$u_{x_{i,j}}$
CIAE	3.260	0.078	0.024	0.176	0.139	1.057	0.025
NMIJ	3.070	0.055	0.018	-0.015	0.115	0.995	0.018
NPL	2.879	0.078	0.027	-0.206	0.139	0.933	0.025
PTB	3.129	0.115	0.037	0.045	0.183	1.014	0.037
$\bar{R}_j$	3.085	0.079	0.026				
χ_j^2	12.19						

Table 1.3 Results for the E-Detector (20 kPa) inside the PE moderator

E-Detector (20 kPa) + 3″ PE Sphere: j = 3							
	$R_{i,j}$ / cm^2	$u_{i,j}$ / cm^2	$u_{i,j} / R_{i,j}$	$\delta R_{i,j}$ /cm^2	$U_{\delta R_{i,j}}$ /cm^2	$x_{i,j}$	$u_{x_{i,j}}$
CIAE NMIJ NPL PTB	0.262 0.224 0.204 0.217	0.007 0.005 0.005 0.008	0.025 0.021 0.026 0.035	0.035 -0.003 -0.023 -0.010	0.011 0.009 0.010 0.012	1.155 0.988 0.900 0.956	0.029 0.021 0.024 0.033
$\overline{R}_j$ χ^2_j	0.227 48.26	0.012	0.055				

Table 1.4 Results for the G-Detector (200 kPa) inside the PE moderator

G-Detector (200 kPa) + 3″ PE Sphere: j = 4							
	$R_{i,j}$ / cm^2	$u_{i,j}$ / cm^2	$u_{i,j} / R_{i,j}$	$\delta R_{i,j}$ /cm^2	$U_{\delta R_{i,j}}$ /cm^2	$x_{i,j}$	$u_{x_{i,j}}$
CIAE NMIJ NPL PTB	1.560 1.355 1.236 1.322	0.037 0.031 0.033 0.047	0.024 0.023 0.027 0.036	0.192 -0.013 -0.132 -0.046	0.065 0.058 0.060 0.077	1.140 0.990 0.903 0.966	0.027 0.023 0.024 0.035
$\overline{R}_j$ χ^2_j	1.368 43.43	0.069	0.050				

Fig. 7 shows the relative deviations $\delta R_{i,j} / \overline{R}_j$ for all investigated combinations of detectors and the moderator sphere. The error bars show the expanded relative uncertainties $U_{\delta R_{i,j}} / \overline{R}_j$ (k = 2) while the dashed lines show the relative standard uncertainties $u_{\overline{R}_j} / \overline{R}_j$ (k = 1) of the arithmetic mean. The final combined results $\overline{x}_i$ for all participants and their uncertainties $u_{\overline{x}_i}$ are shown in table 2. The deviations D_i to the KCRV 1 cm^2/cm^2 and the DOEs D_{ij} are indicated in table 3 and fig. 8.

Table 2: Final combined results $\overline{x}_i$ of the participants and standard uncertainties (k = 1) $u_{\overline{x}_i}$.

	$\overline{x}_i$	$u_{\overline{x}_i}$
CIAE NMIJ NPL PTB	1.103 0.993 0.918 0.987	0.027 0.019 0.025 0.036

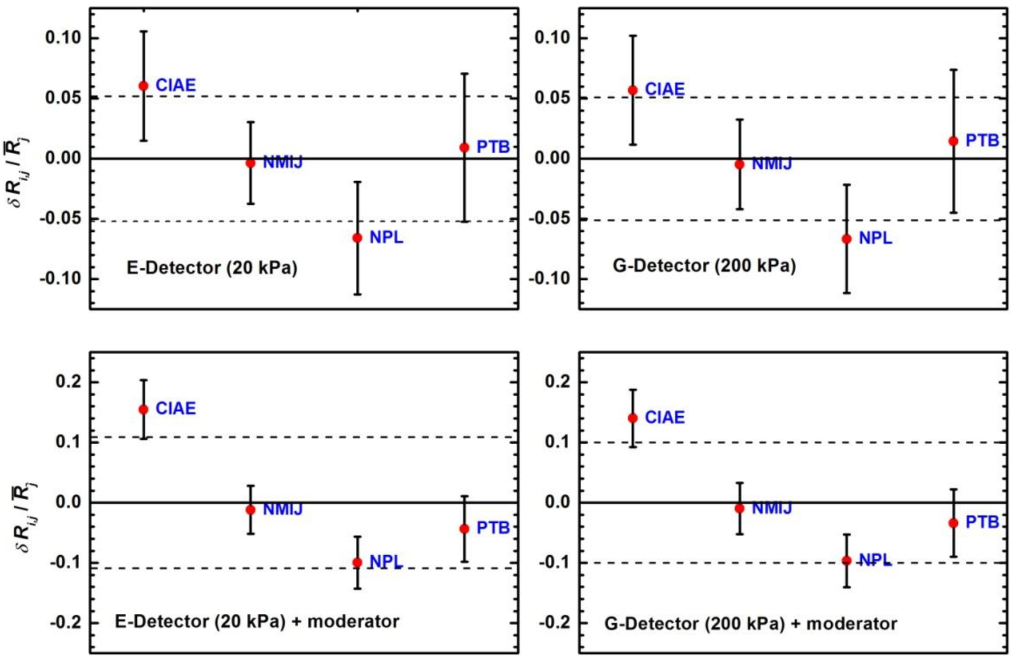

Fig. 7 Deviations $\delta R_{i,j}$ of the results from the arithmetic mean. The deviations and their expanded uncertainties (k = 2) are normalised to the respective arithmetic means $\overline{R}_j$ for better visibility only, i.e. the error bars do not include the uncertainties of the arithmetic means. The dashed lines show the standard uncertainties (k = 1) of the arithmetic means $\overline{R}_j$ calculated using eq. (10).

Table 3: Deviations D_i and degrees of equivalence (DOE) D_{ij} between the different participants. The expanded uncertainties (k = 2) are denoted by U_i and U_{ij}, respectively.

Lab. *j* ⟹

Lab. *i* ⇓

			CIAE		NMIJ		NPL		PTB	
	D_i	U_i	D_{ij}	U_{ij}	D_{ij}	U_{ij}	D_{ij}	U_{ij}	D_{ij}	U_{ij}
CIAE	0.103	0.054			0.110	0.065	0.185	0.073	0.116	0.090
NMIJ	-0.007	0.038	-0.110	0.065			0.075	0.063	0.006	0.081
NPL	-0.082	0.050	-0.185	0.073	-0.075	0.063			-0.069	0.088
PTB	-0.013	0.072	-0.116	0.090	-0.006	0.081	0.069	0.088		

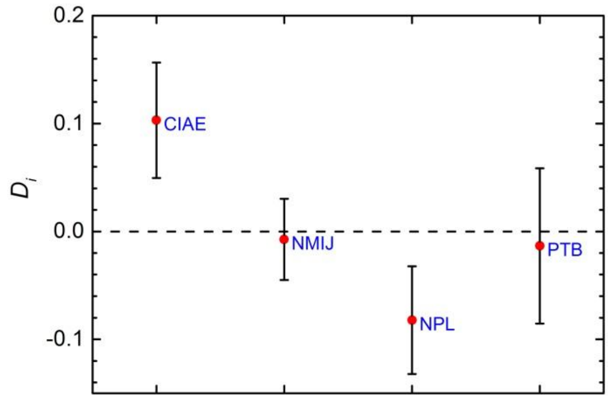

Fig. 8 Deviations D_i of the results from the KCRV 1 cm^2/cm^2 and their expanded uncertainties U_i.

6. Discussion and Conclusions

In general, the results obtained by the PTB and the NMIJ agree reasonably well. As demonstrated in fig. 7, the relative deviation of NPL results from the arithmetic means is about -6.6 % and -9.8 % for the bare detectors and the detectors in the moderator, respectively. These almost constant deviations suggest that the reason could be related to a normalisation problem of the fluence measurement. On the other hand, the CIAE results for the bare detectors show almost the same absolute deviation, but to the opposite side. For the detectors in the moderator, the CIAE results are clearly deviating from the other results by about 16 %. This suggests that there is a problem related to the correct determination of the spectral distribution of the collimated neutron beam used to irradiate the transfer instruments. However, the small number of results delivered in this key comparison makes all these conclusions somewhat uncertain.

The fluence responses of the bare detectors and the detectors covered by the moderator sphere were calculated using MCNPX [WIE12] based on the nominal ^{3}He pressures specified by the manufacturer, i.e. 20 kPa for the E-detector and 200 kPa for the G-detector. These data were communicated to the evaluator only after the measurements had been finished and the reports filed at the BIPM.

Similar calculations were carried out for the 200 kPa A-detector used in the PTB Bonner sphere spectrometer NEMUS, but for a ^{3}He pressure of 220 kPa. For this pressure better agreement was found between the measured and calculated fluence response of NEMUS over the entire energy range from thermal to 20 MeV [WIE12]. The A-detector used in NEMUS and the G-detector are similar in design and the control readings of the two detectors obtained from the stability checks in the HANNA facility agreed within 0.5 %. Hence, it can be concluded that the same improvement of the performance of NEMUS would also be obtained for the G-detector used in the present comparison. Table 3 shows a comparison of the calculated fluence response values R_{nom} and R_{cor} averaged over a Maxwellian reference distribution with kT = 25.3 meV with the mean values $\overline{R}$ reported in tables 1.1 – 1.4.

Table 3 Response for the spectral reference distribution with $kT = 25.3$ meV. The experimental results obtained for the G-detector in the present key comparison and the results calculated using MCNPX for the nominal and the adjusted ^{3}He pressures are denoted by $\overline{R}$, R_{nom} and R_{cor}, respectively.

	$\overline{R}$ / cm^2	R_{nom} / cm^2	R_{cor} / cm^2
E-det.	0.372 ± 0.019	0.392 ± 0.010	
G-det.	3.085 ± 0.158	3.013 ± 0.151	3.108
E-det. + mod.	0.227 ± 0.025	0.252 ± 0.013	
G-det. + mod.	1.368 ± 0.137	1.291 ± 0.039	1.323

The sensitivity of the present key comparison to the spectral distribution can be investigated further by calculating the ratio R_{bare}/R_{mod} of the response at reference conditions of the bare 200 kPa G-detector to that of the G-detector in the moderator sphere. In fig. 9 the experimental values are compared with calculated data for spectral distributions with a thermal component Φ_{th} with temperature kT and an epithermal sub-cadmium fluence Φ_{epi}, cf. eq. (6). The uncertainties indicated for the experimental values are approximate values calculated from the budgets reported by the participants. They include the correlation between the measured response values for the bare detector and the detector in the moderator sphere. For an 'ideal' measurement, i.e. with all corrections carried out correctly, the experimental data should group around the line corresponding to $\Phi_{epi} = 0$ and the temperature $kT = 25.3$ meV. The lines corresponding to $\Phi_{epi} > 0$ show the expected location of the data if an undetected additional epithermal spectral contribution would have been present.

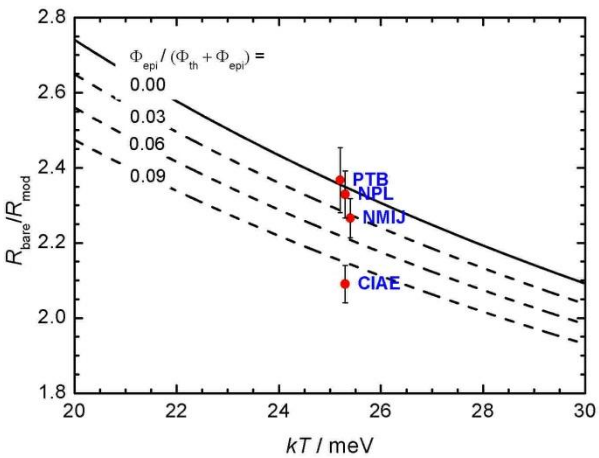

Fig. 9 Ratio of the response R_{bare} for the bare 200 kPa detector and the response R_{mod} of this detector inside the moderator sphere. The solid and the dashed lines show the response ratios calculated for a spectral distribution with a thermal fluence Φ_{th} (temperature kT) and an epithermal sub-cadmium fluence Φ_{epi}. The calculations were carried out for an effective ^{3}He pressure of 220 kPa. The results of the key comparison (red circles) are slightly offset from the reference temperature $kT = 25.3$ meV to make the error bars visible.

This analysis supports the conclusion made above. There is no evidence of problems with the spectral distributions reported by the NPL and the PTB. Also the NMIJ result is almost consistent with the expected value. The CIAE result, however, is clearly deviating and could only be explained by a wrong determination of the temperature of the thermal part or by an undetected epithermal contribution.

The results obtained in this comparison highlight the need to control the spectral distribution in thermal neutron beams. However, a reinvestigation of the problems encountered in the present comparison is greatly hampered by the present unavailability of two of the four participating facilities.

Acknowledgements

This key comparison was initiated by Dr. H. Klein of the PTB during his time as the chairperson of the CCRI(III). The authors would like to thank Dr. B. Wiegel for many helpful discussions and A. Kasper and S. Löb for their continuing support during the organisation of the measurements.

All participants appreciate the support they received from their co-workers. In particular, D.J. Thomas acknowledges the important contribution of his retired colleague P. Kolkowski who carried out and analysed most of the measurements at the NPL.

References

[ALE06] A.V. Alevra, 'All-in-one Spectrometry Analogue Processor AIOSAP-01, Manual', Braunschweig 2006

[AXT70] E.J. Axton, 'Results of the intercomparison of the thermal neutron flux density unit (1966-1968)', Metrologia **6** (1070) 25-32

[BEC64] K.H. Beckurts and K. Wirtz, 'Neutron Physics', Springer-Verlag Berlin, Göttingen, Heidelberg, New York, 1964

[BOE04] R. Böttger, H. Friedrich, H. Janssen, 'The PTB Thermal Neutron Reference Field at GeNF', PTB Report PTB-N-47, Physikalisch-Technische Bundesanstalt Braunschweig 2004, ISBN 3-86590-199-7

[CHE07] J. Chen *et al.* 'International Key Comparison of Neutron Fluence Measurements in Monoenergetic Neutron Fields - CCRI(III)-K10' Metrologia **44** (2007), Technical Supplement, 06005

[COX07] M.G. Cox, 'The evaluation of key comparison data: determining the largest consistent subset', Metrologia **44** 187-200 (2007)

[RAT05] G. Ratel, 'Evaluation of the uncertainty of the degree of equivalence', Metrologia **42** (2005) 140-144

[THO10] D.J. Thomas, V.E. Lewis, H. Klein, P.J. Allisy-Roberts, 'International Key Comparison of 24 keV Neutron Fluence Measurements (1993-2009) - CCRI(III)-K1', Metrologia **47** (2010), Technical Supplement, 06014

[THO11] D.J. Thomas, R. Nolte and V. Gressier, 'What is neutron metrology and why is it needed?', Metrologia **48** (2011) S225-S238

[WIE12] B. Wiegel, private communication, 2012

[X-503] X-5 Monte Carlo Team, 'MCNP – A General Monte Carlo N-Particle Transport Code, Version 5', Report LA-UR-03-1987, Los Alamos National Laboratory, April 24, 2003

Appendices

1. **Report of the CIAE**
2. **Report of the NMIJ**
3. **Report of the NPL**
4. **Report of the PTB**

中国原子能科学研究院
CHINA INSTITUTE OF ATOMIC ENERGY

Report of Key Comparison for Thermal Neutron Fluence Measurements at CIAE

Jun CHEN,
Chunjuan LI,
Yina LIU,
Jianqing WANG,
Yanling YAO

Contents

page

Foreword

Key comparison for thermal neutron fluence measurements, organized by the Section-Ⅲ of the Consultative Committee for Ionizing Radiation (CCRI), had been performed at China Institute of Atomic Energy (CIAE) from June to August of 2007. A collimated thermal neutron beam is available for calibrating the responses of the transfer instruments provided by PTB as pilot laboratory. The thermal neutron field had been characterized by means of the methods described in the report. For the reason that the primary national standard for thermal neutron measurements in China has not been established yet, no a documentation of the traceability to primary national standard can be attached to the report to submit to the organizer.

1 Basic facility

A thermal neutron field established at thermal column of a nuclear reactor of 2MW was used to perform the comparison. A photograph of the experimental hall is shown in Figure A.1. Neutrons are collimated by an eduction tube to be a beam. A small collimator sometimes is inserted into the eduction tube in order to limit the size of neutron beam spot or neutron flux. The structure of the neutron eduction tube is sketched in Figure B.1.

Because the neutron beam can not cover the sensitive area of the transfer instrument, a scanning device shown in Figure A.2 was used to perform a simulation from narrow beam radiation to broad radiation. Detectors can be installed on the scanning device and be positioned precisely by a theodolite, a gradienter and a distance gauge. A ^{3}He proportional counter was used for monitoring the fluctuation of neutron fluence rate with time. In addition, the environmental conditions in the experiment hall, such as temperature, humidity and air pressure, can be measured by a thermometer, a hygrometer and a barometer.

For a convenient narration in the following text, the relative experimental coordinates are plotted in Figure C.1 and the irradiation conditions corresponding to the measurements mentioned in the report are labeled as two cases as follows: (1) “case 1” denotes that the small collimate is inserted into the neutron eduction tube; (2) “case 2” denotes that the small collimate is drawn out from the neutron eduction tube. A reference point was set in the central line of the neutron beam and at a distance of 50mm from the beam port. The responses of the transfer instruments were calibrated at the reference point where the neutron fluence had been determined.

2 Characterization of thermal neutron field

2.1 Neutron energy spectrum

Neutron energy spectrum of the thermal neutron field was determined using the time-of-flight technique. A chopper, which is made of a piece of 1mm thick cadmium sandwiched by two pieces of 0.5mm thick stainless steel, with two symmetrical slits of 2mm in width and 5mm in length, was used to obtain neutron pulses. The chopper could be driven by a motor to be up to 3500 rotations per minute. The start signals of neutron flight were produced by a photoelectric system and the stop signals by a ^{3}He proportional counter. A schematic diagram of the measuring system is shown in Figure D.1

The measurements for neutron energy spectrum were performed in “case 1” so that the edge of the chopper was able to shield the neutron beam. Neutron flight time spectra were measured at two distances as 132.2cm and 152.5cm. Consequently, the actual start time of neutron flight could be calculated by the relationship between neutron flight time and neutron flight distance to be 163.27μs±5.35μs. The channel width of MCA and the linearity of TAC had been calibrated using a pulse generator to generate the neutron start signals instead of the photoelectric system.

Figure 1 shows the measured neutron energy spectrum at the reference point. Background spectra were subtracted from the measured spectrum, and the corrections for the effect of air attenuation and the detection efficiency of the ^{3}He counter, shown in Figure 2 and Figure 3, were considered.

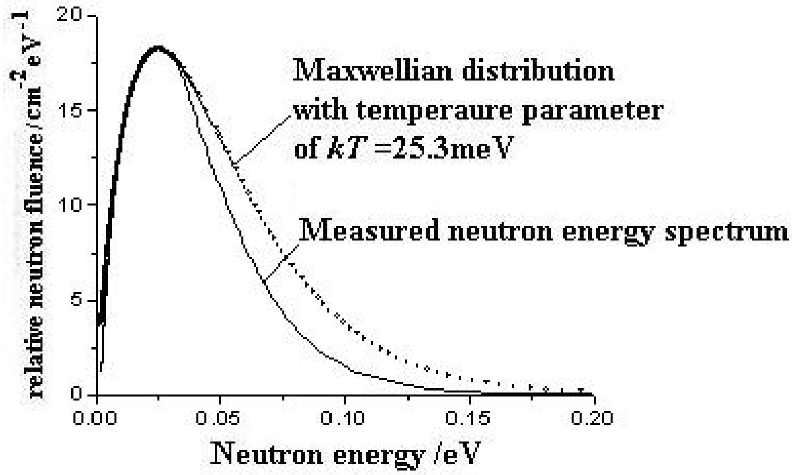

Figure 1—Measured neutron energy spectrum and a Maxwellian fluence distribution with the temperature parameter of kT=25.5meV

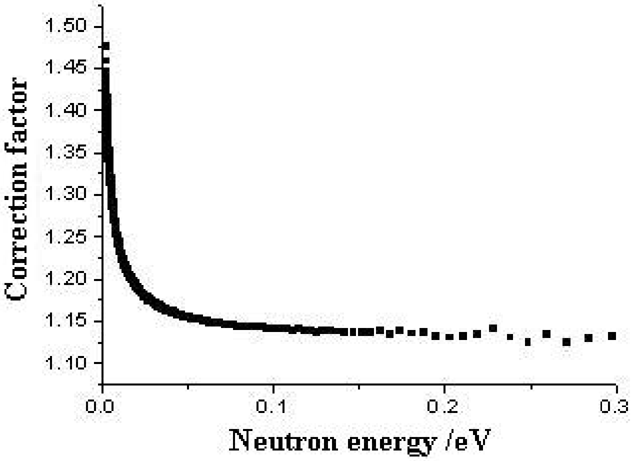

Figure 2—Correction factor of air attenuation as a function of neutron energy

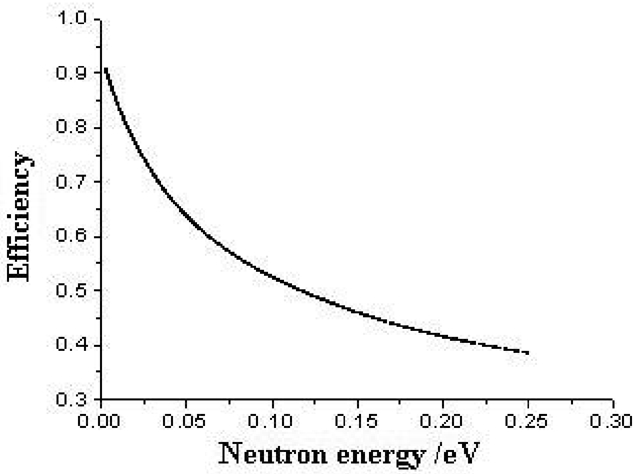

Figure 3—Efficiency of the ^{3}He counter as a function of neutron energy

2.2 Neutron fluence rate

The neutron fluence rate at the reference point was measured by the activation of gold foils in “case 2”. Details of the used gold foils are described in Table 1.

Table 1—Details of the gold foils used in the neutron fluence measurement

Number of gold foils	Mass /mg	Remarks
1#	7.97	The gold foil is 10mm in diameter and 5μm in thickness, and was used as a reference of the activity measurements.
2#	151.19	The gold foil is 15mm in diameter and 40μm in thickness, and was used to measure the thermal neutron fluence.
3#	62.13	The gold foil is 14mm in diameter and 20μm in thickness, and was also used to measure the thermal neutron fluence.
4#	8.05	The gold foil is 10mm in diameter and 5μm in thickness, and was used to check the effect of epithermal neutrons.
5#	31.75	The gold foil is 10mm in diameter and 20μm in thickness, and was also used to check the effect of epithermal neutrons.

In order to obtain enough radioactive statistics, a “thick” gold foil (2# or 3#) irradiated for about six hours at the reference point was used to determine the neutron fluence. It is inevitable, however, that the “thick” gold foil presents a lower emitting efficiency of β rays that is of disadvantage to the measurement of β-γ coincidence. And then a “thin” gold foil (1#) irradiated for six seconds in the core of the reactor was used as a reference of the activity measurements. In addition, the effect of the epithermal neutrons with energy of several eV to the activation of 2# or 3# gold foil was checked by irradiating another “thick” gold foil (5#) covered with another “thin” gold foil (4#) on its surface toward the neutron beam.

The activity of 1# gold foil was measured absolutely by a 4πβ-γ coincidence standard equipment. The spectra of γ rays emitted from the gold foils mentioned above, shown in Figure 4, were measured using a well-type NaI spectrometer. Consequently, the activities of the gold foils with the number 2#, 3#, 4#, and 5# could be determined by normalizing the peak counts of 411keV γ rays emitted from each of them to those of 411keV γ rays emitted from 1# gold foil.

The measured data and the results of the activities of the gold foils are listed in Table 2 and Table 3.

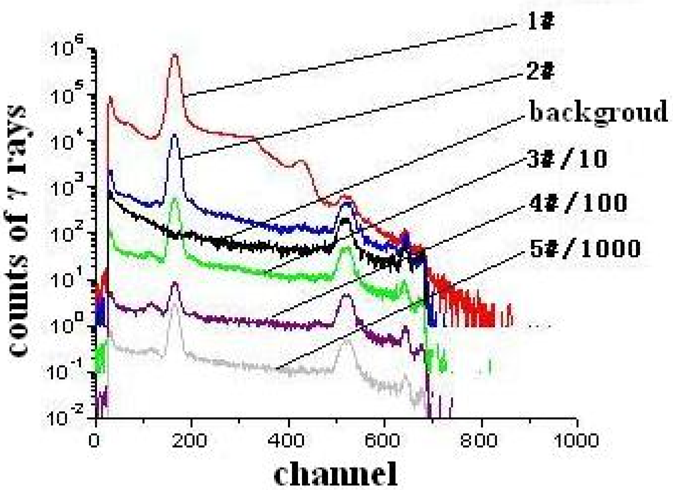

Note: 1#,2#,3#,4#,5# denote the measured spectra of γ rays emitted from 1#,2#,3#,4#,5# gold foils respectively.

Figure 4—Spectra of γ rays from the gold foils measured by the well-type NaI spectrometer

Table 2—Data for the gold foils measured by the well-type NaI spectrometer

Number of gold foils	Dates of measurements	Start time of measurements	Real time /s	Live time /s	Net peak counts of 411keV γ rays
1#	2007.08.28	9:53:18	1790.78	1500	13714671±5166
2#	2007.08.25	17:51:22	1500	1494.16	237498±629
3#	2007.08.26	20:11:42	1500	1496.86	97764±389
4#	2007.08.27	15:11:21	1500	1498.48	11905±134
5#	2007.08.27	15:45:42	1500	1497.82	47151±269

Table 3—Results of the activities of the gold foils

Number of gold foils	Normalized date and time	Net counts of 411keV γ rays corrected for dead-time	Relative activities at normalized time /Bq	relative activities normalized to 1# gold foil
1#	2007.08.28 9:53:18	16373306	9167.504	1
2#		238426	80.21123	8.74952×10^{-3}
3#		97969	43.70665	4.76756×10^{-3}
4#		11917	6.51661	7.10838×10^{-4}
5#		47220	25.98036	2.83396×10^{-3}

Number of gold foils	Date and time of activity measurement	Activity at measuring time /Bq	Activity at normalized time /Bq	Dates and time of irradiation stop	Activity at the time of irradiation stop /Bq
1#	2007.09.03 14:11:48	3202.5	15692.56		
2#				2007.08.25 17:39:00	2.73296×10^{2}
3#				2007.08.26 20:06:00	1.12163×10^{2}
4#				2007.08.27 15:04:00	1.36476×10^{1}
5#				2007.08.27 15:04:00	5.44103×10^{1}

As a result, the thermal neutron fluence rate at the reference point can be determined by Equation (1):

$$\varphi = \frac{k_{\varphi} k_{\mathrm{s}} A}{N_{\mathrm{Au}} \overline{\sigma_{(\mathrm{n},\gamma)}} (1 - \mathrm{e}^{-\lambda(t_1 - t_0)})} \qquad (1)$$

here, k_{φ} is the correction factor for the fluctuation of neutron fluence rate during irradiation; k_{s} is the correction factor for the losses of the neutrons absorbed by gold foil; A is the activity of gold foil; N_{Au} is the number of ^{197}Au nuclei in gold foil; $\overline{\sigma_{(\mathrm{n},\gamma)}}$ is the spectrum-averaged cross-section of the ^{197}Au(n,γ) reaction"; λ is the decay constant of ^{198}Au nucleus; t_1 is the stop time of irradiation; t_0 is the start time of irradiation. The spectrum-averaged cross-section of the ^{197}Au(n,γ) reaction $\overline{\sigma_{(\mathrm{n},\gamma)}}$ can be calculated by Equation (2):

$$\overline{\sigma_{(\mathrm{n},\gamma)}} = \frac{\int_0^\infty \Phi(E)\sigma_{(\mathrm{n},\gamma)}(E)\mathrm{d}E}{\int_0^\infty \Phi(E)\mathrm{d}E} \tag{2}$$

here, E is neutron energy; $\Phi(E)$ is the spectral neutron fluence in "case 2"; $\sigma_{(\mathrm{n},\gamma)}(E)$ is the cross-sections of the ^{197}Au(n,γ) reaction as a function of neutron energy.

In Equation (1), the correction factors k_φ and k_s can be calculated by Equation (3) and Equation (4) respectively:

$$k_\varphi = \frac{n(1-\mathrm{e}^{-\lambda(t_1-t_0)/n})}{\mathrm{e}^{\lambda(t_1-t_0)}-1} \cdot \frac{\sum_{i=1}^{n} C_i \mathrm{e}^{i\lambda(t_1-t_0)/n}}{\sum_{i=1}^{n} C_i} \tag{3}$$

here, n is the recorded times of the counts of monitor during radiation; λ is the decay constant of ^{198}Au nucleus; t_1 is the stop time of irradiation; t_0 is the start time of irradiation; C_i is the counts of monitor in i^{th} time interval.

$$k_\mathrm{s} = \frac{n_1 \overline{\sigma_a} d}{1-\mathrm{e}^{-n_1\overline{\sigma_a}d}} \tag{4}$$

here, n_1 is the number density of ^{197}Au nuclei in gold foil; $\overline{\sigma_a}$ is the spectrum-averaged neutron absorption cross-section of gold; d is the thickness of gold foil.

The neutron fluence normalized a monitor count at the reference point is listed in Table 4.

Table 4—Normalized neutron fluence at the reference point

Parameters	2# gold foil	3# gold foil
Activities of the gold foils /Bq	2.73296×10^{2}	1.12163×10^{2}
Number of ^{197}Au nuclei in the gold foils	4.62176×10^{20}	1.89923×10^{20}
Spectrum-averaged Cross-section of the ^{197}Au(n,γ) reaction /cm^2	9.39324×10^{-23}	
Decay constant of ^{198}Au nucleus /s^{-1}	2.97663×10^{-6}	2.97663×10^{-6}
Irradiation time /s	21900	21660
Correction factor k_{φ}	0.9998	0.9999
Correction factor k_s	1.0123	1.0058
neutron fluence rate /cm$^{-2}\cdot$s^{-1}	1.010×10^{5}	1.013×10^{5}
Monitor counts in irradiation time	5321391	5247337
Neutron fluence normalized to a monitor count /cm^{-2}	**4.155×10^{2}**	**4.180×10^{2}**

By calculation, the fact that the specific activity of 5# gold foil is greater of 1% than that of 4# gold foil, is opposite to the expected result that can be resulted from the epithermal neutrons. The discrepancy between the specific activities of 4# and 5# gold foils may arise from the statistic deviations of the peak counts of 411keV γ rays.

2.3 Spatial distributions of neutron fluence

The spatial distributions of neutron fluence in the neutron beam, shown in Figure 5, were measured by sweeping a ^{235}U fission chamber across the neutron beam.

2.4 Ratio of cadmium

Ratio of cadmium of the thermal neutron field, be approximate 479, was measured by irradiating a gold foil with and without a cadmium cover of 1mm in thickness in the neutron beam.

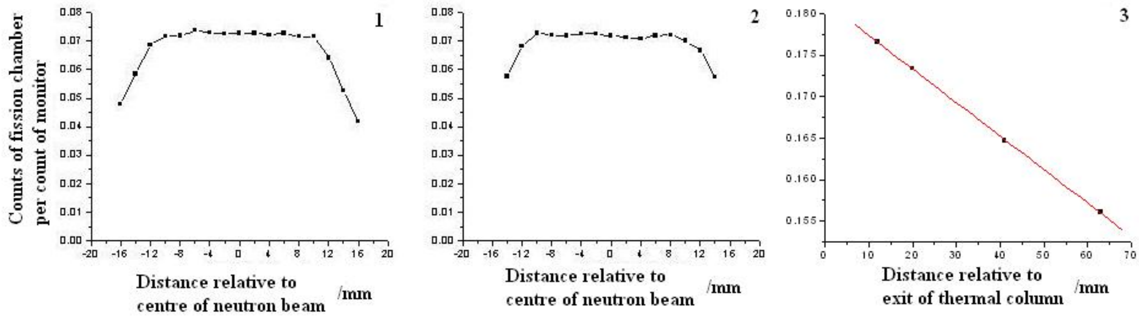

Key

1 Neutron fluence distribution in x direction

2 Neutron fluence distribution in y direction

3 Neutron fluence distribution in z direction

Figure 5—Spatial distributions of neutron fluence in the neutron beam

3 Calibrations of responses of transfer instruments

The responses of the transfer instruments were calibrated in “case 1” in order to obtain the appropriate count rates. Since the neutron beam can not cover the sensitive area of the transfer instrument, a scanning procedure was performed to simulate broad beam irradiation.

The discrimination threshold of the discriminator D1 had been checked before the calibration. Each of the counters, in turn, was fixed on the scanning device to perform a scanning procedure. The scanning step is 4mm for the bare counters and is 8mm for the counters with the polythene moderator. Background neutrons were also measured by moving the counters outside the neutron beam.

Due to very low count rate, the counters with the cadmium cover were just operated by fixing their sensitive centers at the reference point rather than by scanning them. The contribution of the neutrons above the cadmium threshold was taken into account as a correction.

The pulse-height spectra of the transfer instruments are shown in Figure 6. The data measured by the transfer instruments are listed in Table 5 and are shown in Figure 7 by graphic representation. The original data measured by the transfer instruments is given in a spreadsheet file.

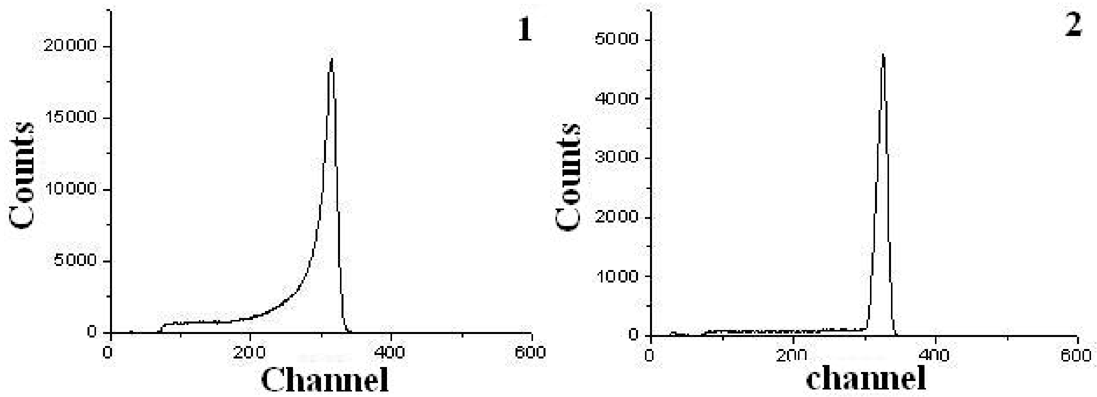

Key

1 Pulse-height spectrum of the 200kPa ^3He counter

2 Pulse-height spectrum of the 20kPa ^3He counter

Figure 6—Pulse-height spectra of the transfer instruments

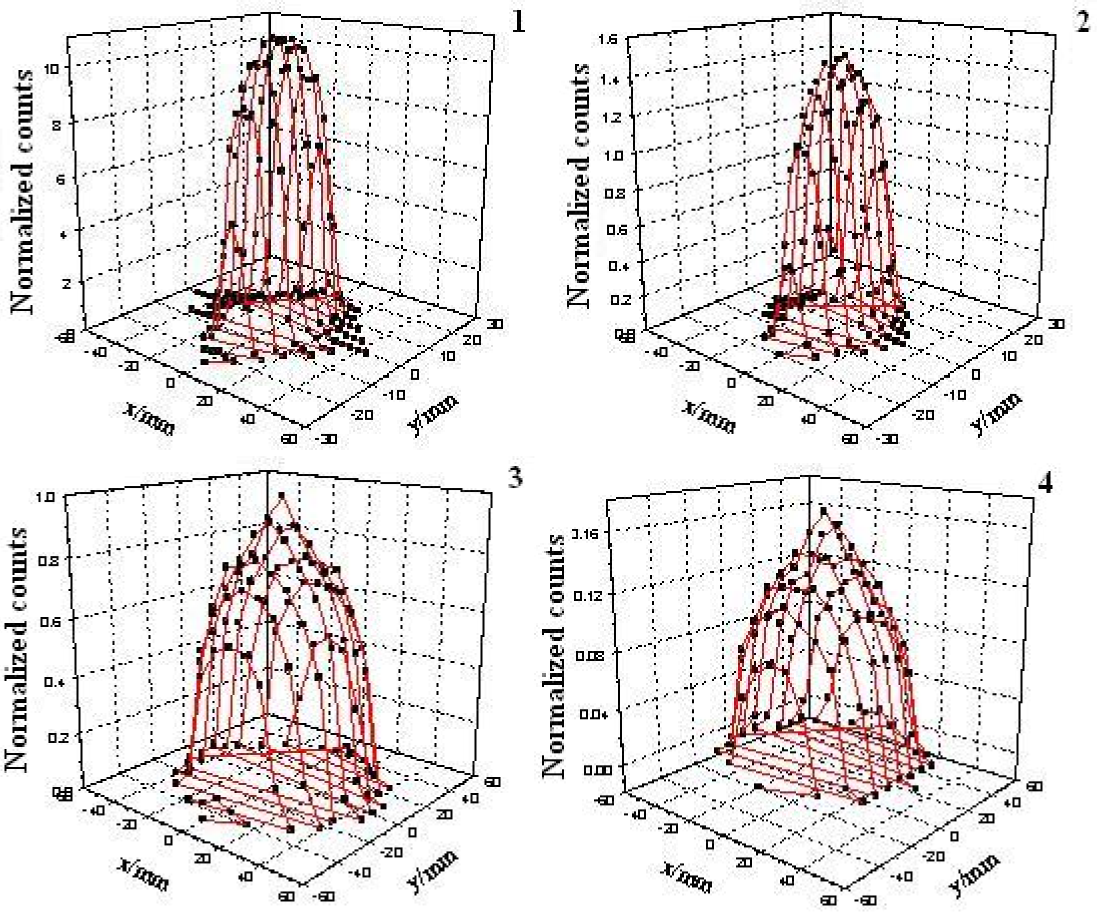

Key

1 Graph plotted with the data of the bare 200kPa ^3He counter

2 Graph plotted with the data of the bare 20kPa ^3He counter

3 Graph plotted with the data of the 200kPa ^3He counter with polythene moderator

4 Graph plotted with the data of the 20kPa ^3He counter with polythene moderator

Figure 7—Graphical representations of the data measured by the transfer instruments

Table 5—Data measured by the transfer instruments

Transfer instruments	Normalized total counts of the detector for the scanning procedure a)	Normalized counts of the detector at the reference point b)	Normalized counts of the detector with the cadmium cover at the reference point b)
Bare 200kPa ^{3}He counter	428.27183	10.66916	8.2806×10^{-4}
Bare 20kPa ^{3}He counter	52.22266	1.49696	5.6602×10^{-5}
200kPa ^{3}He counter with polythene moderator	45.42909	1.00564	3.4605×10^{-3}
20kPa ^{3}He counter with polythene moderator	7.61351	0.17491	5.0243×10^{-4}

a) The normalized total counts, i.e. N_{tot} in Equation (6), were obtained by adding up the normalized counts of the detector at each scanning point which had been corrected for dead time and had subtracted background counts from.

b) The normalized counts, i.e. $N_{(0,0)}$ and $N_{(0,0)}^{(Cd)}$ in Equation (15), were corrected for dead time and subtracted background counts from.

In order to transfer the neutron fluence without the small collimator to that with the small collimator, a ^{235}U fission ionization chamber, whose structure is described in Annex E, was used for the purpose. Figure 8 shows the pulse-height spectra of the fission chamber with regard to the two irradiation conditions. The data from the measurements of the fission chamber are listed in Table 6.

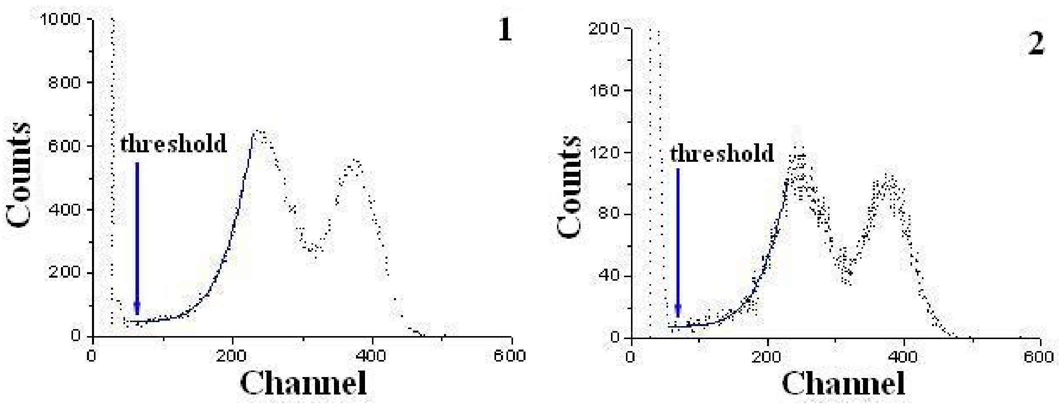

Key

1 Pulse-height spectrum of the ^{235}U fission chamber in "case 2"

2 Pulse-height spectrum of the ^{235}U fission chamber in "case 1"

Figure 8—Pulse-height spectra of the ^{235}U fission chamber

Table 6—Data from the measurements of the ^{235}U fission ionization chamber

Irradiation conditions	Real time /s	Live time /s	Counts of fission fragments above threshold	Counts of monitor
Without the small collimator	3000	2993.68	116669	745237
With the small collimator	20000	19969.74	20281	4864476

According to the comparison protocol, the response $\boldsymbol{R}_{\mathbf{ref}}$ of the transfer instrument, for a homogeneous unidirectional irradiation neutron field with a Maxwellian fluence distribution characterized by the temperature parameter $\boldsymbol{kT}$**=25.3meV**, shall be determined. The response $\boldsymbol{R}_{\mathbf{ref}}$ can be given by Equation (5):

$$R_{\mathrm{ref}} = \prod_{i=1}^{n} k_i \cdot \frac{(N/M_N - k^{(\mathrm{Cd})} N^{(\mathrm{Cd})} / M_N^{(\mathrm{Cd})})}{(\Phi / M_\Phi)} \tag{5}$$

here, k_i is correction factors, $n \geq 2$ denotes the number of k_i ; N is the counts of the transfer instrument without cadmium cover; $N^{(\mathrm{Cd})}$ is the counts of the transfer instrument with cadmium cover; M_N is the counts of monitor during the measurement of the transfer instrument without cadmium cover; $M_N^{(\mathrm{Cd})}$ is the counts of monitor during the measurement of the transfer instrument with cadmium cover; $k^{(\mathrm{Cd})}$ is the correction factor for the neutrons above the cadmium cut-off energy(0.68eV) absorbed by the cadmium cover; Φ is the measured neutron fluence below the cadmium cut-off energy; M_Φ is the counts of monitor during the measurement of the neutron fluence.

Considering a scanning procedure to be performed and the effect of the neutrons above the cadmium threshold as a correction, Equation (6) can be simply written as:

$$R_{\text{ref}} = \prod_{i=1}^{n} k_i \cdot \frac{N_{\text{tot}}}{\phi} \tag{6}$$

here, N_{tot} is the normalized total counts of the counter in a scanning procedure which had been corrected for dead time and had subtracted background counts from; ϕ is the normalized neutron fluence of the simulated broad beam radiation field below the cadmium cut-off energy at the reference point.

For the scanning procedure that simulates narrow beam radiation into broad beam radiation, ϕ can be given by Equation (7):

$$\phi = \frac{iI_1}{S} \tag{7}$$

here, i is the number of scanning points; I_1 is the normalized neutron flux below the cadmium cut-off energy at the reference point in "case 1"; S is the total scanning area, $S = i \cdot \Delta x \Delta y$, Δx is the scanning step in x direction, Δy is the scanning step in y direction.

Then, I_1 can be determined with the fission chamber by Equation (8):

$$I_1 = \phi_1 S_1 = \frac{k_{1,\text{f}} N_{1,\text{f}} F_1 S_1}{N_1 \overline{\sigma_{(\text{n,f}),1}} M_1} \tag{8}$$

here, ϕ_1 is the normalized neutron fluence below the cadmium cut-off energy at the reference point in "case 1"; S_1 is the cross-sectional area of the neutron beam at the reference point in "case 1"; $k_{1,\text{f}}$ is the correction factors of the counts of fission fragments measured in "case 1"; $N_{1,\text{f}}$ is the counts of fission fragments above discrimination threshold measured in "case 1" and corrected for dead-time; F_1 is a proportion factor of the neutron fluence below cadmium cut-off energy to the total neutron fluence in "case 1"; N_1 is the number of ^{235}U nuclei contained in the uranium sample layer in the area of S_1, $N_1 = \rho S_1 d_1$, ρ is the number density of ^{235}U nuclei in the uranium sample layer, d_1 is the mean thickness of the uranium sample layer covered by the neutron beam in "case 1"; $\overline{\sigma_{(n,f),1}}$ is the spectrum-averaged cross-section of the ^{235}U(n,f) reaction in "case 1"; M_1 is the counts of monitor during the measurement of fission chamber in "case 1".

Similarly, the normalized neutron flux below the cadmium cut-off energy at the reference point in "case 2" I_2 can be determined with the fission chamber by Equation (9):

$$I_2 = \phi_2 S_2 = \frac{k_{2,f} N_{2,f} F_2 S_2}{N_2 \overline{\sigma_{(n,f),2}} M_2} \tag{9}$$

here, ϕ_2 is the normalized neutron fluence below the cadmium cut-off energy at the reference point in "case 2"; S_2 is the area of the uranium sample layer (in "case 2", the uranium sample layer can be covered by the neutron beam); $k_{2,f}$ is the correction factors of counts of fission fragments measured in "case 2"; $N_{2,f}$ is the counts of fission fragments above discrimination threshold measured in "case 2" and corrected for dead-time; F_2 is a proportion factor of the neutron fluence below cadmium cut-off energy to the total neutron fluence in “case 2”; N_2 is the number of ^{235}U nuclei in the uranium sample layer, $N_2 = \rho S_2 d_2$, ρ is the number density of ^{235}U nuclei in the uranium sample layer, d_2 is the mean thickness of the uranium sample layer”; $\overline{\sigma_{(\mathrm{n,f}),2}}$ is the spectrum-averaged cross-section of the ^{235}U(n,f) reaction in “case 2”; M_2 is the counts of monitor during the measurement of fission chamber in “case 2”.

If the presuppositions, as (1) the neutron energy spectrum at the reference point is hardly changed by the small collimator and (2) the ^{235}U sample layer of the fission chamber presents a well uniformity, are tenable, i.e., F_1=F_2, $\overline{\sigma_{(\mathrm{n,f}),1}} = \overline{\sigma_{(\mathrm{n,f}),2}}$ and d_1=d_2, then the normalized neutron flux below the cadmium cut-off energy at the reference in “case 1” point I_1can be obtained by dividing Equation (8) by Equation (9):

$$I_1 = \phi_2 S_2 \cdot \frac{k_{1,\mathrm{f}} N_{1,\mathrm{f}} M_2}{k_{2,\mathrm{f}} N_{2,\mathrm{f}} M_1} \tag{10}$$

The demonstrations for these presuppositions are described in Annex F.

Then, the response $\boldsymbol{R}_{\mathbf{ref}}$ of the transfer instrument can be determined by Equation (11):

$$R_{\mathrm{ref}} = \prod_{i=1}^{n} k_i \cdot \frac{N_{\mathrm{tot}} \Delta x \Delta y}{I_1} = \prod_{i=1}^{n} k_i \cdot \frac{N_{\mathrm{tot}} \Delta x \Delta y}{\phi_2 S_2} \cdot \frac{k_{2,\mathrm{f}} N_{2,\mathrm{f}} M_1}{k_{1,\mathrm{f}} N_{1,\mathrm{f}} M_2} \tag{11}$$

Where the correction factor $k_{1,\mathrm{f}}$ or $k_{2,\mathrm{f}}$ shall be a product of the correction factors as follows: (ⅰ) the correction factor for the count losses of fission fragments below discrimination threshold; (ⅱ) the correction factor for the absorption of fission fragments by the ^{235}U sample layer and (iii) the correction factor for the neutron scattering and absorption resulted from the structure of the fission chamber. For the purpose of the fission chamber used in the experiment, however, only the correction factor (iii) is necessary to be considered. The correction factors $k_{1,\mathrm{f}}$ and $k_{2,\mathrm{f}}$ were calculated by the MCNP code.

Taking account of those measured results mentioned above and the demonstration of the presupposition (1), in fact, it can be demonstrated that the neutrons above the cadmium threshold in the thermal neutron field are very few and can be ignored, i.e., F_1=F_2=1.

The correction factor k_1 for the actual spectral distribution deviated from a Maxwellian distribution with the temperature parameter kT=25.3meV was calculated by Equation (12) and Equation (13):

$$k_1 = \frac{\int_0^{\infty} (\Phi_E^{(\mathrm{ref})} / \Phi^{(\mathrm{ref})}) r(E) \mathrm{d}E}{\int_0^{E_{\mathrm{Cd}}} (\Phi_E / \Phi) r(E) \mathrm{d}E} \tag{12}$$

and,

$$\frac{\Phi_E^{(\mathrm{ref})} \mathrm{d}E}{\Phi^{(\mathrm{ref})}} = (\frac{E}{kT}) \mathrm{e}^{(-E/kT)} \frac{\mathrm{d}E}{kT} \tag{13}$$

here, ($\Phi_E^{(\mathrm{ref})} / \Phi^{(\mathrm{ref})}$) is the normalized spectral fluence of a Maxwellian distribution with the temperature parameter kT=25.3meV; (Φ_E / Φ) is the actual normalized spectral fluence; $r(E)$ is the relative response of the transfer instrument.

The dead-time correction factor k_2 had been considered by Equation (14) in the data processing:

$$k_2 = \frac{1}{1 - n\tau} \tag{14}$$

here, n is the count rate of the transfer instrument; τ is the dead-time of the transfer instrument, τ=(7.2±0.9)μs.

In addition, the term of Equation (5) for the effect of the neutrons above cadmium cut-off energy is considered as a correction factor k_3 that is calculated by Equation (15):

$$k_3 = 1 - N_{(0,0)}^{(\mathrm{Cd})} / N_{(0,0)} \tag{15}$$

here, $N_{(0,0)}^{(\mathrm{Cd})}$ is the normalized counts of the counter with the cadmium cover when its sensitive center is positioned at the reference point; $N_{(0,0)}$ is the normalized counts of the counter without the cadmium cover in the same situation.

The data and results of the responses of the transfer instruments are listed in Table 7 (see next page).

Table 7—Data and results of the responses of the transfer instruments

<table>
<tr><th rowspan="4">Transfer instruments</th><th colspan="8">Parameters [a)] and values</th></tr>
<tr><td>ϕ_2 /cm^{-2}</td><td>S_2 /cm^2</td><td>$k_{1,\mathrm{f}}$</td><td>$k_{2,\mathrm{f}}$</td><td>$N_{1,\mathrm{f}}$</td><td>$N_{2,\mathrm{f}}$</td><td>M_1</td><td>M_2</td></tr>
<tr><td>4.167×10^{2} [b)]</td><td>1.7671</td><td>1.0673</td><td>1.0499</td><td>20312</td><td>116915</td><td>4864476</td><td>745237</td></tr>
<tr><td>N_{tot}</td><td colspan="2">$\Delta x\Delta y$ /cm^2</td><td colspan="2">k_1</td><td>k_3</td><td colspan="2">$\boldsymbol{R}_{\mathbf{ref}}$ **/ cm^2**</td></tr>
<tr><td>Bare 200kPa ^{3}He counter</td><td>428.27183</td><td colspan="2">0.16</td><td colspan="2">0.9476</td><td>0.9999</td><td colspan="2">**3.26**</td></tr>
<tr><td>Bare 20kPa ^{3}He counter</td><td>52.22266</td><td colspan="2">0.16</td><td colspan="2">0.9387</td><td>1.0000</td><td colspan="2">**0.394**</td></tr>
<tr><td>200kPa ^{3}He counter with polythene moderator</td><td>45.42909</td><td colspan="2">0.64</td><td colspan="2">1.0728</td><td>0.9966</td><td colspan="2">**1.56**</td></tr>
<tr><td>20kPa ^{3}He counter with polythene moderator</td><td>7.61351</td><td colspan="2">0.64</td><td colspan="2">1.0726</td><td>0.9971</td><td colspan="2">**0.262**</td></tr>
<tr><td colspan="9">a) Symbols corresponding to these parameters are indicated in the Equations from (8) to (15).
b) The result is the mean value of the normalized neutron fluence measured respectively by 2# and 3# gold foils.</td></tr>
</table>

4 Evaluation of uncertainties for calibrations of responses of transfer instruments

4.1 Mathematical model

The mathematical model for the response of the transfer instrument can be established as follows:

$$R_{\mathrm{ref}} = \prod_{i=1}^{n} k_i \cdot \frac{N_{\mathrm{tot}} \Delta x \Delta y}{\phi_2 S_2} \cdot \frac{k_{2,\mathrm{f}} N_{2,\mathrm{f}} M_1}{k_{1,\mathrm{f}} N_{1,\mathrm{f}} M_2} \tag{16}$$

and,

$$\phi_2 = \frac{k_{\varphi} k_{\mathrm{s}} A t}{N_{\mathrm{Au}} \overline{\sigma_{(\mathrm{n},\gamma)}} (1 - \mathrm{e}^{-\lambda (t_1 - t_0)}) M_{\Phi}} \tag{17}$$

here, t is the irradiation time of the gold foil (2# or 3#); M_{Φ} is the counts of monitor during the irradiation of the gold foil (2# or 3#); the meanings of other symbols is the same as that in Equation (1) and Equation (11).

4.2 Origins of uncertainties

The origins of the uncertainties for the calibration of the response of the transfer instrument are described as follows:

(a) Uncertainty due to the unevenness of the ^{235}U sample layer.

(b) Uncertainty of the activity of the “thick” gold foil (2# or 3#).

(c) Uncertainty of the spectrum-averaged cross-section of the ^{197}Au(n,γ) reaction.

(d) Uncertainty of the area of the ^{235}U sample layer.

(e) Uncertainty of the normalized total counts of the transfer instrument.

(f) Uncertainty of the normalized counts of fission fragments.

(g) Uncertainty due to the correction factors.

(h) Others described as follows:

Values of the integral quantities, such as the spectrum-averaged cross-sections of the $^{235}U(n,f)$ and $^{197}Au(n,\gamma)^{198}Au$ reactions, were found to present a tiny difference (< 0.1%) for the change of the neutron energy spectrum owing to the use of the small collimator. In addition, the uncertainty due to the discrepancy of the position of detectors was assessed to be approximately 0.07%, taking into account the result of the spatial distribution of neutron fluence in z direction.

4.3 Evaluated results of uncertainties

The evaluated results of the uncertainties for the calibrations of responses of the transfer instruments are given in Table 8 (see next page). The details are described in Annex G.

Table 8 Evaluated results of uncertainties for the calibrations of the responses of the transfer instruments

Origins of uncertainties	Relative uncertainties /%				Type of evaluation methods
	Bare 200kPa ^{3}He counter	Bare 20kPa ^{3}He counter	200kPa ^{3}He counter with polythene moderator	20kPa ^{3}He counter with polythene moderator	
Uncertainty due to the unevenness of the ^{235}U sample layer of the fission chamber	1.8	1.8	1.8	1.8	A
Uncertainty of the activity of the gold foils（2# or 3#）	0.50	0.50	0.50	0.50	B
Uncertainty of the spectrum-averaged cross section of the $^{197}Au(n,\gamma)$ reaction	0.44	0.44	0.44	0.44	B
Uncertainty of the area of the ^{235}U sample layer	0.16	0.16	0.16	0.16	B
Uncertainty of the normalized total counts of the transfer instrument	0.84	0.85	0.85	0.90	A
Uncertainty of the normalized counts of fission fragments	0.78	0.78	0.78	0.78	A
Uncertainty due to the correction factors	0.85	0.85	0.85	0.85	B
Relative Combined standard uncertainties /%	**2.4**	**2.4**	**2.4**	**2.5**	

Annex A

Basic facility

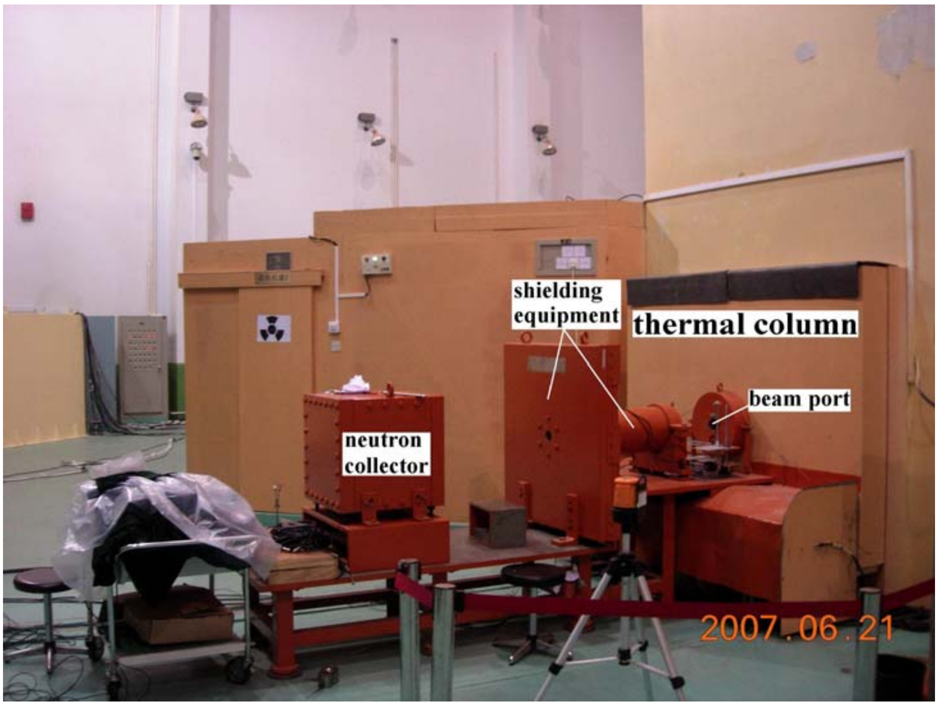

Figure A.1—Experimental hall

Fig. A.2—Scanning device

Annex B

Neutron eduction tube of thermal column

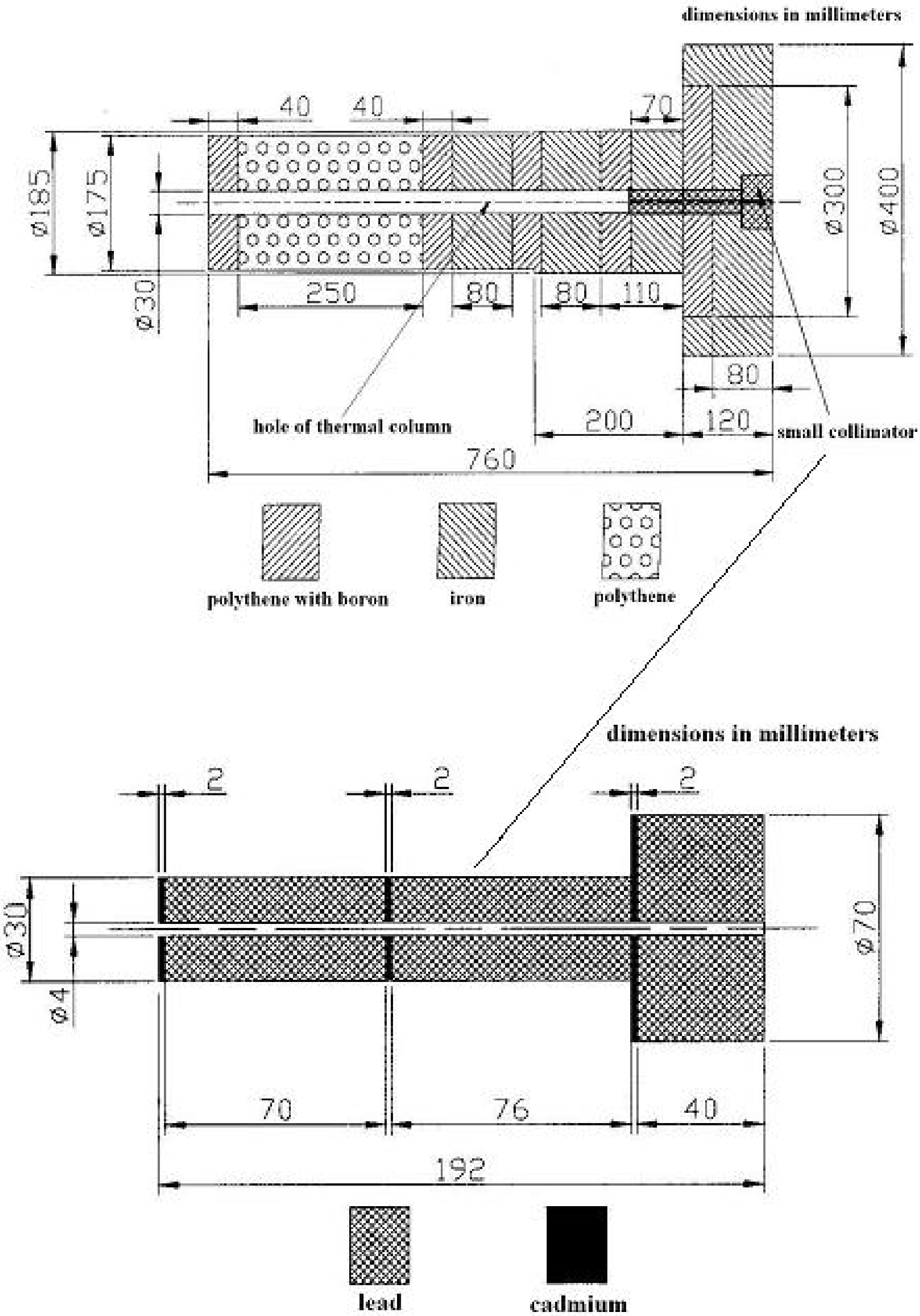

Figure B.1—Schematic diagrams of the neutron eduction tube of thermal column

Annex C
Graphical representation of relative experimental coordinates

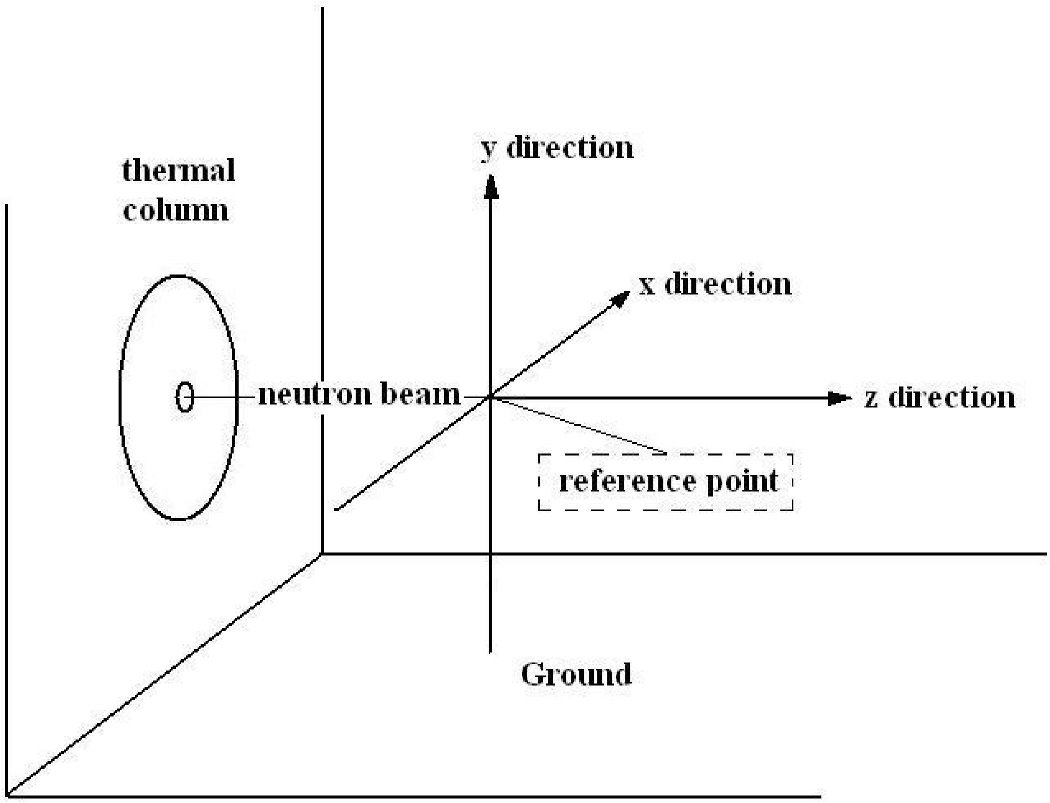

Figure C.1—schematic diagram of the relative experimental coordinates

Annex D
Measuring system for thermal neutron energy spectrum

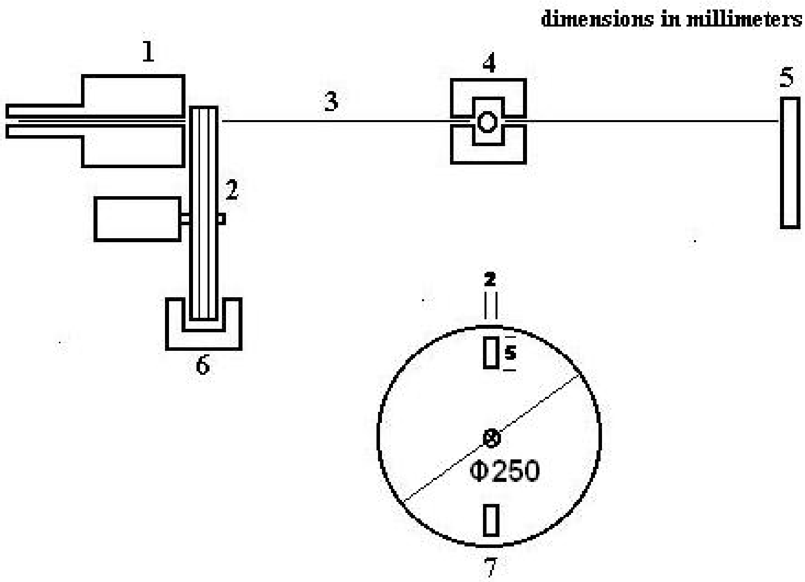

Key

1 **Small collimator**

2 **Chopper**

3 **Neutron beam**

4 **^{3}He proportional counter with a shield of polythene mixed with boron**

5 **^{3}He proportional counter used as monitor**

6 **Photoelectric system**

7 **Obverse view of the chopper**

Figure D.1—Schematic diagram of the measuring system for thermal neutron energy spectrum

Annex E

Description of structure of ^{235}U fission ionization chamber

The ^{235}U fission ionization chamber is a parallel-plate type of chamber with an outer-wall of brass. The outer-diameter of the lateral wall is 70mm and the inner-diameter is 67mm. The thickness of the bottom wall is 0.6mm. A collector of 0.5mm thick brass and a backing of 0.35mm thick stainless steel with a uranium sample layer are fixed in the chamber by a ring of 0.5mm thick aluminum and three braces. The uranium sample layer contains natural uranium of 330.6μg with 90.09% abundance of ^{235}U. The brace is assembled with a bar of teflon covered with some sleeves of teflon and those of brass. These sleeves can either insulate the collector from the wall of the fission chamber or connect the backing with the outer-wall. The distance of collector-to-backing can be adjusted conveniently by using the sleeves with different lengths. A schematic diagram of the ^{235}U fission ionization chamber is shown in Figure E.1.

While the fission chamber is used, a mixture of argon gas of 90% and methane of 10% flows through the chamber and the collector is biased with a positive voltage.

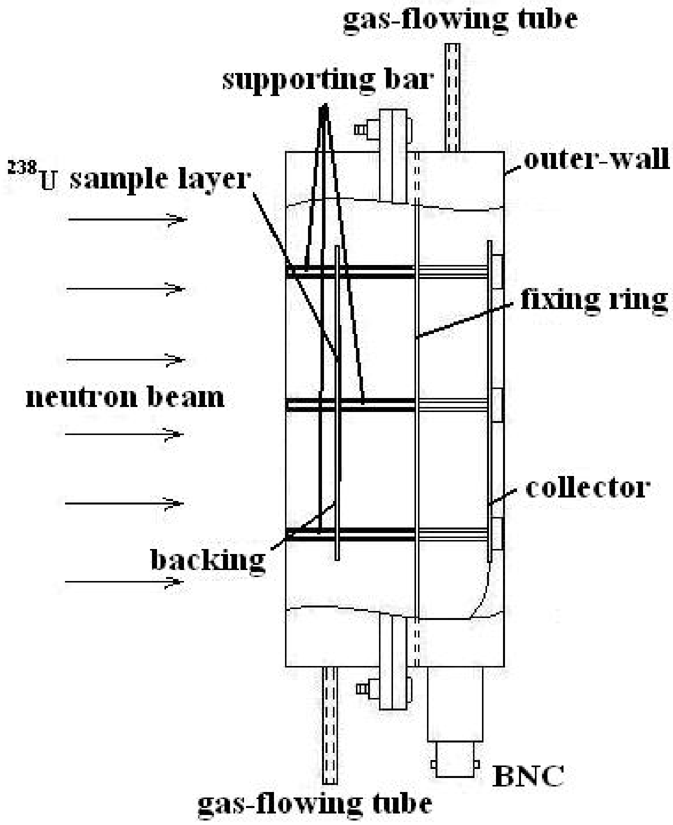

Figure E.1—Schematic diagram of the ^{235}U fission ionization chamber

Annex F

Demonstration of presuppositions

F.1 Influence of the small collimator on the neutron energy spectrum

In order to check the influence of the small collimator on the neutron energy spectrum, the MCNP code was used for a calculation. Due to a relative calculation, the initial source was described as the measured neutron energy spectrum. The neutron spectral fluence at the reference point was tallied while the small collimator is in the neutron eduction tube. The result is shown in Figure F.1.

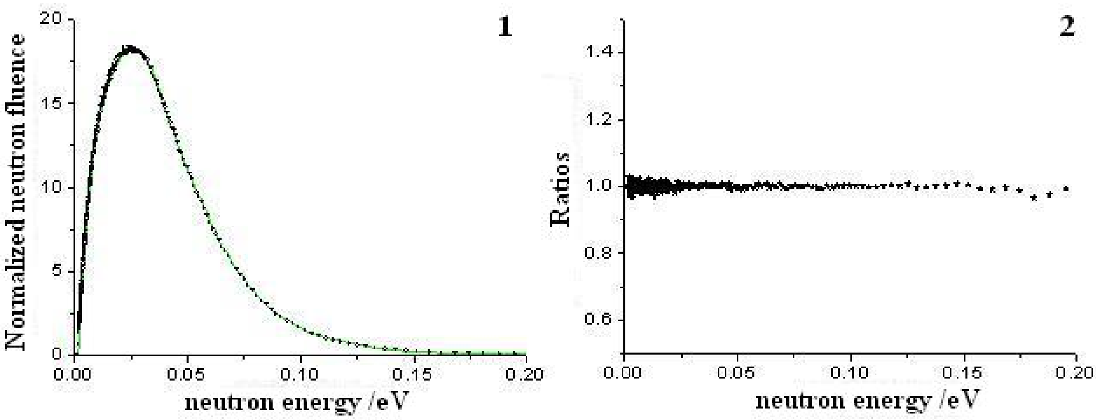

Key

1 Solid line corresponds to the initial neutron energy spectrum; Dots correspond to the calculated neutron energy spectrum

2 The ratios of the calculated spectral neutron fluence to the initial spectral neutron fluence

Figure F.1—Results calculated with the MCNP code for checking the influence of the small collimator on the neutron energy spectrum

F.2 Uniformity of the ^{235}U sample layer

The uniformity of the ^{235}U sample layer was measured with a 2π multi-wire proportional chamber. The ^{235}U sample layer was covered with an aluminum foil with a hole of 4mm in diameter. By altering the position of the hole over the ^{235}U sample layer, a group of α particle counts could be obtained. The data are listed in Table F.1.

Table F.1—Result of the measurement of the uniformity of the ^{235}U sample layer

Number of positions	Measuring time /s	α particle counts			Mean counts of α particles at each position
1	300	13331	13584	13358	13424.3
2	300	13919	13994	13905	13939.3
3	300	14348	14401	14233	14327.3
4	300	13828	13942	13864	13878.0
5	300	13875	13847	13825	13849.0
6	300	13889	13897	13732	13839.3
7	300	13941	14077	13821	13946.3
8	300	13615	13754	13542	13637.0
9	300	13669	13563	13651	13627.7
10	300	13796	13616	13624	13678.7
Value averaged over the mean counts of α particles at each position					**13814.7(1±0.018)**

Annex G
Evaluation of uncertainties for calibration of response of transfer instrument

(a) Uncertainty due to the unevenness of the ^{235}U sample layer

The uncertainty u_1 due to the unevenness of the ^{235}U sample layer can be calculated by Equation (G.1) according to the data listed in Table F.1:

$$u_1 = s(N_\alpha) / \overline{N_\alpha} = \frac{1}{\overline{N_\alpha}} \sqrt{\frac{\sum_{i=1}^{n} (N_{\alpha,i} - \overline{N_\alpha})^2}{n-1}} \tag{G.1}$$

here, $N_{\alpha,i}$ is the mean counts of α particles at each position of the ^{235}U sample layer; $\overline{N_\alpha}$ is the value averaged over the mean counts of α particles at each position of the ^{235}U sample layer.

(b) Uncertainty of the activity of the "thick" gold foil

The uncertainty u_2 of the activity of the "thick" gold foil (2# or 3#) is mainly derived from the relative deviation $s(N_\gamma)$ of the peak counts of 411keV γ rays emitted by the "thick" gold foil (the relative deviation of the peak counts of 411keV γ rays emitted by the "thin" gold foil can be ignored) and the uncertainty $u(A_t)$ of activity of the "thin" gold foil (1#). u_2 is calculated by Equation (G.2):

$$u_2 = \sqrt{s^2(N_\gamma) + u^2(A_t)} \tag{G.2}$$

here, $s(N_\gamma)$ can be obtained from the data in Table 2; $u(A_t)$ is equal to 0.3% given by the laboratory of activity measurements at CIAE.

(c) Uncertainty of the spectrum-averaged cross-section of the

^{197}Au(n,γ) reaction

The uncertainty u_3 of the spectrum-averaged cross-section of the ^{197}Au(n,γ) reaction is resulted from the energy resolution of the measured neutron energy spectrum and the evaluated uncertainty of the cross-section of the ^{197}Au(n,γ) reaction from the ENDF/B-Ⅶ database. The uncertainty u_3 is evaluated as follows:

1) The resolving energy ΔE_i at each energy of the measured neutron energy spectrum can be calculated by Equation (G.3):

$$\Delta E_i = 0.028 E_i^{3/2} (\Delta t / L) \tag{G.3}$$

here, E_i is neutron energy (eV); Δt is the resolving time (μs) of the measuring system which includes the components as follows: a) the component produced by the width of the slit of the chopper (48.5μs), b) the resolving time of electronics system (～6μs) and c) the component resulted from the error of the actual time of the neutron start signals (5.35μs).

Then, Δt can be calculated to be equal to 49.16μs; L is the distance of neutron flight (m), L = 1.3223m.

2) The cross-sections $\sigma_{(n,\gamma),\max}(E_i)$ and $\sigma_{(n,\gamma),\min}(E_i)$ of the ^{197}Au(n,γ) reaction corresponding to the energies $(E_i - \Delta E_i)$ and $(E_i + \Delta E_i)$ can be obtained by interpolating the cross-section data from the ENDF/B-Ⅶ database. Thus the standard deviation $s(\sigma_{(n,\gamma)}(E_i))$ of the cross-section of the ^{197}Au(n,γ) reaction at the energy E_i can be determined by

Equation (G.4), taking into account the evaluated uncertainty $u(\sigma_{(n,\gamma)})$ of the cross-section of the ^{197}Au(n,γ) reaction:

$$s(\sigma_{(n,\gamma)}(E_i)) = \frac{\sigma_{(n,\gamma),\max}(E_i)(1+u(\sigma_{(n,\gamma)})) - \sigma_{(n,\gamma),\min}(E_i)(1-u(\sigma_{(n,\gamma)}))}{2\sqrt{3}} \quad \text{(G.4)}$$

Where $u(\sigma_{(n,\gamma)})$ is equal to 0.14%.

Consequently, the relative uncertainty u_3 is calculated by Equation (G.5) which is deduced from Equation (2):

$$u_3 = \frac{1}{\overline{\sigma_{(n,\gamma)}}} \sqrt{\sum_{i=1}^{n} (\frac{\Phi(E_i)}{\Phi} \cdot (E_{i+1} - E_i) \cdot s(\sigma_{(n,\gamma)}(E_i))^2} \quad \text{(G.5)}$$

here, $\overline{\sigma_{(n,\gamma)}}$ is the spectrum-averaged cross-section of the ^{197}Au(n,γ) reaction; $\Phi(E_i)/\Phi$ is the normalized spectral neutron fluence; $(E_{i+1} - E_i)$ is the energy intervals of the measured neutron energy spectrum.

(d) Uncertainty of the area of the ^{235}U sample layer

The uncertainty u_4 of the area of the ^{235}U sample layer is derived from the limits of the permissible error of the vernier caliper which was used to measure the diameter of the ^{235}U sample-made pattern. The relative uncertainty u_4 can be calculated by Equation (G.6), taking into account an even distribution:

$$u_4 = 2s(d)/d = \frac{2\Delta_{\mathrm{V}}}{\sqrt{3} \cdot d} \quad \text{(G.6)}$$

here, Δ_{V} is the limits of the permissible error of the vernier caliper，Δ_{V} =±0.02mm；d is the diameter of the ^{235}Usample layer，d=15mm.

(e) Uncertainty of the normalized total counts of the transfer instrument

The uncertainty u_5 of the normalized total counts of the transfer instrument is derived from the relative statistical deviation of the total counts of the transfer instrument and the relative statistical deviation of the counts of monitor at each scanning point. Hence, the relative uncertainty u_5 can be calculated by Equation (G.7):

$$u_5 = \sqrt{\frac{1}{N'_{\mathrm{tot}}} + \frac{1}{M_{N'}}} \tag{G.7}$$

here, N'_{tot} is the total counts of the transfer instrument; $M_{N'}$ is the counts of monitor at each scanning point.

(f) Uncertainty of the normalized counts of fission fragments

The uncertainty u_6 of the normalized counts of fission fragments is derived from the relative statistical deviations of the counts of fission fragments and the relative statistical deviations of the counts of monitor in the two irradiation conditions. The relative uncertainties u_6 can be calculated by Equation (G.8):

$$u_6 = \sqrt{\frac{1}{N'_{1,\mathrm{f}}} + \frac{1}{N'_{2,\mathrm{f}}} + \frac{1}{M_1} + \frac{1}{M_2}} \tag{G.8}$$

here, $N'_{1,\mathrm{f}}$ is the counts of fission fragments above discrimination threshold in "case 1"; $N'_{2,\mathrm{f}}$ is the counts of fission fragments above discrimination threshold in "case 2"; M_1 is the counts of monitor during the measurement of the fission chamber in “case 1”; M_2 is the counts of monitor during the measurement of the fission chamber in “case 2”.

(g) Uncertainty due to the correction factors

The uncertainty u_7 due to the correction factors in Equation (16) and Equation (17) is attributed to the uncertainties of $k_{1,\mathrm{f}}$ and $k_{2,\mathrm{f}}$. The contributions of other correction factors can be ignored. The uncertainties of $k_{1,\mathrm{f}}$ and $k_{2,\mathrm{f}}$ can be resulted from the various aspects of the calculations performed with the MCNP program, such as the degree to which the initial conditions simulate the actual irradiation geometry, the uncertainties in nuclear cross-sections, the statistical uncertainties, etc., however, the overall uncertainty of $k_{1,\mathrm{f}}$ or $k_{2,\mathrm{f}}$ may be estimated to be not greater than 10%. Therefore, the uncertainties due to the correction factors $k_{1,\mathrm{f}}$ and $k_{2,\mathrm{f}}$ can be obtained to be approximately 0.68% and 0.50% respectively, considering the magnitude of the correction factors. And then the relative uncertainty u_6 can be calculated by Equation (G.9) to be approximately 0.85%.

$$u_7 = \sqrt{u^2(k_{1,\mathrm{f}}) + u^2(k_{2,\mathrm{f}})} \tag{G.9}$$

here, $u(k_{1,\mathrm{f}})$ is the relative uncertainty of the correction factor $k_{1,\mathrm{f}}$; $u(k_{2,\mathrm{f}})$ is the relative uncertainty of the correction factor $k_{2,\mathrm{f}}$.

Conclusively, the standard uncertainty $u(R_{\mathrm{ref}})$ of the response of the transfer instrument is combined with the uncertainties analyzed above:

$$u(R_{\mathrm{ref}}) = \sqrt{u_1^2 + u_2^2 + u_3^2 + u_4^2 + u_5^2 + u_6^2 + u_7^2} \tag{G.10}$$

Report on measurements at the National Metrology Institute of Japan for the CCRI(III)-K8 key comparison

1. Introduction

The National Metrology Institute of Japan (NMIJ) is the first participant of the CCRI(III)-K8 key comparison for thermal neutron fluence measurements. Measurements were made with transfer instruments in a standard thermal neutron field from November to December 2006. The results are summarized in this report.

2. Calibration facility and characterization methods of the neutron field

The facility has a graphite pile which is a rectangular prism, 230 cm wide, 190 cm deep and 190 cm high, consisting of graphite blocks stacked on a base iron board on a concrete floor. It has a vertical guide hole from the top to the center for mounting radioactive neutron sources. The neutrons from the sources are moderated and thermalized inside the graphite pile. A standard thermal neutron field was established by placing a 148 GBq Am-Be source at the center of the graphite pile [1].

The graphite pile also contains structures for embedding small samples such as activation foils in addition to several guide holes for inserting small neutron detectors. Some of the graphite blocks can be withdrawn to increase the internal space. Bulky neutron detectors such as neutron survey meters are normally positioned outside the pile.

The thermal neutron fluence rate is determined by gold activation using the cadmium difference method. Normally, gold foils with diameters of 20 mm, placed in aluminum or cadmium covers with thicknesses of 1 mm, are used. The induced activity in the irradiated gold foil is determined by counting gamma rays (412 keV) using a well-type NaI(Tl) scintillation detector with a crystal 12.7 cm in diameter and 12.7 cm in length and a well 2.8 cm in diameter and 5.1 cm in depth.

The detection efficiency ε of the NaI detector is calibrated using irradiated gold foils for which the induced activity has been determined by absolute measurements using $4\pi\beta$–γ coincidence counting equipment [2] to count beta rays (maximum energy of 960 keV) and gamma rays (412 keV) [3]. The $4\pi\beta$–γ equipment is fully simulated with the EGS5 code [4] to correct for overcounting in the beta detectors due mainly to internal conversion electrons and gamma rays.

Neutron transport in the graphite pile is simulated using the MCNPX code [5] to obtain the coefficient used to convert the measured saturated activity to the thermal neutron fluence rate. In the simulation, the Am-Be source generates neutrons with the energy distribution recommended by the International Organization for Standardization (ISO) [6]. The MCNPX calculation also yields the spectral neutron fluence, which is provided to customers when requested.

3. Spectral neutron fluence rate, total neutron fluence rate and traceability to primary national standards

A graphite block was removed from the pile to allow transfer instruments to be irradiated at a distance of 90 cm from the source as shown in Figure 1. All transfer instruments were positioned so that the centers of their SP9 counters exactly coincided. Two gold foils were prepared, 25 μm thick and 20 mm in diameter, in 1-mm-thick aluminum and cadmium cases, respectively, and were irradiated separately at the same position as the center of the SP9 counter. After irradiation, the foils were removed from their cases and set in the well-type NaI detector to determine the count rate for gamma rays under the saturated condition. The difference in the saturated count rate between the aluminum and cadmium cases yielded the net saturated count rate c due to activation by only those neutrons with energies below 0.68 eV. The net saturated count rate c was converted to the net saturated activity ρ using the detection efficiency ε of the well-type NaI detector. This was converted using the coefficient η obtained by the MCNPX calculation to the net neutron fluence rate $\phi_{\mathrm{Au}}^{\mathrm{org}}$ below 0.68 eV originally present in the void space corresponding to the gold foil under irradiation.

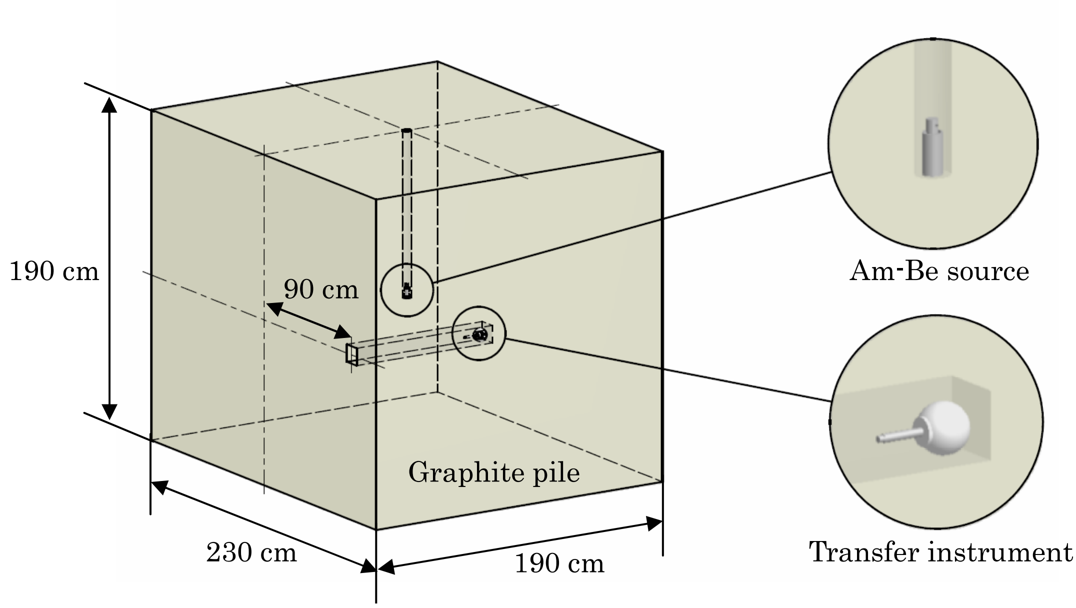

Figure 1: Irradiation setup for transfer instruments in the graphite pile.

The net original neutron fluence rate $\phi_{\mathrm{Au}}^{\mathrm{org}}$ was found to be 1.25×10^3 cm^{-2}s^{-1}. It should be noted that the effective neutron field that neutron detectors actually sense can differ slightly from that shown here, since the presence of the detector itself can disturb the surrounding field.

Figure 2 shows the spectral neutron fluence rate originally present in the void space calculated using the MCNPX code. For neutron spectral fluence distributions in the thermal and slowing down regions, the formula,

$$\phi(E) = \phi_{\mathrm{t}} \frac{E}{(kT)^2} \exp\left(-\frac{E}{kT}\right) + \phi_{\mathrm{n}} \frac{\Delta}{E}$$

has been widely used where T, ϕ_{t}, ϕ_{n} and Δ respectively represent the neutron temperature, the thermal neutron fluence rate, the nonthermal neutron fluence rate per unit lethargy and the joining function [7]. The neutron spectral fluence distribution shown in Figure 2 was fitted using this formula with T = 304 K (kT = 26.2 meV), ϕ_{t} = 1.25×10^3 cm^{-2}s^{-1} and ϕ_{n} = 2.16 cm^{-2}s^{-1}.

The primary standard instrument of the thermal neutron fluence rate standard at NMIJ is the 4πβ–γ coincidence counting equipment, which is used for absolute measurement of the induced activity in gold foils irradiated in the standard thermal neutron field. This equipment also acts as the primary standard instrument of the radioactivity standard at NMIJ.

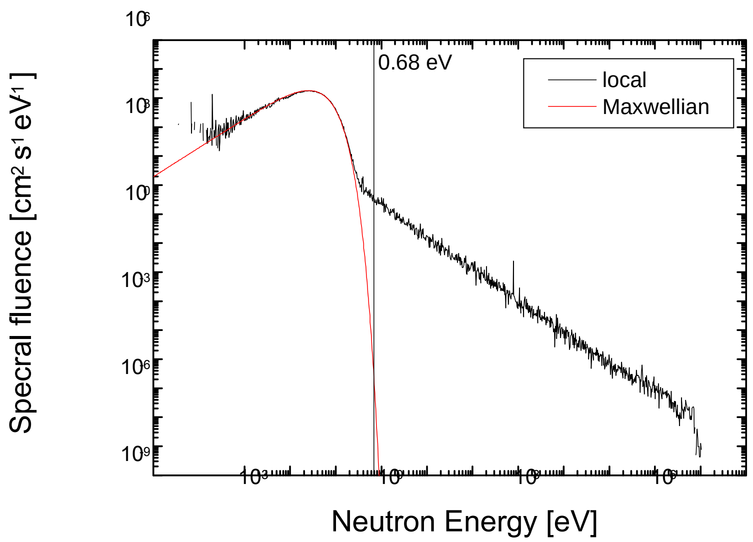

Figure 2: Spectral neutron fluence rate originally present at the measurement location in the local neutron field calculated with the MCNPX code. A Maxwellian spectral distribution with a temperature parameter of 25.3 meV is also shown for comparison.

4. Measurements carried out with the transfer instruments

Each transfer instrument was connected to the AIOSAP module and operated as directed in the protocol. The unipolar signals from the AIOSAP module were fed to a multichannel analyzer (AMPTEK MCA8000A) and processed to obtain pulse-height spectra. The pulse-height spectra of the transfer instruments are shown for 20 kPa in Figure 3 and for 200 kPa in Figure 4. Each figure includes a vertical line at 15 % and 50 % of the pulse height of the main peak. It can be seen that the 15 % threshold

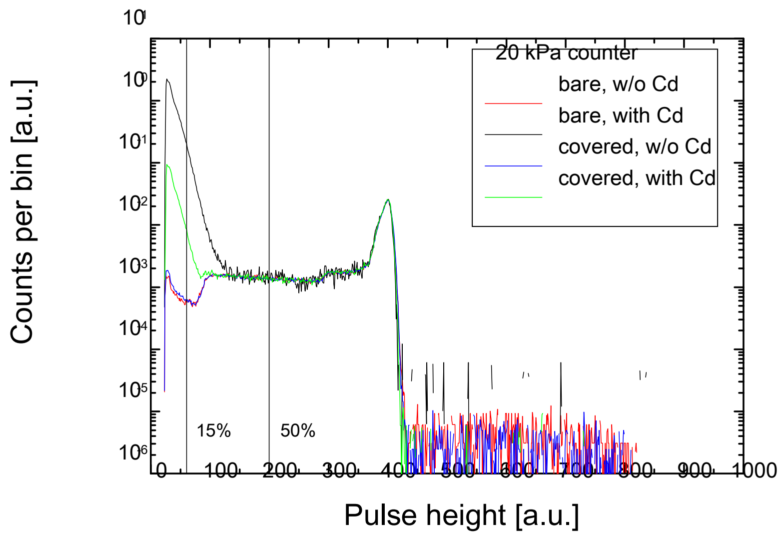

Figure 3: Pulse-height spectra of the transfer instruments with a nominal ^{3}He pressure of 20 kPa.

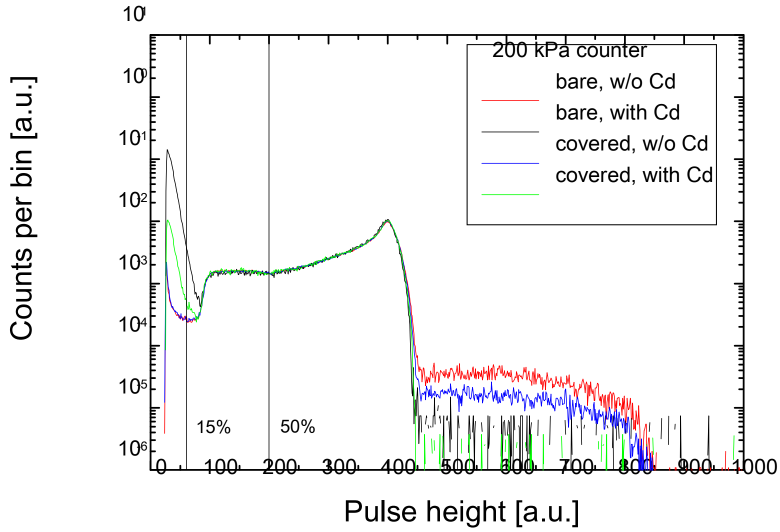

Figure 4: Pulse-height spectra of the transfer instruments with a nominal ^{3}He pressure of 200 kPa.

succeeds in discriminating events induced by photons or electronic noise from those caused by the ^{3}He(n,p)^{3}H reaction for the transfer instruments without cadmium shielding but fails for those with cadmium shielding. It was therefore decided not to use the output pulses from the discriminator D1 and instead to take the summation of counts above the 15 % threshold in the pulse-height spectra to obtain the reading N^{0} for the case without cadmium shielding. To obtain the value N^{Cd} for the case with cadmium shielding, counts above 50 % were summed and then multiplied by the ratio of the no-shielding count above 15 % to that above 50 %. The multichannel analyzer provides the real time and the live time during data acquisition. In this analysis, the former was regarded as the reading of the neutron fluence monitor. Dead time losses were considered by using the live time to convert the counts into the count rates.

5. Evaluation of the response of the transfer instruments

The response R_{local} was first determined for each transfer instrument without cadmium shielding for neutrons with energies below 0.68 eV at the measurement position, which was defined by the ratio between n and $\phi_{\mathrm{TI}}^{\mathrm{eff}}$ where $\phi_{\mathrm{TI}}^{\mathrm{eff}}$ represents the net effective neutron fluence rate sensed by the transfer instrument below 0.68 eV and n is the net count rate of the transfer instrument under the irradiation of $\phi_{\mathrm{TI}}^{\mathrm{eff}}$.

Transfer instruments were embedded in the MCNPX calculations based on the configuration shown in reference [8]. The ^{3}He pressures in the SP9 counter were adjusted so that the calculations and the measurements agreed with regard to the ratio of the count rate of the transfer instruments to the saturated activity in the gold foil. The difference between the actual cadmium cut off and the present nominal threshold energy of 0.68 eV was taken into account in addition to the attenuation of neutrons with energies above 0.68 eV in the cadmium shield, and the total count rate for each transfer instrument with cadmium shielding was converted into the net count rate for the transfer instrument without cadmium shielding due to neutrons above 0.68 eV, which was subsequently subtracted from the total count rate of the transfer instrument without cadmium shielding to obtain n.

The net original neutron fluence rate for each transfer instrument differed slightly from that for the gold foil since an intensity gradient was present in the fluence distribution of the local neutron field. Since transfer instruments absorbed neutrons, local dips were formed in the neutron field. We converted $\phi_{\mathrm{Au}}^{\mathrm{org}}$ into $\phi_{\mathrm{TI}}^{\mathrm{eff}}$ by taking into account all of these factors in the MCNPX calculation.

Finally we converted R_{local} into the response R_{ref} corresponding to the reference condition specified in the protocol, in which neutrons are irradiated homogeneously and

Table 1: Summary of the values of R_{ref} with standard uncertainties with a coverage factor of 1 obtained for all transfer instruments.

Detector	R_{ref} [cm^2]	Uncertainty [%]
20 kPa, bare	0.3703	1.4
200 kPa, bare	3.070	1.8
20 kPa, covered	0.2242	2.1
200 kPa, covered	1.355	2.3

unidirectionally with a Maxwellian spectral distribution and a temperature parameter kT = 25.3 meV. The local neutron field was almost omnidirectional with a spectral distribution (see Figure 2) only slightly different from the reference condition and this was taken into account in the MCNPX calculation in the conversion process. Table 1 summarizes the values of R_{ref} and their standard uncertainties with a coverage factor of 1 obtained for all transfer instruments.

6. Evaluation of the uncertainty budgets

The uncertainty budgets of R_{ref}, R_{local}, n, $\phi_{\mathrm{Tl}}^{\mathrm{eff}}$ are summarized for the 20 kPa and 200 kPa bare counters in Appendices 2 and 3 respectively and for the 20 kPa and 200 kPa counters covered with a polyethylene sphere in Appendices 4 and 5 respectively. The uncertainty budgets of $\phi_{\mathrm{Au}}^{\mathrm{org}}$, ρ, c and ε are summarized in Appendix 6. All uncertainties are specified as standard uncertainties with a coverage factor of 1. The symbols used in the uncertainty budgets are listed in the nomenclature in Appendix 1.

References

[1] H. Harano, T. Matsumoto, T. Shimoyama, Y. Sato, A. Uritani, Y. Hino, K. Kudo, T. Michikawa, "Convenient Method of Relative Calibration of the Neutron Source Emission Rate Between Different Source Types," IEEE Transactions on Nuclear Science, **53**, 1413-1417 (2006).

[2] "Particle Counting in Radioactivity Measurements," ICRU 52 (1994).

[3] E. Schönfeld and R. Dersch, "Table of Radionuclides," Monographile BIPM-5, **2**, 121-128 (2004).

[4] H. Hirayama, Y. Namito, A. F. Bielajew, S. J. Wilderman, W.R. Nelson, "The EGS5 Code System," SLAC-R-730 (2005).

[5] D. B. Pelowitz, “MCNPX user’s manual version 2.5.0,” Los Alamos National Laboratory, LA-CP-05-0369 (2005).

[6] “Reference Neutron Radiations Part1: Characteristics and Methods of Production,” ISO 8529-1 (2001).

[7] K. H. Beckurtz and K. Wirtz, “Neutron Physics,” Springer-Verlag Berlin, Gottingen, Heidelberg, New York (1964).

[8] B. Wiegel, A. V. Alevra, B. R. L. Siebert, “Calculations of the Response Functions of Bonner Spheres with a Spherical ^{3}He Proportional Counter Using a Realistic Detector Model,” PTB-N-21, Braunschweig (1994).

Appendix 1: Nomenclature of the symbols used in uncertainty budgets.

$$R_{\mathrm{ref}} = k_{\mathrm{spec}} k_{\mathrm{dir}} R_{\mathrm{local}} \tag{1}$$

$$R_{\mathrm{local}} = \frac{n}{\phi_{\mathrm{TI}}^{\mathrm{eff}}} \tag{2}$$

$$n = \frac{\nu_{\mathrm{DT}}^{0} \nu_{\delta}^{0} \nu_{\mathrm{ROI}}^{0} N^{0}}{t_{\mathrm{R}}^{0}} - \frac{\nu_{\mathrm{DT}}^{\mathrm{Cd}} \nu_{\mathrm{AmBe}}^{\mathrm{Cd}} \nu_{\mathrm{abs}}^{\mathrm{Cd}} \nu_{0.68}^{\mathrm{Cd}} \nu_{\delta}^{\mathrm{Cd}} \nu_{\mathrm{ROI}}^{\mathrm{Cd}} \nu_{15/50}^{\mathrm{Cd}} N^{\mathrm{Cd}}}{t_{\mathrm{R}}^{\mathrm{Cd}}} \tag{3}$$

$$\phi_{\mathrm{TI}}^{\mathrm{eff}} = f_{\mathrm{AmBe}} f_{\mathrm{eff/org}} f_{\mathrm{TI/Au}} \phi_{\mathrm{Au}}^{\mathrm{org}} \tag{4}$$

$$\phi_{\mathrm{Au}}^{\mathrm{org}} = \eta \rho \tag{5}$$

$$\rho = \frac{c}{\varepsilon} \tag{6}$$

$$c = \frac{\chi_{25,\mathrm{GP}}^{\mathrm{Al}} \chi_{\delta,\mathrm{NaI}}^{\mathrm{Al}} \chi_{\delta,\mathrm{GP}}^{\mathrm{Al}} \chi_{\infty}^{\mathrm{Al}} c^{\mathrm{Al}}}{\chi_{25,\mathrm{NaI}}^{\mathrm{Al}}} - \frac{\chi_{\mathrm{AmBe}}^{\mathrm{Cd}} \chi_{\mathrm{abs}}^{\mathrm{Cd}} \chi_{0.68}^{\mathrm{Cd}} \chi_{25,\mathrm{GP}}^{\mathrm{Cd}} \chi_{\delta,\mathrm{NaI}}^{\mathrm{Cd}} \chi_{\delta,\mathrm{GP}}^{\mathrm{Cd}} \chi_{\infty}^{\mathrm{Cd}} c^{\mathrm{Cd}}}{\chi_{25,\mathrm{NaI}}^{\mathrm{Al}}} \tag{7}$$

$$\varepsilon = \frac{e_{25} e_{\delta,\mathrm{NaI}} c_{\mathrm{NaI}} (1+K)}{e_{\delta,4\pi\beta\gamma} A} \tag{8}$$

Quantity	Unit	Definition
R_{ref}	cm^{2}	Response of each transfer instrument without cadmium shielding under the reference condition.
k_{spec}	-	Conversion factor for the difference in the spectral distribution between the local and reference conditions.
k_{dir}	-	Conversion factor for the difference in the irradiating direction between the local and reference conditions.
R_{local}	cm^{2}	Response of each transfer instrument without cadmium shielding under the irradiation below 0.68 eV in the local neutron field.
n	s^{-1}	Count rate of each transfer instrument without cadmium shielding under the irradiation below 0.68 eV in the local neutron field.
$\phi_{\mathrm{TI}}^{\mathrm{eff}}$	cm^{-2}s^{-1}	Effective neutron fluence rate sensed by each transfer instrument without cadmium shielding below 0.68 eV in the local neutron field.

v_{DT}^{0}	-	Dead time correction factor for each transfer instrument without cadmium shielding.
v_{δ}^{0}	-	Correction factor for deviation in positioning each transfer instrument without cadmium shielding in the graphite pile.
v_{ROI}^{0}	-	Correction factor for deviation in setting the region of interest above the 15 % threshold in the pulse-height spectrum of each transfer instrument without cadmium shielding.
N^{0}	-	Reading of each transfer instrument without cadmium shielding obtained by summing the counts above the 15 % threshold in the pulse-height spectra.
t_{R}^{0}	s	Real time of measurement with each transfer instrument without cadmium shielding.
$v_{\mathrm{DT}}^{\mathrm{Cd}}$	-	Dead time correction factor for each transfer instrument with cadmium shielding.
$v_{\mathrm{AmBe}}^{\mathrm{Cd}}$	-	Decay correction factor for the Am-Be source.
$v_{\mathrm{abs}}^{\mathrm{Cd}}$	-	Correction factor for the attenuation of neutrons above 0.68 eV in the cadmium shield.
$v_{0.68}^{\mathrm{Cd}}$	-	Correction factor for the difference between the actual cadmium cut off and the present nominal threshold energy 0.68 eV.
v_{δ}^{Cd}	-	Correction factor for deviation in positioning each transfer instrument with cadmium shielding in the graphite pile.
$v_{\mathrm{ROI}}^{\mathrm{Cd}}$	-	Correction factor for deviation in setting the region of interest above the 50 % threshold in the pulse-height spectrum of each transfer instrument with cadmium shielding.
$v_{15/50}^{\mathrm{Cd}}$	-	Ratio of the fraction between above the 15 % and 50 % thresholds in the pulse-height spectrum of each transfer instrument without cadmium shielding.
N^{Cd}	-	Reading of each transfer instrument with cadmium shielding obtained by summing the counts above the 50 % threshold in the pulse-height spectra.
$t_{\mathrm{R}}^{\mathrm{Cd}}$	s	Real time of measurement with each transfer instrument with cadmium shielding.
f_{AmBe}	-	Decay correction factor for the Am-Be source.

$f_{\mathrm{eff/org}}$	-	Conversion factor between the original and effective neutron fluence rate below 0.68 eV in the local neutron field for each transfer instrument without cadmium shielding allowing for the dip in the fluence distribution formed by the absorption.
$f_{\mathrm{TI/Au}}$	-	Conversion factor of the original neutron fluence rate below 0.68 eV in the local neutron field for the gold foil to that for each transfer instrument without cadmium shielding allowing for the intensity gradient in the fluence distribution.
$\phi_{\mathrm{Au}}^{\mathrm{org}}$	cm^{-2}s^{-1}	Original neutron fluence rate below 0.68 eV in the local neutron field for the gold foil.
η	cm^{-2}	Original neutron fluence rate below 0.68 eV for the gold foil required to induce unit saturated activity in the gold foil in the local neutron field.
ρ	s^{-1}	Saturated activity in the gold foil induced by neutrons below 0.68 eV in the local neutron field.
c	s^{-1}	Count rate of the well-type NaI detector for the saturated activity in the 25 μm gold foil irradiated in the aluminum case with neutrons below 0.68 eV in the local neutron field.
ε		Detection efficiency of the well-type NaI detector for the induced activity in the 25 μm gold foil.
$\chi_{25,\mathrm{GP}}^{\mathrm{Al}}$	-	Correction factor for the induced activity in the gold foil irradiated in the aluminum case in the local neutron field allowing for the deviation of the actual gold foil thickness from 25 μm.
$\chi_{\delta,\mathrm{NaI}}^{\mathrm{Al}}$	-	Correction factor for deviation in positioning the gold foil in the well-type NaI detector after irradiation in the aluminum case.
$\chi_{\delta,\mathrm{GP}}^{\mathrm{Al}}$	-	Correction factor for deviation in positioning the gold foil in the aluminum case in the graphite pile.
$\chi_{\infty}^{\mathrm{Al}}$	-	Conversion factor of the count rate of the well-type NaI detector for the activity in the gold foil irradiated in the aluminum case expected at the end of irradiation into the saturated value.
c^{Al}	s^{-1}	Count rate of the well-type NaI detector for the activity in the gold foil irradiated in the aluminum case in the local neutron field expected at the end of irradiation.

$\chi_{25,\mathrm{NaI}}^{\mathrm{Al}}$	-	Correction factor for the detection efficiency of the well-type NaI detector allowing for the deviation of the actual thickness of the gold foil irradiated in the aluminum case from 25 μm.
$\chi_{\mathrm{AmBe}}^{\mathrm{Cd}}$	-	Decay correction factor for the Am-Be source.
$\chi_{\mathrm{abs}}^{\mathrm{Cd}}$	-	Correction factor for the attenuation of neutrons above 0.68 eV in the cadmium case.
$\chi_{0.68}^{\mathrm{Cd}}$	-	Correction factor for the difference between the actual cadmium cut off and the present nominal threshold energy 0.68 eV.
$\chi_{25,\mathrm{GP}}^{\mathrm{Cd}}$	-	Correction factor for the induced activity in the gold foil irradiated in the cadmium case in the local neutron field allowing for the deviation of the actual gold foil thickness from 25 μm.
$\chi_{\delta,\mathrm{NaI}}^{\mathrm{Cd}}$	-	Correction factor for deviation in positioning the gold foil in the well-type NaI detector after irradiation in the cadmium case.
$\chi_{\delta,\mathrm{GP}}^{\mathrm{Cd}}$	-	Correction factor for deviation in positioning the gold foil in the cadmium case in the graphite pile.
$\chi_{\infty}^{\mathrm{Cd}}$	-	Conversion factor of the count rate of the well-type NaI detector for the activity in the gold foil irradiated in the cadmium case expected at the end of irradiation into the saturated value.
c^{Cd}	s^{-1}	Count rate of the well-type NaI detector for the activity in the gold foil irradiated in the cadmium case in the local neutron field expected at the end of irradiation.
$\chi_{25,\mathrm{NaI}}^{\mathrm{Cd}}$	-	Correction factor for the detection efficiency of the well-type NaI detector allowing for the deviation of the actual thickness of the gold foil irradiated in the cadmium case from 25 μm.
e_{25}	-	Correction factor for the detection efficiency of the well-type NaI detector allowing for the deviation of the actual thickness of the reference gold foil from 25 μm.
$e_{\delta,\mathrm{NaI}}$	-	Correction factor for deviation in positioning the reference gold foil in the well-type NaI detector.
c_{NaI}	s^{-1}	Count rate of the well-type NaI detector for the activity in the reference gold foil expected at the end of irradiation.
K	-	Correction factor for overcounting in the beta detectors of the

		$4\pi\beta-\gamma$ coincidence counting equipment mainly ascribed to internal conversion electrons and gamma rays.
$e_{\delta,4\pi\beta\gamma}$	-	Correction factor for deviation in positioning the reference gold foil in the $4\pi\beta-\gamma$ coincidence counting equipment.
A	s^{-1}	Apparent activity in the reference gold foil measured with the $4\pi\beta-\gamma$ coincidence counting equipment expected at the end of irradiation.

Appendix 2: Uncertainty budgets for the 20 kPa bare counter.

$$R_{\mathrm{ref}} = k_{\mathrm{spec}} k_{\mathrm{dir}} R_{\mathrm{local}}$$

Quantity	Unit	x_i	$u(x_i)$	c_i	$u_i(y)$	$u_i(y)/y$
k_{spec}	-	1.0155	0.0007	3.647E-01	2.461E-04	0.07 %
k_{dir}	-	1.0311	0.0062	3.592E-01	2.235E-03	0.60 %
R_{local}	cm^2	0.35368	0.00446	1.047E+00	4.670E-03	1.26 %
R_{ref}	cm^2	0.37034			0.00518	1.40 %

$$R_{\mathrm{local}} = \frac{n}{\phi_{\mathrm{TI}}^{\mathrm{eff}}}$$

Quantity	Unit	x_i	$u(x_i)$	c_i	$u_i(y)$	$u_i(y)/y$
n	s^{-1}	440.13	2.40	8.036E-04	1.925E-03	0.54 %
$\phi_{\mathrm{TI}}^{\mathrm{eff}}$	$cm^{-2}s^{-1}$	1244.4	14.2	2.842E-04	4.023E-03	1.14 %
R_{local}	cm^2	0.35368			0.00446	1.26 %

$$n = \frac{\nu_{\mathrm{DT}}^{0}\nu_{\delta}^{0}\nu_{\mathrm{ROI}}^{0}N^{0}}{t_{\mathrm{R}}^{0}} - \frac{\nu_{\mathrm{DT}}^{\mathrm{Cd}}\nu_{\mathrm{AmBe}}^{\mathrm{Cd}}\nu_{\mathrm{abs}}^{\mathrm{Cd}}\nu_{0.68}^{\mathrm{Cd}}\nu_{\delta}^{\mathrm{Cd}}\nu_{\mathrm{ROI}}^{\mathrm{Cd}}\nu_{15/50}^{\mathrm{Cd}}N^{\mathrm{Cd}}}{t_{\mathrm{R}}^{\mathrm{Cd}}}$$

Quantity	Unit	x_i	$u(x_i)$	c_i	$u_i(y)$	$u_i(y)/y$
ν_{DT}^{0}	-	1.0047	0.0007	4.384E+02	2.896E-01	0.07 %
ν_{δ}^{0}	-	1.0000	0.0050	4.404E+02	2.202E+00	0.50 %
ν_{ROI}^{0}	-	1.0000	0.0006	4.404E+02	2.643E-01	0.06 %
N^{0}	-	264260	514	1.667E-03	8.568E-01	0.19 %
t_{R}^{0}	s	602.80	0.01	7.306E-01	7.306E-03	0.00 %
$\nu_{\mathrm{DT}}^{\mathrm{Cd}}$	-	1.0001	0.0000	3.025E-01	1.329E-07	0.00 %
$\nu_{\mathrm{AmBe}}^{\mathrm{Cd}}$	-	1.0000	0.0000	3.025E-01	1.537E-10	0.00 %
$\nu_{\mathrm{abs}}^{\mathrm{Cd}}$	-	1.0626	0.0188	2.847E-01	5.343E-03	0.00 %
$\nu_{0.68}^{\mathrm{Cd}}$	-	0.7959	0.0612	3.800E-01	2.326E-02	0.01 %
$\nu_{\delta}^{\mathrm{Cd}}$	-	1.0000	0.0050	3.025E-01	1.512E-03	0.00 %
$\nu_{\mathrm{ROI}}^{\mathrm{Cd}}$	-	1.0000	0.0006	3.025E-01	1.815E-04	0.00 %
$\nu_{15/50}^{\mathrm{Cd}}$	-	1.2210	0.0100	2.477E-01	2.477E-03	0.00 %
N^{Cd}	-	10545	103	2.868E-05	2.946E-03	0.00 %
$t_{\mathrm{R}}^{\mathrm{Cd}}$	s	36002.52	0.01	8.402E-06	8.402E-08	0.00 %
n	s^{-1}	440.13			2.40	0.54 %

$$\phi_{\mathrm{TI}}^{\mathrm{eff}} = f_{\mathrm{AmBe}}\, f_{\mathrm{eff/org}}\, f_{\mathrm{TI/Au}}\, \phi_{\mathrm{Au}}^{\mathrm{org}}$$

Quantity	Unit	x_i	$u(x_i)$	c_i	$u_i(y)$	$u_i(y)/y$
f_{AmBe}	-	1.0040	0.0000	1.239E+03	6.324E-07	0.00 %
$f_{\mathrm{eff/org}}$	-	0.9850	0.0045	1.263E+03	5.692E+00	0.46 %
$f_{\mathrm{TI/Au}}$	-	1.0035	0.0010	1.240E+03	1.292E+00	0.10 %
$\phi_{\mathrm{Au}}^{\mathrm{org}}$	$cm^{-2}s^{-1}$	1254.0	13.0	9.924E-01	1.290E+01	1.04 %
$\phi_{\mathrm{TI}}^{\mathrm{eff}}$	$cm^{-2}s^{-1}$	1244.4			14.2	1.14 %

Appendix 3: Uncertainty budgets for the 200 kPa bare counter.

$$R_{\mathrm{ref}} = k_{\mathrm{spec}} k_{\mathrm{dir}} R_{\mathrm{local}}$$

Quantity	Unit	x_i	$u(x_i)$	c_i	$u_i(y)$	$u_i(y)/y$
k_{spec}	-	1.0137	0.0014	3.028E+00	4.278E-03	0.14 %
k_{dir}	-	1.0326	0.0065	2.973E+00	1.941E-02	0.63 %
R_{local}	cm^2	2.9325	0.0503	1.047E+00	5.270E-02	1.72 %
R_{ref}	cm^2	3.0697			0.0563	1.83 %

$$R_{\mathrm{local}} = \frac{n}{\phi_{\mathrm{TI}}^{\mathrm{eff}}}$$

Quantity	Unit	x_i	$u(x_i)$	c_i	$u_i(y)$	$u_i(y)/y$
n	s^{-1}	3567.6	26.0	8.220E-04	2.133E-02	0.73 %
$\phi_{\mathrm{TI}}^{\mathrm{eff}}$	$cm^{-2}s^{-1}$	1216.6	18.9	2.410E-03	4.560E-02	1.56 %
R_{local}	cm^2	2.9325			0.0503	1.72 %

$$n=\frac{\nu_{DT}^{0}\nu_{\delta}^{0}\nu_{ROI}^{0}N^{0}}{t_{R}^{0}}-\frac{\nu_{DT}^{Cd}\nu_{AmBe}^{Cd}\nu_{abs}^{Cd}\nu_{0.68}^{Cd}\nu_{\delta}^{Cd}\nu_{ROI}^{Cd}\nu_{15/50}^{Cd}N^{Cd}}{t_{R}^{Cd}}$$

Quantity	Unit	x_i	$u(x_i)$	c_i	$u_i(y)$	$u_i(y)/y$
ν_{DT}^{0}	-	1.0415	0.0054	3.426E+03	1.834E+01	0.51 %
ν_{δ}^{0}	-	1.0000	0.0050	3.568E+03	1.784E+01	0.50 %
ν_{ROI}^{0}	-	1.0000	0.0003	3.568E+03	1.070E+00	0.03 %
N^{0}	-	713615	845	5.000E-03	4.224E+00	0.12 %
t_{R}^{0}	s	208.29	0.01	1.713E+01	1.713E-01	0.00 %
ν_{DT}^{Cd}	-	1.0001	0.0000	4.365E-01	1.918E-07	0.00 %
ν_{AmBe}^{Cd}	-	1.0000	0.0000	4.366E-01	2.219E-10	0.00 %
ν_{abs}^{Cd}	-	1.0618	0.0185	4.112E-01	7.623E-03	0.00 %
$\nu_{0.68}^{Cd}$	-	0.8073	0.0578	5.407E-01	3.125E-02	0.00 %
ν_{δ}^{Cd}	-	1.0000	0.0050	4.366E-01	2.183E-03	0.00 %
ν_{ROI}^{Cd}	-	1.0000	0.0003	4.366E-01	1.310E-04	0.00 %
$\nu_{15/50}^{Cd}$	-	1.2170	0.0100	3.587E-01	3.587E-03	0.00 %
N^{Cd}	-	10545	103	4.140E-05	4.251E-03	0.00 %
t_{R}^{Cd}	s	25202.00	0.01	1.732E-05	1.732E-07	0.00 %
n	s^{-1}	3567.6			26.0	0.73 %

$$\phi_{TI}^{eff}=f_{AmBe}f_{eff/org}f_{TI/Au}\phi_{Au}^{org}$$

Quantity	Unit	x_i	$u(x_i)$	c_i	$u_i(y)$	$u_i(y)/y$
f_{AmBe}	-	1.0040	0.0000	1.212E+03	6.183E-07	0.00 %
$f_{eff/org}$	-	0.9629	0.0111	1.263E+03	1.405E+01	1.15 %
$f_{TI/Au}$	-	1.0035	0.0010	1.212E+03	1.263E+00	0.10 %
ϕ_{Au}^{org}	$cm^{-2}s^{-1}$	1254.0	13.0	9.702E-01	1.261E+01	1.04 %
ϕ_{TI}^{eff}	$cm^{-2}s^{-1}$	1216.6			18.9	1.56 %

Appendix 4: Uncertainty budgets for the 20 kPa counter covered with the polyethylene sphere.

$$R_{\mathrm{ref}} = k_{\mathrm{spec}} k_{\mathrm{dir}} R_{\mathrm{local}}$$

Quantity	Unit	x_i	$u(x_i)$	c_i	$u_i(y)$	$u_i(y)/y$
k_{spec}	-	0.9889	0.0077	2.267E-01	1.737E-03	0.77 %
k_{dir}	-	1.0169	0.0102	2.205E-01	2.242E-03	1.00 %
R_{local}	cm^2	0.22296	0.00381	1.006E+00	3.829E-03	1.71 %
R_{ref}	cm^2	0.22420			0.00477	2.13 %

$$R_{\mathrm{local}} = \frac{n}{\phi_{\mathrm{TI}}^{\mathrm{eff}}}$$

Quantity	Unit	x_i	$u(x_i)$	c_i	$u_i(y)$	$u_i(y)/y$
n	s^{-1}	270.18	1.48	8.252E-04	1.217E-03	0.55 %
$\phi_{\mathrm{TI}}^{\mathrm{eff}}$	$cm^{-2}s^{-1}$	1211.8	19.6	1.840E-04	3.608E-03	1.62 %
R_{local}	cm^2	0.22296			0.00381	1.71 %

$$n = \frac{\nu_{\mathrm{DT}}^{0}\nu_{\delta}^{0}\nu_{\mathrm{ROI}}^{0}N^{0}}{t_{\mathrm{R}}^{0}} - \frac{\nu_{\mathrm{DT}}^{\mathrm{Cd}}\nu_{\mathrm{AmBe}}^{\mathrm{Cd}}\nu_{\mathrm{abs}}^{\mathrm{Cd}}\nu_{0.68}^{\mathrm{Cd}}\nu_{\delta}^{\mathrm{Cd}}\nu_{\mathrm{ROI}}^{\mathrm{Cd}}\nu_{15/50}^{\mathrm{Cd}}N^{\mathrm{Cd}}}{t_{\mathrm{R}}^{\mathrm{Cd}}}$$

Quantity	Unit	x_i	$u(x_i)$	c_i	$u_i(y)$	$u_i(y)/y$
ν_{DT}^{0}	-	1.0029	0.0004	2.745E+02	1.134E-01	0.04 %
ν_{δ}^{0}	-	1.0000	0.0050	2.753E+02	1.377E+00	0.51 %
ν_{ROI}^{0}	-	1.0000	0.0006	2.753E+02	1.652E-01	0.06 %
N^{0}	-	330382	575	8.333E-04	4.790E-01	0.18 %
t_{R}^{0}	s	1203.51	0.01	2.288E-01	2.288E-03	0.00 %
$\nu_{\mathrm{DT}}^{\mathrm{Cd}}$	-	1.0001	0.0000	5.137E+00	2.257E-06	0.00 %
$\nu_{\mathrm{AmBe}}^{\mathrm{Cd}}$	-	1.0000	0.0000	5.138E+00	2.611E-09	0.00 %
$\nu_{\mathrm{abs}}^{\mathrm{Cd}}$	-	1.0354	0.0106	4.962E+00	5.267E-02	0.02 %
$\nu_{0.68}^{\mathrm{Cd}}$	-	0.9532	0.0140	5.390E+00	7.572E-02	0.03 %
$\nu_{\delta}^{\mathrm{Cd}}$	-	1.0000	0.0050	5.138E+00	2.569E-02	0.01 %
$\nu_{\mathrm{ROI}}^{\mathrm{Cd}}$	-	1.0000	0.0006	5.138E+00	3.083E-03	0.00 %
$\nu_{15/50}^{\mathrm{Cd}}$	-	1.2190	0.0100	4.215E+00	4.215E-02	0.02 %
N^{Cd}	-	107618	328	4.774E-05	1.566E-02	0.01 %
$t_{\mathrm{R}}^{\mathrm{Cd}}$	s	25202.35	0.01	2.039E-04	2.039E-06	0.00 %
n	s^{-1}	270.18			1.48	0.55 %

$$\phi_{\mathrm{TI}}^{\mathrm{eff}} = f_{\mathrm{AmBe}}\, f_{\mathrm{eff/org}}\, f_{\mathrm{TI/Au}}\phi_{\mathrm{Au}}^{\mathrm{org}}$$

Quantity	Unit	x_i	$u(x_i)$	c_i	$u_i(y)$	$u_i(y)/y$
f_{AmBe}	-	1.0040	0.0000	1.207E+03	6.159E-07	0.00 %
$f_{\mathrm{eff/org}}$	-	0.9603	0.0119	1.262E+03	1.504E+01	1.24 %
$f_{\mathrm{TI/Au}}$	-	1.0023	0.0007	1.209E+03	8.369E-01	0.07 %
$\phi_{\mathrm{Au}}^{\mathrm{org}}$	$cm^{-2}s^{-1}$	1254.0	13.0	9.664E-01	1.256E+01	1.04 %
$\phi_{\mathrm{TI}}^{\mathrm{eff}}$	$cm^{-2}s^{-1}$	1211.8			19.6	1.62 %

Appendix 5: Uncertainty budgets for the 200 kPa counter covered with the polyethylene sphere.

$$R_{\mathrm{ref}} = k_{\mathrm{spec}} k_{\mathrm{dir}} R_{\mathrm{local}}$$

Quantity	Unit	x_i	$u(x_i)$	c_i	$u_i(y)$	$u_i(y)/y$
k_{spec}	-	0.9896	0.0077	1.369E+00	1.049E-02	0.77 %
k_{dir}	-	1.0153	0.0102	1.334E+00	1.355E-02	1.00 %
R_{local}	cm^2	1.3481	0.0253	1.005E+00	2.543E-02	1.88 %
R_{ref}	cm^2	1.3546			0.0307	2.26 %

$$R_{\mathrm{local}} = \frac{n}{\phi_{\mathrm{TI}}^{\mathrm{eff}}}$$

Quantity	Unit	x_i	$u(x_i)$	c_i	$u_i(y)$	$u_i(y)/y$
n	s^{-1}	1622.7	9.4	8.308E-04	7.812E-03	0.58 %
$\phi_{\mathrm{TI}}^{\mathrm{eff}}$	$cm^{-2}s^{-1}$	1203.7	21.5	1.120E-03	2.407E-02	1.79 %
R_{local}	cm^2	1.3481			0.0253	1.88 %

$$n = \frac{\nu_{\mathrm{DT}}^{0}\nu_{\delta}^{0}\nu_{\mathrm{ROI}}^{0}N^{0}}{t_{\mathrm{R}}^{0}} - \frac{\nu_{\mathrm{DT}}^{\mathrm{Cd}}\nu_{\mathrm{AmBe}}^{\mathrm{Cd}}\nu_{\mathrm{abs}}^{\mathrm{Cd}}\nu_{0.68}^{\mathrm{Cd}}\nu_{\delta}^{\mathrm{Cd}}\nu_{\mathrm{ROI}}^{\mathrm{Cd}}\nu_{15/50}^{\mathrm{Cd}}N^{\mathrm{Cd}}}{t_{\mathrm{R}}^{\mathrm{Cd}}}$$

Quantity	Unit	x_i	$u(x_i)$	c_i	$u_i(y)$	$u_i(y)/y$
ν_{DT}^{0}	-	1.0190	0.0025	1.625E+03	4.034E+00	0.25 %
ν_{δ}^{0}	-	1.0000	0.0050	1.655E+03	8.277E+00	0.51 %
ν_{ROI}^{0}	-	1.0000	0.0004	1.655E+03	6.622E-01	0.04 %
N^{0}	-	993257	997	1.667E-03	1.661E+00	0.10 %
t_{R}^{0}	s	611.41	0.01	2.708E+00	2.708E-02	0.00 %
$\nu_{\mathrm{DT}}^{\mathrm{Cd}}$	-	1.0004	0.0000	3.271E+01	1.336E-03	0.00 %
$\nu_{\mathrm{AmBe}}^{\mathrm{Cd}}$	-	1.0000	0.0000	3.272E+01	0.000E+00	0.00 %
$\nu_{\mathrm{abs}}^{\mathrm{Cd}}$	-	1.0353	0.0106	3.160E+01	3.348E-01	0.02 %
$\nu_{0.68}^{\mathrm{Cd}}$	-	0.9551	0.0135	3.426E+01	4.612E-01	0.03 %
$\nu_{\delta}^{\mathrm{Cd}}$	-	1.0000	0.0050	3.272E+01	1.636E-01	0.01 %
$\nu_{\mathrm{ROI}}^{\mathrm{Cd}}$	-	1.0000	0.0004	3.272E+01	1.309E-02	0.00 %
$\nu_{15/50}^{\mathrm{Cd}}$	-	1.2150	0.0100	2.693E+01	2.693E-01	0.02 %
N^{Cd}	-	163394	404	2.002E-04	8.094E-02	0.00 %
$t_{\mathrm{R}}^{\mathrm{Cd}}$	s	6002.31	0.01	5.451E-03	5.451E-05	0.00 %
n	s^{-1}	1622.7			9.4	0.58 %

$$\phi_{\mathrm{TI}}^{\mathrm{eff}} = f_{\mathrm{AmBe}}\, f_{\mathrm{eff/org}}\, f_{\mathrm{TI/Au}}\phi_{\mathrm{Au}}^{\mathrm{org}}$$

Quantity	Unit	x_i	$u(x_i)$	c_i	$u_i(y)$	$u_i(y)/y$
f_{AmBe}	-	1.0040	0.0000	1.199E+03	6.117E-07	0.00 %
$f_{\mathrm{eff/org}}$	-	0.9538	0.0139	1.262E+03	1.748E+01	1.45 %
$f_{\mathrm{TI/Au}}$	-	1.0023	0.0007	1.201E+03	8.313E-01	0.07 %
$\phi_{\mathrm{Au}}^{\mathrm{org}}$	$cm^{-2}s^{-1}$	1254.0	13.0	9.599E-01	1.247E+01	1.04 %
$\phi_{\mathrm{TI}}^{\mathrm{eff}}$	$cm^{-2}s^{-1}$	1203.7			21.5	1.79 %

Appendix 6: Uncertainty budgets in fluence determination.

$$\phi_{\mathrm{Au}}^{\mathrm{org}} = \eta\rho$$

Quantity	Unit	x_i	$u(x_i)$	c_i	$u_i(y)$	$u_i(y)/y$
η	cm^{-2}	25.952	0.139	4.832E+01	6.719E+00	0.54 %
ρ	s^{-1}	48.318	0.429	2.595E+01	1.112E+01	0.89 %
$\phi_{\mathrm{Au}}^{\mathrm{org}}$	$cm^{-2}s^{-1}$	1254.0			13.0	1.04 %

$$\rho = \frac{c}{\varepsilon}$$

Quantity	Unit	x_i	$u(x_i)$	c_i	$u_i(y)$	$u_i(y)/y$
c	s^{-1}	29.420	0.183	1.642E+00	3.003E-01	0.62 %
ε	-	0.6089	0.0039	7.935E+01	3.058E-01	0.63 %
ρ	s^{-1}	48.318			0.429	0.89 %

$$c = \frac{\chi^{\mathrm{Al}}_{25,\mathrm{GP}}\chi^{\mathrm{Al}}_{\delta,\mathrm{NaI}}\chi^{\mathrm{Al}}_{\delta,\mathrm{GP}}\chi^{\mathrm{Al}}_{\infty}c^{\mathrm{Al}}}{\chi^{\mathrm{Al}}_{25,\mathrm{NaI}}} - \frac{\chi^{\mathrm{Cd}}_{\mathrm{AmBe}}\chi^{\mathrm{Cd}}_{\mathrm{abs}}\chi^{\mathrm{Cd}}_{0.68}\chi^{\mathrm{Cd}}_{25,\mathrm{GP}}\chi^{\mathrm{Cd}}_{\delta,\mathrm{NaI}}\chi^{\mathrm{Cd}}_{\delta,\mathrm{GP}}\chi^{\mathrm{Cd}}_{\infty}c^{\mathrm{Cd}}}{\chi^{\mathrm{Al}}_{25,\mathrm{NaI}}}$$

Quantity	Unit	x_i	$u(x_i)$	c_i	$u_i(y)$	$u_i(y)/y$
$\chi^{\mathrm{Al}}_{25,\mathrm{GP}}$	-	1.0135	0.0027	2.938E+01	7.936E-02	0.27 %
$\chi^{\mathrm{Al}}_{\delta,\mathrm{NaI}}$	-	1.0000	0.0020	2.977E+01	5.955E-02	0.20 %
$\chi^{\mathrm{Al}}_{\delta,\mathrm{GP}}$	-	1.0000	0.0050	2.977E+01	1.489E-01	0.51 %
$\chi^{\mathrm{Al}}_{\infty}$	-	1.8594	0.0000	1.601E+01	6.374E-05	0.00 %
c^{Al}	s^{-1}	15.809	0.018	1.883E+00	3.454E-02	0.12 %
$\chi^{\mathrm{Al}}_{25,\mathrm{NaI}}$	-	1.0006	0.0001	2.976E+01	3.487E-03	0.01 %
$\chi^{\mathrm{Cd}}_{\mathrm{AmBe}}$	-	1.0000	0.0000	-3.544E-01	1.801E-10	0.00 %
$\chi^{\mathrm{Cd}}_{\mathrm{abs}}$	-	1.0232	0.0046	-3.463E-01	1.609E-03	0.01 %
$\chi^{\mathrm{Cd}}_{0.68}$	-	0.9886	0.0023	-3.585E-01	8.166E-04	0.00 %
$\chi^{\mathrm{Cd}}_{25,\mathrm{GP}}$	-	1.0163	0.0033	-3.487E-01	1.137E-03	0.00 %
$\chi^{\mathrm{Cd}}_{\delta,\mathrm{NaI}}$	-	1.0000	0.0020	-3.544E-01	7.087E-04	0.00 %
$\chi^{\mathrm{Cd}}_{\delta,\mathrm{GP}}$	-	1.0000	0.0050	-3.544E-01	1.772E-03	0.01 %
$\chi^{\mathrm{Cd}}_{\infty}$	-	1.5561	0.0000	-2.277E-01	1.001E-06	0.00 %
c^{Cd}	s^{-1}	0.2217	0.0093	-1.598E+00	1.481E-02	0.05 %
$\chi^{\mathrm{Cd}}_{25,\mathrm{NaI}}$	-	1.0009	0.0002	-3.540E-01	6.526E-05	0.00 %
c	s^{-1}	29.420			0.183	0.62 %

$$\varepsilon = \frac{e_{25}e_{\delta,\mathrm{NaI}}c_{\mathrm{NaI}}(1+K)}{e_{\delta,4\pi\beta\gamma}A}$$

Quantity	Unit	x_i	$u(x_i)$	c_i	$u_i(y)$	$u_i(y)/y$
e_{25}	-	0.9989	0.0002	6.096E-01	1.383E-04	0.02 %
$e_{\delta,\mathrm{NaI}}$	-	1.0000	0.0020	6.089E-01	1.218E-03	0.20 %
c_{NaI}	s^{-1}	367.60	0.54	1.656E-03	8.887E-04	0.15 %
K	-	0.0372	0.0056	5.871E-01	3.276E-03	0.54 %
$e_{\delta,4\pi\beta\gamma}$	-	1.0000	0.0020	6.089E-01	1.218E-03	0.20 %
A	s^{-1}	625.47	0.61	9.735E-04	5.906E-04	0.10 %
ε	-	0.6089			0.0039	0.63 %

National Physical Laboratory

NPL REPORT IR 29

The NPL contribution to CCRI key comparison K8 of thermal neutron fluence measurements

P K Kolkowski and D J Thomas

JULY 2013

National Measurement System

July 2013

NATIONAL PHYSICAL LABORATORY

The NPL contribution to CCRI key comparison K8 of thermal neutron fluence measurements

by

P. Kolkowski and D.J. Thomas

Neutron Metrology Group
Acoustics & Ionising Radiation Division

Abstract
The results of NPL's experiments as part of the CCRI key comparison, K8, of thermal neutron fluence measurements are presented. Two detectors were provided for the comparison, and measurements were performed for both detectors, with and without the polyethylene moderating sphere provided. These measurements were performed with the detectors orientated both parallel and perpendicular to the neutron beam from the column of the NPL thermal pile.

ISSN 1754-2952

National Physical Laboratory
Hampton Road, Teddington, Middlesex, TW11 0LW

This report details the results of NPL’s participation in a CCRI key comparison of thermal neutron fluence production and measurement. A restricted report was originally produced, printed as NPL REPORT AIR(RES)024, and was sent to the evaluator. The results of the comparison have now been made public so this report has been re designated as IR 29 and published as a NOT RESTRICTED report.

Approved on behalf of the Managing Director, NPL by Bajram Zeqiri,
Knowledge Leader, Acoustics & Ionising Radiation Team,

Contents

Figures **Page**

Tables **Page**

1 INTRODUCTION

This report details the NPL contribution to CCRI key comparison, K8, of thermal neutron calibration capabilities. There is no standard technique that is used by national metrology institutes (NMIs) for producing thermal neutron calibration fields. They can be reactor-based systems, or can be based on a neutron source, or sources, in a moderating assembly. The neutron source can be either a radionuclide source, or on accelerator-driven one. Probably because of the diversity of the facilities, this is the first CCRI thermal neutron comparison to have been organised.

The comparison involved circulating two SP9 spherical ^{3}He proportional counters as thermal neutron detectors – see the protocol at Appendix A. These have response functions which decrease with a roughly 1/*v* dependence on energy over the thermal region, where *v* is the neutron velocity. They differed in gas pressure and hence sensitivity; one, serial no. 8916-104, contained 200 kPa of the gas and the other, serial no. 9313-111, only 20 kPa. This allowed measurements to be made over a wide range of different neutron fluence rates, up to roughly 10^{5} cm^{-2} s^{-1}, although this range does not extend to the fluences typically found in, or close to, the core of a reactor. In addition a 7.62 cm (3") diameter polyethylene moderating sphere was made available. Either of the SP9 counters could be positioned at the centre of this sphere to provide a neutron detector with a very different response function for thermal neutrons, in fact one that increases with energy over the thermal region. The motivation for using of this combination of instruments was to obtain information on the neutron spectra at the various participating laboratories. Basically, the ratio of the responses of the bare and moderated instruments gives an indication of the mean energy of the thermal distribution.

The detectors were circulated to the participating labs together with a set of battery-operated electronics and the protocol. This explained how to use the equipment, and also detailed the quantity to be reported. This quantity is simply the response of the devices in terms of counts per unit fluence; however, the results need to be corrected to the response which would be obtained in a particular thermal neutron distribution. This approach was necessary so that results from the various laboratories with different thermal neutron fields could be compared.

Thermal neutron fluences are commonly measured using thin activation foils. These are usually irradiated both bare and under a thermal neutron absorbing cadmium cover to derive information about the ratio of the neutron fluence rate above and below the cadmium cut-off energy, which is about 0.5 eV for 1 mm of cadmium. This is the approach adopted at NPL and the foils used are 0.05 mm thick gold. Without detailed information about the thermal neutron spectrum, obtained for example using a mechanical chopper device, the interpretation of activation measurements involves making various assumptions about the spectrometric and directional characteristics of the field.

Thermal fluences derived from activation measurements are normally quoted using the convention of Westcott *et al.*[(1)]. This assumes that the neutron spectrum can be described in terms of a thermal Maxwellian peak and a 1/*E* slowing down component, and the approach is applicable when using foils of materials such as gold which have a cross section which essentially varies inversely as the neutron velocity, i.e. “obeys the 1/*v* law”. The directional characteristics need to be known to derive some of the parameters used in the analysis with this convention. Fluence distributions tend to be either isotropic or approximate to beam geometry. For the present measurements the thermal neutron field was essentially a beam.

In the Westcott convention, the quantity derived is the product of a neutron density, n, and a particular velocity, $v_o = 2200$ m s^{-1}. This is a measure of the fluence rate, although not a precise one because the velocity v_o is not the correct average velocity of the neutrons. The reason for using the Westcott approach is that the exact spectrum in most thermal neutron fields is not known, but the use of this convention allows measurements, e.g. of cross sections, to be compared without confusion.

When foil irradiations are performed with and without a cadmium cover a number of different Westcott fluence rates can be derived. In order to determine true fluence rates information is needed on the average velocity of the neutrons, and for this a value is required for the effective temperature, T, of the Maxwellian distribution. (The peak energy of the Maxwellian distribution is at kT, where k is the Boltzmann constant.) With this information the true fluence rates can be derived. Information on the estimation of the temperature of the NPL thermal column field is given in section 2.3. (The Maxwellian temperature is in fact required even to derive nv_0, but the result is not very sensitive to the exact value of T.)

In activation foil measurements the thermal fluence rates are derived from the saturated activity induced in the foils, The expressions relating the saturated activity of the bare foil, D_0, and of the cadmium covered foil, $D_0(Cd)$, to the Westcott fluence rates can be found in various references[2,3,4], and are given below for the most commonly used fluence rates.

$$\phi_W = nv_0 = \frac{1}{G_t} \cdot \frac{(D_0 - D_0(Cd).F)}{N\sigma_0 g} \cdot \frac{R}{(R-1)} \tag{1}$$

$$\phi_W(th) = n_{th}v_0 = \frac{1}{G_t} \cdot \frac{(D_0 - D_0(Cd).F)}{N\sigma_0 g} \tag{2}$$

$$\phi_W(M) = n_M v_0 = nv_0 \left[1 - \frac{4r}{(\pi\mu)^{1/2}} \right] \tag{3}$$

$$\phi_W(1/E) = n_{1/E}v_0 = nv_0 - n_M v_0 \tag{4}$$

$$\phi'_W(1/E) = n'_{1/E}\, v_0 = n_{th}v_0 - n_M v_0 \tag{5}$$

Where:

ϕ_W	is the total fluence rate in the Westcott convention,
G_t	is the thermal neutron self-shielding factor, (it depends on the directional characteristics of the field),
N	number of gold atoms per mg of foil,
σ_0	cross section for 2200 m s^{-1} neutrons,
F	is a correction factor for attenuation of epi-cadmium neutrons in cadmium,
g	is a measure of the departure of the cross section from a $1/v$ dependence in the Maxwellian region (it has a slight dependence on the Maxwellian temperature T),

R is the cadmium ratio for an ideal $1/v$ detector, which can be derived from the cadmium ratio, $R_{Cd} = D_0 / D_0(Cd)$, measured for the activation foil,

$\phi_W(th)$ is the sub-cadmium-cut-off fluence rate, sometimes called simply the thermal fluence, in the Westcott convention,

n_{th} is the neutron density in the sub-cadmium-cut-off region,

$\phi_W(M)$ is the Maxwellian fluence rate in the Westcott convention,

n_M is the neutron density in the Maxwellian distribution,

r is a measure of the relative intensity of the epithermal component, (expressions for r can be found in references 2 and 3),

μ defines the lower limit, E_Δ, of the $1/E$ component, $E_\Delta = \mu kT$,

$\phi_W(1/E)$ is the total $1/E$ neutron fluence rate in the Westcott convention,

$n_{1/E}$ is the total neutron density in the $1/E$ distribution,

$\phi'_W(1/E)$ is the $1/E$ neutron fluence rate, in the Westcott convention, in the region between E_Δ and the cadmium cut-off energy E_{Cd}, and

$n'_{1/E}$ is the neutron density in the $1/E$ distribution in the region between E_Δ and the cadmium cut-off energy E_{Cd}.

If the value for the effective temperature, T, of the Maxwellian is known, a value for, $\bar{v}_M$, the mean velocity for the Maxwellian distribution can be derived(2-4):

$$\frac{\bar{v}_M}{v_0} = \left[\frac{4T}{\pi T_0}\right]^{1/2} \tag{6}$$

where:

T_0 is 293.6 K, i.e. the temperature corresponding to the velocity v_0.

The $1/E$ component is assumed to extend from some lower energy limit E_Δ up to the maximum energy in the spectrum. The average velocity $\bar{v}_{1/E}$ can be calculated from:

$$\frac{\bar{v}_{1/E}}{v_0} = \frac{\ln(E_{\max} / E_\Delta)}{2E_0^{1/2}\left[E_\Delta^{-1/2} - E_{max}^{-1/2}\right]} \tag{7}$$

where:

E_{max} is the maximum energy of the $1/E$ component.

If E_{max} is set to the cadmium cut-off energy, E_{Cd}, the value derived for $\bar{v}_{1/E}/v_0$, indicated here by $\bar{v}'_{1/E}/v_0$, is for the $1/E$ fluence below this energy, i.e. in the thermal region. Thus $\bar{v}$ is available for both components of the fluence below this energy, and the true sub-cadmium-cut-off fluence rate $\phi(th)$ can be derived from:

$$\phi(th) = n_{th}\bar{v}_{th} = n_M\bar{v}_M + n'_{1/E}\,\bar{v}'_{1/E} = n_M v_0 \cdot \frac{\bar{v}_M}{v_0} + n'_{1/E}\, v_0 \cdot \frac{\bar{v}'_{1/E}}{v_0} \tag{8}$$

If the SP9 detectors for the comparison exercise are irradiated in the thermal column field both bare and with a cadmium cover, and the thermal neutron count rate is determined by subtracting the under cadmium counts from the bare counts, then the fluence which produced these counts is given by eq. (8) .

2 THE NPL THERMAL NEUTRON FACILITY

2.1 History and construction

Thermal neutron fluence standards have been available at NPL since the facility, commonly known as the thermal pile, was set up in the late 1960s by Ryves and Paul[5]. The pile consists of a large graphite block within which fast neutrons are produced by bombarding two beryllium targets, located on either side of a central irradiation cavity, with deuterons from the NPL 3.5 MV Van de Graaff accelerator. The graphite moderates these neutrons producing a well thermalized field at the bottom of the cavity. Figure 1 shows a schematic view of the pile.

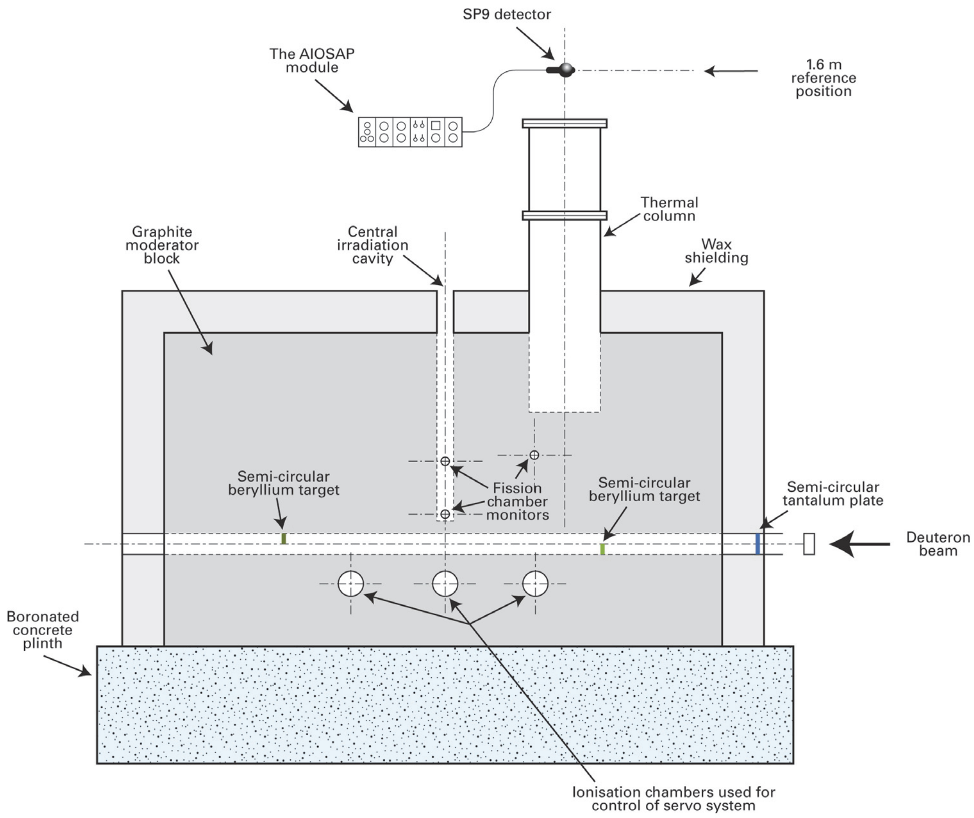

Figure 1. Side-on schematic view of the NPL thermal pile.

The arrangement of the targets as two semi-circular plates, in combination with a semi-circular tantalum 'dump' plate just outside the pile, see Figure 2, allows accurate control of the neutron production. The system, described in detail in reference 5, is designed to provide a stable neutron fluence rate at the bottom of the central irradiation cavity, and this fluence rate is controlled by an ionisation chamber situated immediately below the cavity. A servo-system compares the voltage developed by the ion chamber current with a pre-set reference voltage. The fluence rate is then kept constant at a level determined by the reference voltage. Historically this is referred to as the 'demand level'. Provided the incident deuteron beam intensity remains reasonably constant the servo-system maintains a thermal neutron fluence rate that varies by <± 0.2% over a period of several hours. This is achieved by using steering plates to either move the deuteron beam further onto the tantalum, to reduce the fluence rate, or further onto the beryllium targets, to increase the rate. In this way the system maintains a constant fluence in the cavity regardless of small changes in the total beam current from the Van de Graaff. Two additional ion chambers, situated to the left and right of the central chamber, provide signals to steer the beam vertically between the beryllium targets to keep the yield from the two targets equal and thus minimise the fluence gradient across the floor of the cavity. This cavity is designed for irradiating devices to relatively high neutron fluences, up to 10^7 cm^{-2} s^{-1}. Devices such as SP9 counters are, however, more easily irradiated in the field of the thermal column shown to the left of the cavity in Figure 1.

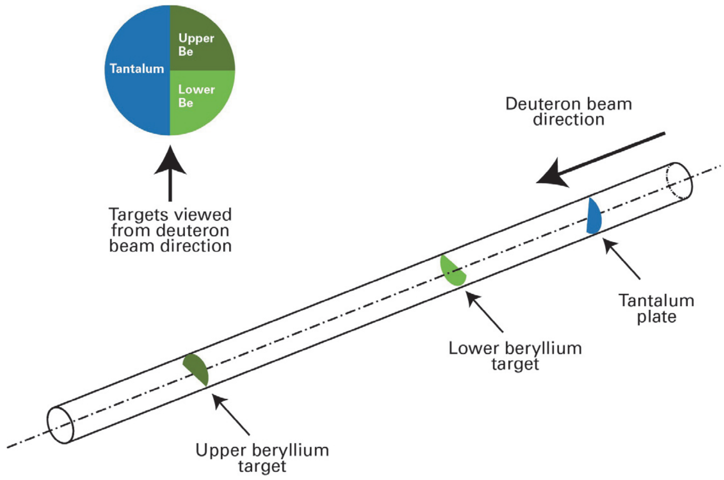

Figure 2. Arrangement of the two beryllium targets and the tantalum plate.

The column consists of a larger diameter hole, also in the top of the pile, but situated so that it is almost over one of the beryllium targets. A stainless steel tube, cadmium-lined on its curved surface, but not on its base, is placed in the hole. The tube is available in sections and can be adjusted in half metre steps, from 1 m to 3 m. When the tube is 1.5 m long or more it can be evacuated to reduce attenuation of the thermal beam. The neutron beam emerging from this tube is reasonably uniform. Over a horizontal circular area of about 10 cm diameter the decrease in fluence from the centre to the extremity of this area is < 1%. For a horizontal circular area of 30 cm diameter the fluence at the extremity is about 6% less than that at the centre. The intensity falls off as the height increases, and the maximum thermal fluence rate achievable at a height of 1 m is about 4 x 10^4 cm^{-2} s^{-1}. Experience has shown that, the control system, although designed to maintain an accurately constant fluence rate at the bottom of the central cavity, also maintains a very constant fluence rate in the beam of the column. The location of the SP9 detectors in the beam of the column during the comparison measurements is shown in Figure 1.

2.2 Monitoring

During the SP9 counter measurements the neutron fluence was continuously monitored by two Centronic, pulsed ^{235}U fission chambers. One is permanently positioned in the graphite between the bottom of the thermal column and the beryllium target (FC_C, type FC4A/100/U235) and the other at a fixed position to one side of the central irradiation cavity (FC_H , type FC4B/20/U235) approximately 60 cm from the axis of the thermal column*.

* Two fission chambers are shown close to the central cavity in Figure 1. FC_H is the upper one of these two.

These monitors were calibrated in terms of the neutron fluence rate at a reference position, 1.6 m above the base of the thermal column, using the gold foil activation technique. The 1.6 m position was chosen so that the required fluence rates could easily be achieved whilst keeping dead time corrections for the SP9 counters reasonably low.

Calibration of the monitors was performed mid-way through the measurements with the SP9 counters. A pair of gold foils, both 1 cm^2 in area and weighing approximately 96 mg, were irradiated, one foil being enclosed in a 1 mm thick cadmium metal box in order to enable the epi-thermal neutron correction to be determined. The foils were mounted on a low mass jig that positioned each foil on a horizontal plane about 4 cm from the central axis of the thermal column at the same height as the SP9 counters were positioned. They were sufficiently far apart that scatter between the foils was negligible.

The foils were 4πβ-counted in shielded, low-background, proportional counters. The observed count rates were corrected for counter background, dead-time, decay during counting, and for non-saturation during the irradiation. The quantity derived for each foil was the saturated β count rate per mg of gold. Foil activities were then derived using β-counting efficiencies determined by 4πβ-γ coincidence counting following irradiation of the foils in the GLEEP reactor at Harwell[2]. The measured β-counting efficiency for the bare gold foils was corrected for the effects of different irradiating spectra at GLEEP and NPL by a correction factor derived from the measured ratios of the activities of the bare and cadmium-covered foils (the cadmium ratios). The counting efficiency of the cadmium-covered foils did not require this correction.

Thermal neutron fluence rates were calculated according to the convention of Westcott *et al.*[1]. A value of (98.69 ± 0.28) barn, taken from the evaluation of Carlson *et al.*[6], was used for the gold activation cross section, σ_0. Appendix B shows the printout of the FORTRAN program which was used to derive the various fluence values from the saturated disintegration rates measured for the bare and cadmium covered foils.

2.3 Spectrum of the thermal column field

Two approaches have been used to derive information about the neutron spectrum in the field of the NPL thermal column. One for the fluence above the cadmium cut off energy, and another for the region below this energy.

The epithermal component of the column spectrum consists of primary neutrons which have not been moderated to thermal energies. These neutrons are produced within the pile from the d-Be reaction, and to a lesser extent, from the d-D reaction and from the action of the deuteron beam on contaminants deposited on the beryllium targets and the tantalum plate. All these reactions contribute to the neutron field, but the ratio of the thermal component to the fast and epithermal component will vary slightly depending on the deuteron beam conditions (energy) and the cleanliness of the vacuum system, targets and tantalum plate. This component has been measured using Bonner spheres. The measurements[7] revealed a relatively flat, 1/E, spectrum extending from the thermal region to a maximum energy of about 8 MeV. Although the higher energy fluence is only about 24% of the thermal fluence, the dose equivalent due to the fast component is more than a factor of two greater than that due to the thermal neutrons.

A second approach was used to derive information about the sub-cadmium part of the spectrum. When analysed using the Westcott convention measurements with gold foils, with and without cadmium cover, provide information on the relative fluences in the Maxwellian peak and in the 1/E component of the spectrum. By using an empirical relationship the effective temperature of the Maxwellian peak can also be determined from these measurements(8). This approach is described in NPL Report DQL RN008(9), however, since that report was written it has been realised that the effective temperature varies somewhat with height in the column. The most recent measurements give a value of 22.6 ^{o}C for T-T_m at the height of 1.6 m where the present measurements were made, where T is the effective temperature of the Maxwellian distribution and T_m is the physical temperature of the moderator. This is measured using a thermometer set inside the pile.

3 MEASUREMENTS

The measurements for the comparison were carried out in the second half of February, 2007.

A battery-powered electronics module was supplied for the measurements, the AIOSAP (All-in-one Spectrometry Processor) which consisted of a high voltage supply, analogue pulse processing, and discrimination units. This module was mounted as close as practical to the thermal neutron beam so that the special cables and sockets supplied could be used to optimise the pulse processing – see Figure 3 lower.

The SP9 counter was connected to the unit with all the settings made as directed in Appendix 1. The high voltage control was slowly increased and then ‘locked’ when the appropriate value was indicated in the LED display. On several occasions it was noticed that the voltage would slowly increase for about an hour after the initial ‘power on’ after which it would remain constant at which point the voltage would be reduced to the correct operating value. The increase was as much as 10 volts on one occasion. For this reason the AIOSAP and high voltage were switched on at least two hours prior to the measurements. The discriminator output from the AIOSAP was then connected, via a 30 m 50Ω cable, to an NPL width/delay unit. This unit produces output pulses of a suitable width and height to trigger the scaler card used to record the counts during the measurements. The width of a pulse from this unit is unaffected by the input pulse width and it was set to 6.4 μs for the present measurements.

The electronics for both fission chamber monitors consisted of a high voltage unit, a preamplifier, a main amplifier, a single channel analyser to set a discriminator level above the noise, and a width/delay unit to provide a suitable pulse for counting the events in a scaler. For the column fission chamber short pulse shaping times were used and the dead-time (5.0 ± 0.5 μs) was defined by the width of the pulse from the width/delay unit. For the fission chamber near the central cavity longer pulse shaping times were used in the main amplifier. The pulse from the width/delay unit was set to 10.2 μs, however, subsequent investigation showed that, because of the longer shaping time constants, the overall dead-time per pulse was greater than 10.2 μs and the value used for performing corrections was 11.5 ± 1.0 μs. Before and after any measurements were carried out the ratio of the dead-time corrected fission chamber monitor count rates was compared with previous measurements to check the stability of the monitors.

A locating jig was attached to the top of the thermal column; see Figure 3, which provided a reference plane enabling accurate positioning of the sensitive volume of the bare SP9 counters in all orientations used, and in moderator/cadmium shield assemblies. Sets of pillars of different lengths were used to support the jig so that for every configuration and assembly combination the centre of the sensitive volume was at the reference height of 1.6 m.

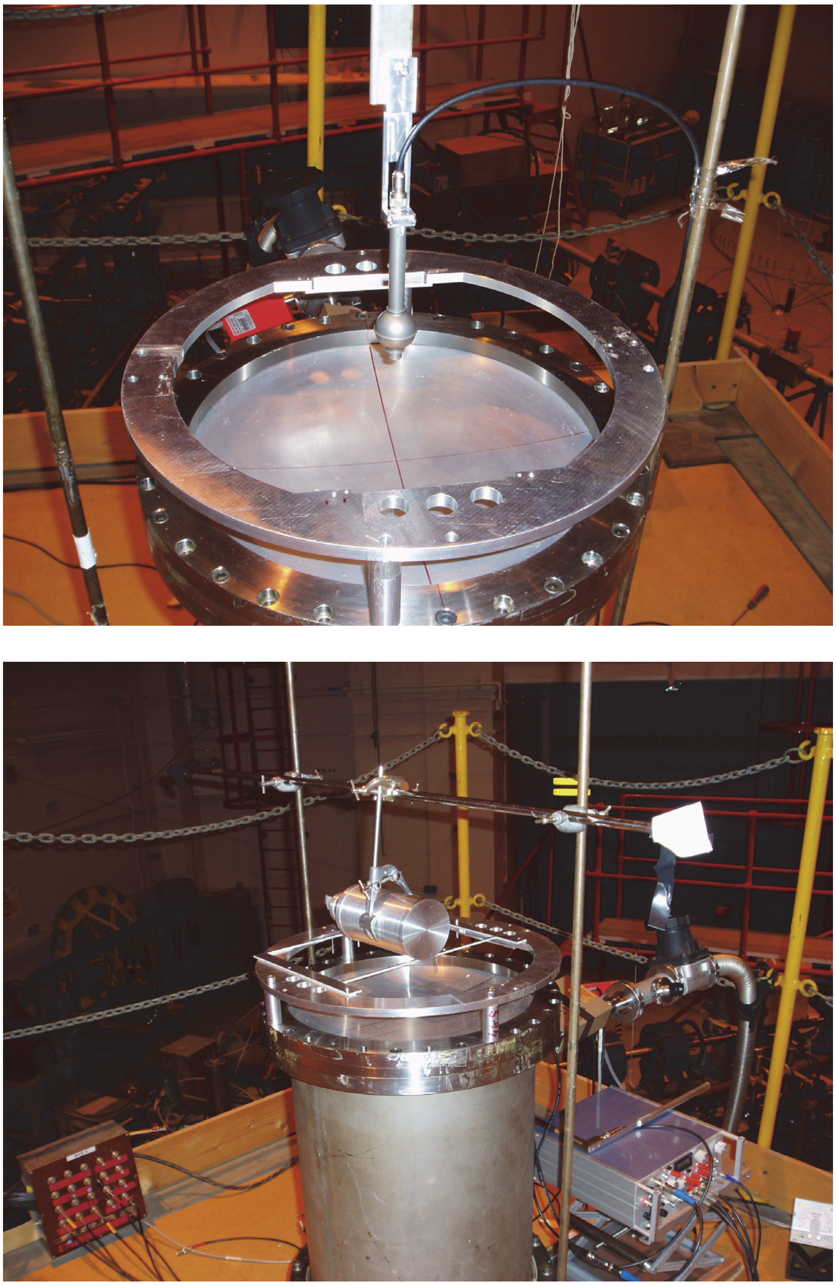

Figure 3. Mounting arrangements for the SP9 counters. Upper picture: SP9 counter bare and parallel to the neutron beam, lower picture SP9 counter in moderator and inside cadmium sleeve mounted perpendicular to the neutron beam.

During all the measurements with the SP9 counter, data were collected via a PC scaler card which recorded: the counts from a precision pulse generator running at 10 Hz, the counts from the SP9 detector, and the counts from the two fission chambers. A measurement consisted of a number of cycles, usually five, each cycle run for 1000 counts from the 10 Hz pulser, i.e. for 100 s. In this way estimates of the statistical uncertainties could be derived from the standard deviation of the cycles as well as from the assumption that Poisson statistics apply. For the measurements with gold foils the counts from the two fission counters were recorded for 100 s cycles throughout the measurement providing information which could be used to correct for any non-uniformity of the irradiation over the period of the measurement.

Table 1 lists the demand levels used for the various measurements performed with the AIOSAP electronics. The levels were chosen to optimise the count rate and in some instances to obtain information about the consistency of the SP9 count rate per unit monitor with demand.

Table 1. Demand levels used for the various measurements with the AIOSAP electronics.

Configuration	Demand level(s)
200 kPa SP9 parallel to the beam no polyethylene moderator	0.1 to 10.0
200 kPa SP9 perpendicular to the beam no polyethylene moderator	0.3
20 kPa SP9 parallel to the beam no polyethylene moderator	0.3 and 3.0
20 kPa SP9 perpendicular to the beam no polyethylene moderator	0.3 and 3.0
200 kPa SP9 parallel to the beam with polyethylene moderator	0.5
200 kPa SP9 perpendicular to the beam with polyethylene moderator	0.5
20 kPa SP9 parallel to the beam with polyethylene moderator	3.0
20 kPa SP9 perpendicular to the beam with polyethylene moderator	3.0

Measurements for all the configurations in Table 1 were performed with and without cadmium cover. For the under-cadmium measurements the SP9 counter was attached to an aluminium base unit and the cover fitted – see Appendix 1. This base unit did not appear to have a cadmium layer, and it was thought that with the SP9 counter perpendicular to the beam there might be a path for thermal neutrons through the base. For this reason an additional cadmium disc was made with a hole at the centre for the SP9 stem and this was fitted on the base unit so that it was on the inside of the final enclosure. However, measurements with and without this disc were consistent within the uncertainties indicating that there was no significant pathway for thermal neutrons through the base.

In addition to collecting data with the AIOSAP electronics some measurements were also performed with conventional NIM electronics units belonging to NPL. The electronics chain consisted of:

- High voltage unit (Tenelec TC953),
- Pre-amplifier (Ortec 142PC),
- Main amplifier (Ortec571),
- Timing Single Channel Analyser (Ortec 551),
- NPL width/delay unit (width of output pulse set to 6.4μs)

The data from these measurements have not been included in the final results for NPL's contribution to this comparison, but have simply been used as a check that results obtained with the AIOSAP unit are consistent with what would be obtained with the sort of electronics NPL would normally use for this type of measurement.

4 ANALYSIS

4.1 Initial processing of the data

As a first step in analysing the data all the scaler counts were transferred to an Excel workbook where dead-time corrections were performed for the counts from the SP9 counter and for the counts from the fission chambers. Ratios of the dead-time corrected individual SP9 counts, N, to those for the two fission chambers were calculated. The fission chamber counts are designated M_C for the column fission chamber, FC_C, and M_H for the chamber close to the access hole, FC_H. Means, standard deviations and values for the standard error of the mean were then calculated for the number of cycles involved in each measurement, i.e. mean values were obtained for N, M_C, M_H, N/M_C, and N/M_H. The demand level, D, is constant for a measurement so a value for N/D is easily derived. The approach of calculating N/M_C and N/M_H values for individual cycles and then deriving a mean of these ratios was taken because any variation in the fluence rate during the cycles will result in variations in the individual N, M_C, and M_H values, but should not affect the ratios. There was, however, little or no indication of variation of the fluence over the majority of the measurements. The above analysis was performed for all configurations of the SP9 counters and moderating sphere, and also for these configurations enclosed in the appropriate cadmium cover provided.

4.2 Monitor stability

To obtain a value for the fluence response of the SP9 detector, for example from the mean ratio for N/M_C, requires a calibration of the fission counter monitor in terms of neutron fluence per fission chamber count M_C. This is obtained from the gold foil measurement. Because this measurement is made at one particular time, and for one particular demand level, it is essential that the monitors are stable. To check the performance of the monitors their ratios were investigated both as a function of demand level and of time. Figure 4 shows the ratios of M_H/M_C, M_C/D, and M_H/D as a function of demand. In all cases the uncertainties in the ratios increase as the demand increases because of the uncertainty in the dead-time correction. All the ratios are for measurements with an SP9 counter, except for one of the measurements at a demand of 10 which was that for the irradiation of the gold foils. Note that the majority of measurements were made for demand levels in the range 0.3 to 3.

The ratio M_H/M_C is constant within the uncertainties over the range of demand levels, indicating that these two monitors agree very well with each other. There is even an indication that the assigned uncertainties, due mainly to statistics at low demand level and the uncertainty in the dead-time correction at higher demand levels, might be a little large in view of the level of agreement.

For the ratio M_C/D the values are reasonably constant except for the one at the lowest demand value of 0.1 where there is a clear suggestion that either M_C is too low or D is too high. There is some indication that this problem may also be present in the data for the next highest demand level of 0.3. Overall, the results for this ratio when viewed for all demand levels, suggest that the uncertainties may be slightly underestimated, but in view of the fact that the plot of the data for M_H/M_C indicates the opposite, i.e. that the fission chamber uncertainties may be slightly overestimated, no changes were made to the uncertainties in M_C/D.

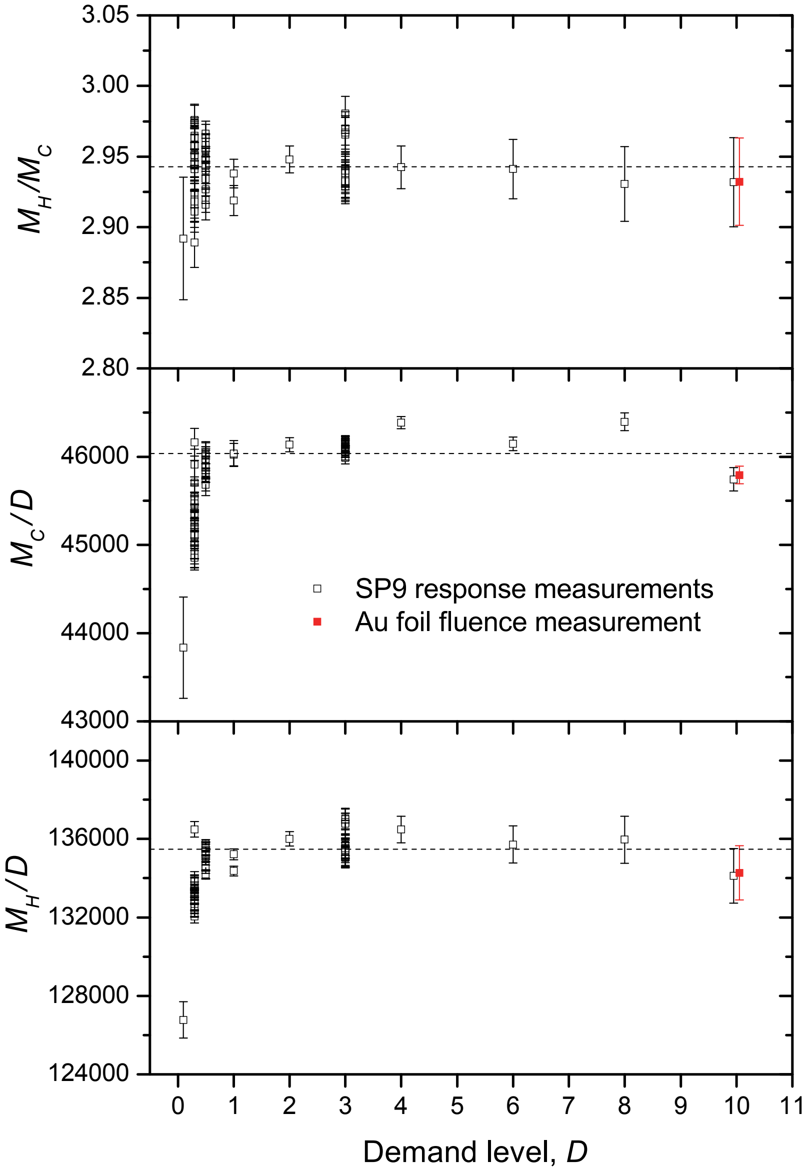

Figure 4. Ratios of monitor readings as a function of demand level for all the measurements performed. The dotted horizontal lines indicate mean values for these ratios over the range of demand values from 0.5 to 10.

The bottom plot in Figure 4 shows the data for M_H/D. These are similar to those for M_C/D, indicating a constant value for demand levels between 0.5 and 10, but with indications that either M_H is too low or D is too high below a demand of 0.5.

From the data in Figure 4 it can be concluded that all three monitors perform well over the range of demands from 0.5 to 10, and that any one could be chosen. The consistency of M_H/M_C over the entire range of demand levels would indicate that the low values for M_C/D and M_H/D for demands below 0.5 are due to problems with the demand as a monitor in this region, however, further data on this issue is available from the variation of the results for the SP9 counters with demand and this is discussed in section 4.3.

In Figure 5 the data for M_C/D are shown, for all demand levels used, as a function of time covering the whole period of the measurements. This figure highlights the consistency of this ratio for demand levels of 0.5 and above and the fact that there is definitely a problem with one of the monitors for the lowest demand level, i.e. 0.1. Except for a couple of data points, the results for data taken at a demand of 0.3 indicate that there may also be a problem with one of the monitors at this demand level. The value of M_C/D is roughly 2% lower for this demand than the average for higher demands. There is no indication of variation of the monitor ratios over the period of the measurements. The data for M_H/D provides similar evidence of the stability of the monitors with time.

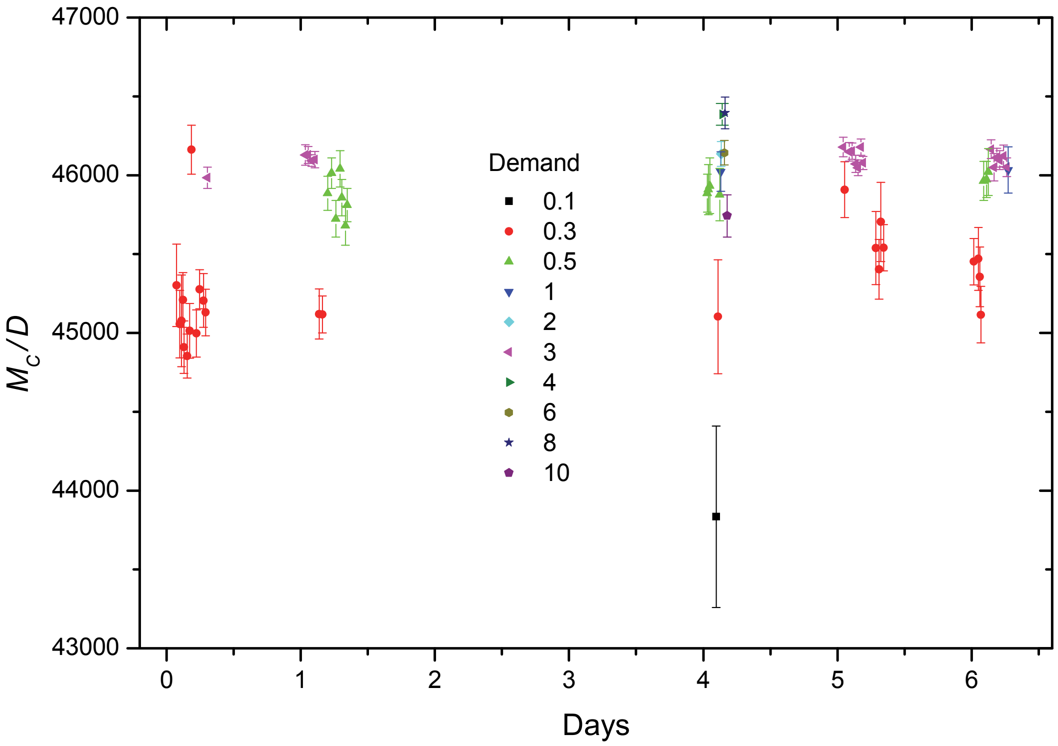

Figure 5. Variation of the ratio M_C/D with time from the first measurement.

4.3 The SP9 counter dead-time when using the AIOSAP electronics

If all corrections that need to be applied to the SP9 counts and to the monitor readings have been applied and are correct, then the quantity ‘SP9 counts per unit monitor reading’ should be constant for all demand levels for a particular SP9 counter configuration. Figure 6 shows this ratio for the three monitors for a series of measurements which were taken over a range of demand levels for a fixed SP9 counter configuration (bare detector mounted parallel to the neutron beam). Dead-time corrections to the SP9 counts were applied assuming a dead-time per pulse from the AIOSAP unit of 7.2 ± 0.9 µs as specified in the protocol. The conventional equation for a non-extending dead time, eq. (9), was used to relate the corrected counts N to the measured counts N' via the measured count rate R' (equal to N' divided by the measurement time T), and the dead-time per pulse τ.

$$N = \frac{N'}{(1 - R' \cdot \tau)} \tag{9}$$

The rather large uncertainties at the higher demand levels are a result of the large dead-time corrections applied to the SP9 counts (42% for a demand of 10). This correction is common to all three sets of data, i.e. they are correlated. This explains why the results for the different monitors agree better than would be expected from a simple consideration of the error bars.

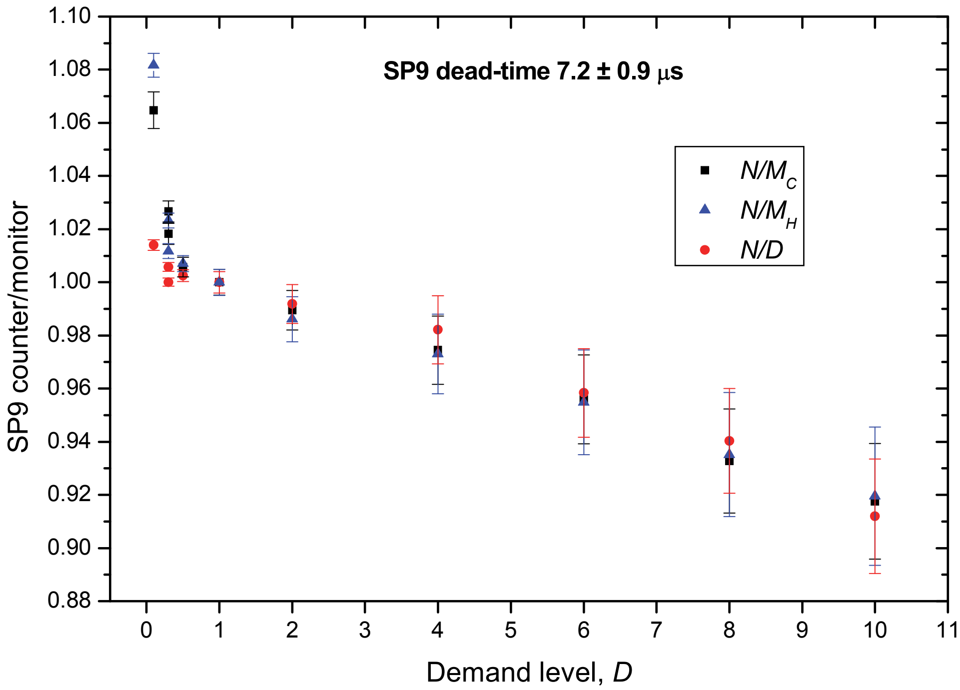

Figure 6. Variation of the counts, N, per unit monitor reading, M_C, M_H or D, as a function of demand for the 200 kPa SP9 counter mounted vertically free in air. The three sets of data are all normalised to unity for the measurement at a demand of 1.0.

In spite of the rather large uncertainties at higher demand levels, resulting from the uncertainty in the dead-time, it is clear that the data are not consistent, and the indications are that the dead-time of 7.2 μs is not applicable, certainly not at the higher demand levels. A check using a double pulser, where the time between pulses could be varied over a range of several μs, indicated that the specified dead-time of 7.2 μs was correct at low count rates. The two-source method was then used to measure the dead-time at higher count rates, similar to those seen at the higher demand levels. Values were obtained which were larger than 7.2 μs. For a combined rate from the two sources that was similar to that at a demand of 10 the dead-time was measured as 8.8 μs. For lower rates the dead time was smaller, but still greater than 7.2 μs. The indications are thus that the dead-time may be rate dependent. Because the two source method uses readings at different count rates to derive the dead-time, its results cannot be relied upon if the dead-time is truly rate dependent, but it does give a clear indication that the dead-time was not 7.2 μs at the higher rates.

It is possible that the dead-time is extending rather than non-extending. An expression relating measured counts to the true number of events which occurred can be written for the case of extending dead-time, but it involves the term $e^{-R\tau}$ where R is the true count rate which is unknown. Allowance was therefore made for the apparently varying dead-time using eq. (10)below:

$$N = \frac{N'}{(1 - R' \cdot (1 + R'/R_0) \cdot \tau)} \tag{10}$$

where R_0 is a constant adjusted manually to make the values of the SP9 counts/monitor constant over the range of demand values used in the measurements. The results are shown in Figure 7.

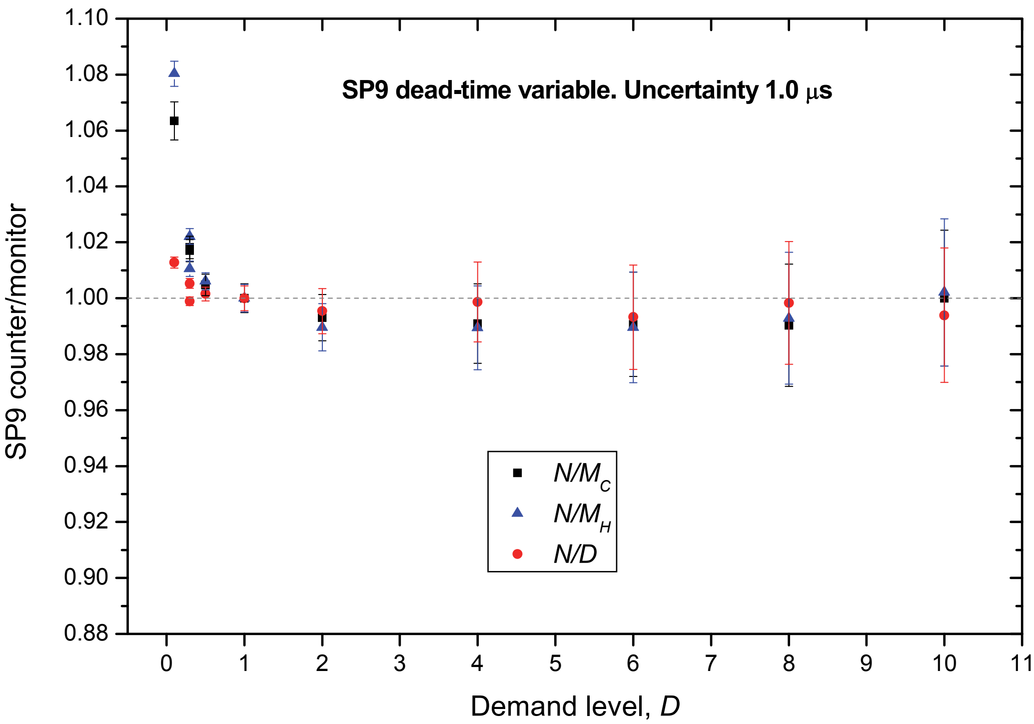

Figure 7. As for Figure 6 but with a variable dead-time.

The optimum value for R_0 was found to be 16000 s^{-1} which resulted in a dead-time of 9.2 μs for a demand of 10 where the SP9 count rate was about 32,000 s^{-1}. For a demand of 0.5 the dead-time was still 7.2 μs. It can be seen that, for this value of R_0, the ratios of the SP9 counts to the various monitor readings are all consistent, within the uncertainties, over the range of demands from 0.5 to 10. This approach has no underlying physical justification. It simply provides a way of performing dead-time corrections which ensure that the ratios of SP9 counts per unit monitor reading have the correct properties as a function of demand level. The assumption of a fixed dead-time of 9.2 μs gave much better overall consistency of the SP9 counts per unit monitor values than a dead-time of 7.2 μs, but not as good consistency as the varying dead-time approach. No reason for the problem with the dead-time of the AIOSAP electronics has yet been discovered. It is possible that it was a result of the combination of the AIOSAP with the width/delay unit used to provide input to the scaler system. Luckily the effect on the final results for the response values is small since the vast majority of the measurements were made at low demand levels where the dead-time corrections are small. To allow for the inexact knowledge of the dead-time an uncertainty of ±1 μs was assigned.

4.4 Data at demand levels of 0.3 or lower

At a demand of 0.1 the ratios of the SP9 counts to the three monitors are inconsistent with the values at higher demand levels, and in view of the problems identified at this demand level when ratios of monitor readings were compared, the single measurement at this demand was not included in the final results.

The data for a demand of 0.3 in Figure 5 and Figure 7, suggest that there may also be a slight problem with the monitoring at this demand level. To investigate this matter results for SP9 counts per unit monitor taken for a demand of 0.3 were compared with data taken at higher demand levels wherever such data were available for a particular detector configuration. Results are shown in Table 2.

Table 2. Ratio of results for SP9 counts, *N*, per unit monitor, *M*, for measurements at a demand of 0.3 to the corresponding results for a demand greater than 0.3.

Configuration	$(N/M)_{D=0.3}/(N/M)_{D>0.3}$		
	FC_C	FC_H	Demand
200 kPa SP9 bare vertical	1.017	1.014	1.001
20 kPa SP9 bare vertical	1.020	1.029	1.007
20 kPa SP9 bare horizontal	1.015	1.019	0.991
Mean value =	1.017	1.021	1.000
Correction factor =	0.991	0.989	1.000
Uncertainty in correction factor =	0.009	0.010	0.009

It appears from Table 2 that $(N/M)_{D=0.3}$ is roughly 2% higher than $(N/M)_{D>0.3}$ for both fission counters, but the ratio $(N/M)_{D=0.3}/(N/M)_{D>0.3}$ is unity within the uncertainties, which are of the order of 1%, when the demand is the monitor. This is a slightly surprising result as both fission chambers would be expected to act as very stable monitors when the fluence rate is changed, whereas the demand value itself is simply a setting for the electronics which controls the overall operation of the thermal pile. Nevertheless, the data point to small problems with the fission chambers at low levels and a correction factor was applied so that the results for *N/M* at a demand of 0.3 were decreased by half the difference between the measured value for $(N/M)_{D=0.3}/(N/M)_{D>0.3}$ and the value expected for a perfect monitor, i.e. unity. The implications that M_C and M_H are low at a demand of 0.3, and are low by roughly the same amount, explains the data for this demand level as shown in Figure 4.

For the cases where the fission chambers were used as monitors uncertainties were assigned to the correction factors which were large enough to cover both the measured value for the ratio and the 'perfect monitor' situation, i.e. a ratio of 1.0. From the data for the demand as monitor it appears that the demand is a good monitor right down to a level of 0.3. The correction factor was therefore unity; however, an uncertainty component was included to cover any possible problems with the demand as monitor and was set to cover the range ratios shown in Table 2.

4.5 Background in the SP9 counters

A check of the background count rates in the two SP9 counters with all neutron-producing equipment switched off revealed an almost zero rate, which was completely negligible compared to the count rates recorded during the measurements. However, with the accelerator beam present in the thermal pile there is the possibility of a neutron background in the room which is not due to deuterons striking the neutron-producing targets in the pile, and which is thus not accurately monitored by the demand level and the fission chambers. One possible mechanism would be from neutron production at the tantalum stop situated where the beam enters the pile, see Figure 1. There must be some deuteron build-up on the tantalum with time. This room background is very difficult to measure, and may vary with the beam current settings. If such a background exists it is likely to be most evident at low count rates in the SP9, and so to investigate its presence the data for the SP9 counts per unit demand have been plotted against demand, see Figure 8. This is essentially the same data as plotted in Figure 7, except that, for clarity, the error bars show only the statistical uncertainties with no contribution for uncertainty in the dead-time.

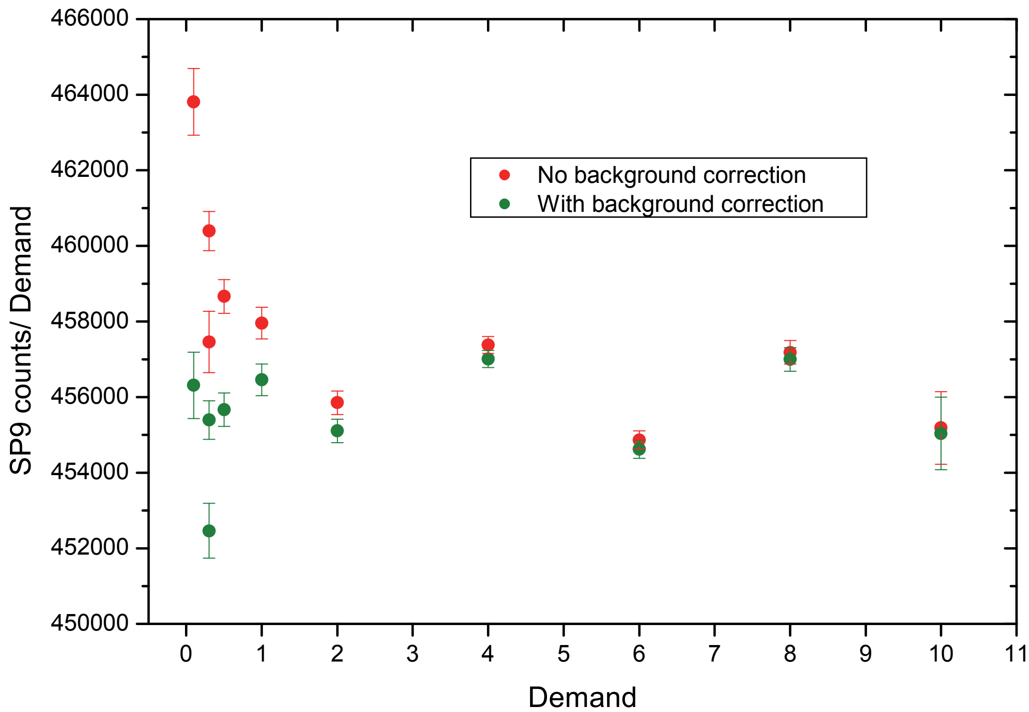

Figure 8. Variation of 200 kPa SP9 counts per unit demand with demand level.

With no background correction the ratio SP9/demand increases as the demand decreases. By applying a background subtraction it was possible to make the ratio reasonably constant as a function of demand. The actual background value was obtained by varying it until the ratio was constant. The effect of this background is small, being of the order of 1% at a demand of 0.3, and becoming a smaller percentage still at higher demands values. (It is evident from Figure 8 that the statistical uncertainty alone is not enough to account for the variations in the ratios as a function of demand and some other component must be present possibly associated with the division of the beam between targets and the tantalum stop.)

The data in Figure 8 indicates the presence of a room background. However, other data do not always support this. Column 4 in Table 2 records ratios of SP9 counts per unit demand for demand levels of 0.3 and levels >3.0. These are reasonably consistent. In one case the value at 0.3 is smaller than at higher demands. In view of the fact that a correction is made for *N/M* at a demand of 0.3 being larger than at higher demands when the fission chambers were used as monitors, see section 4.4, and the fact that most of the data were taken at demands greater than 0.3, no corrections have been made for room background. Nevertheless, an additional uncertainty component of 0.5% has been added to the uncertainty budget to cover possible background effects.

The overall conclusion from the various checks described in section 4 is that, for the highest levels of accuracy, there may be some problems with the monitors at very low demand levels; however, uncertainties have been assigned which allow for these problems.

4.6 Calibration of the monitors

The various investigations of monitor performance indicate that, after the small corrections outlined in section 4.4 have been made to data taken at a demand of 0.3, any of the three monitors can be used with equal validity. (The single datum at a demand of 0.1 is clearly unreliable and was excluded.) For the final results a mean of the data for all three monitors was therefore taken.

As already noted, calibration of the monitors was performed, towards the middle of the measurement campaign, by irradiating a pair of gold foils, one bare and one under cadmium cover. The irradiation was performed for 3 hours at a demand level of 10, and the foil activity determined immediately afterwards. From Figure 4 it can be seen that, although the value for M_C/D was a bit low for the calibration run, there is no valid reason not to accept the results of this calibration for all three monitors. Values for the fluence rates during the monitor calibration and the calibration coefficients, i.e. $\Phi / M_{\Phi i}$, where $M_{\Phi i}$ is the monitor count for monitor *i* during the fluence calibration which gave a fluence value Φ, are given in Table 3. (The index i would be *C* for FC_C, *H* for FC_H and *D* for the demand level.)

Table 3. Values for the fluence rates during the monitor calibration and the fluence per unit monitor for the three monitors.

Quantity	Fluence rate ($cm^{-2}\ s^{-1}$)	Fluence per unit monitor reading $\Phi / M_{\Phi i}$ ($cm^{-2}\ M^{-1}$)		
		FC_C	FC_H	Demand
nv_0	1.495×10^4	3.264	1.113	1494.9
$n_{th}v_0$	1.479×10^4	3.231	1.102	1479.4
$n_m v_0$	1.460×10^4	3.188	1.087	1459.8
$n_{th}\overline{v}_{th}$	1.763×10^4	3.851	1.313	1763.0
$n_m\overline{v}_m$	1.706×10^4	3.726	1.270	1705.9

As a check of the calibration the value obtained for the calibration coefficient for FC_C, was compared with earlier measurements when using gold foils positioned at the height used in this experiment (1.6 m). Monitor FC_C is the one usually employed for irradiations in the thermal column. The results are shown in Table 4 and show very good consistency. Nevertheless, the best value to use for this work is that derived during the present measurement campaign as the fission chamber discriminator setting can vary slightly with time over periods in excess of a few days.

Table 4. Earlier FC_C calibrations with gold foils at a reference height of 1.6 m.

Measurement date	Fluence $n_{th}v_0$ per unit FC_C count ($cm^{-2}\ M^{-1}$)
5th April 2006	3.211
13th June 2006	3.219
19th February 2007 (present measurements)	3.231

4.7 Measurements for the various configurations

The sub sections below give the results for the fluence response of the various detector configurations, for each fluence monitor used, and for two representations of the fluence rate, $\phi_W(th) = n_{th}v_0$ and $\phi(th) = n_{th}\overline{v}_{th}$. For each monitor, *i*, the responses, $R_{\text{W-NPL}i}$ and $R_{\text{NPL}i}$, were calculated using eqs (11) and (12) below

$$R_{\text{W-NPL}i} = \frac{\left(N/M_{Ni} - k^{(\text{Cd})}N^{(\text{Cd})}/M_{Ni}^{(\text{Cd})}\right)}{\left(\Phi_w(th)/M_{\Phi i}\right)} \tag{11}$$

and

$$R_{\text{NPL}i} = \frac{\left(N/M_{Ni} - k^{(\text{Cd})}N^{(\text{Cd})}/M_{Ni}^{(\text{Cd})}\right)}{\left(\Phi(th)/M_{\Phi i}\right)} \tag{12}$$

where:

$R_{\text{W-NPL}i}$	is the response, as measured with monitor *i,* in the sub-cadmium-cut-off Westcott fluence of the NPL thermal column beam,
$R_{\text{NPL}i}$	is the response, as measured with monitor *i,* in the sub-cadmium-cut-off true fluence of the NPL thermal column beam,
N/M_{Ni}	is the bare detector count per monitor *i* count (or reading in the case of the demand as monitor),
$N^{(\text{Cd})}/M_{Ni}^{(\text{Cd})}$	is the detector count per monitor *i* count for the detector under cadmium,
$k^{(\text{Cd})}$	is a correction factor for attenuation of the neutrons above the cadmium-cut-off energy in the cadmium cover,
$\Phi_W(th)/M_{\Phi i}$ and $\Phi(th)$	are the calibration coefficients for monitor *i* for $\phi_W(th)$ and $\phi(th)$.

Values for the cadmium cover correction factor $k^{(Cd)}$ were calculated using the Monte Carlo code MCNP. For both the bare detectors the value was estimated to be 1.000 ± 0.005, and for the detectors within the polyethylene sphere the factor was 0.990 ± 0.005[10].

The values of N/M_{Ni} and $N^{(\text{Cd})}/M_{Ni}^{(\text{Cd})}$ were in most cases derived as a mean of several measurements, sometimes at different demand levels. Uncertainties for the mean values were calculated taking into account statistics (in the SP9 counts and the monitor where applicable), the uncertainty in the dead-time corrections, and those due to the correction for monitoring inconsistency at a demand of 0.3 where necessary. To determine the uncertainties in $R_{\text{W-NPL}i}$ and $R_{\text{NPL}i}$ the uncertainties in N/M_{Ni} and $N^{(\text{Cd})}/M_{Ni}^{(\text{Cd})}$ were combined with those in the relevant $k^{(\text{Cd})}$ factor and those in the monitor counts $M_{\Phi i}$ during the fluence calibration. The aim was to exclude uncertainties that are common to measurements with all three monitors. Thus, the uncertainty in the fluence Φ during the monitor calibration was excluded. The use of mean values for N/M_{Ni} and $N^{(\text{Cd})}/M_{Ni}^{(\text{Cd})}$ from measurements at different demand levels makes it impossible to separate out the dead-time correction uncertainty from the statistical uncertainty in a final uncertainty budget. There is also the fact that the results are correlated because the same SP9 counts are used in the analysis for the three monitors, however, the process described above of deriving mean values for the ratios N/M_{Ni} and $N^{(\text{Cd})}/M_{Ni}^{(\text{Cd})}$ makes this correlation inevitable.

To quantify the level of agreement between results obtained with the different monitors a χ^2/ν value was calculated for each data set using eq. (13):

$$\chi^2/\nu = \sum_{i=1}^{n} \frac{(x_i - \bar{x})^2/\sigma_i^2}{(n-1)} \tag{13}$$

where:

x_i	is the result, $R_{\text{W-NPL}i}$ or $R_{\text{NPL}i}$, derived using a particular monitor,
$\bar{x}$	is the mean result,
σ_i	is the uncertainty in x_i, and
n	is the number of results, 3 in this case.

For each configuration, averaged responses $R_{\text{W-NPL}}$ and R_{NPL}, derived from a weighted mean of the responses $R_{\text{W-NPL}i}$ and $R_{\text{NPL}i}$ obtained with the three monitors, are presented. The uncertainty σ_m quoted for the mean is the larger of the values obtained from the spread of the results as derived from eq. (14):

$$\sigma_m = \sqrt{\frac{\sum_{i=1}^{n}(x_i - \bar{x})^2 w_i}{(n-1)\sum_{i=1}^{n} w_i}} \tag{14}$$

or from the value obtained by combining the individual uncertainties using eq. (15):

$$\sigma_m = \sqrt{1\Big/\sum_{i=1}^{n} w_i} \tag{15}$$

where:

w_i	is the weight for each response given by $w_i = 1/\sigma_i^2$.

Because the SP9 counts are common to all three $R_{\mathrm{NPL}i}$ values there are correlations in the data for which allowance should in principle be made. The SP9 counting uncertainties are, however, small and in view of the rather pessimistic approach outlined above of taking the largest value from eqs (14) and (15), it was felt that the correlations could be neglected.

4.7.1 200 kPa SP9, parallel to the beam, no polyethylene moderator sphere

For this configuration bare detector measurements were performed at 10 different demand levels covering the range from 0.1 to 10, although the datum at a demand of 0.1 was not included in the final results. The mean values for the three monitors are shown in Table 5. All the results have been corrected for the response to epi-cadmium neutrons via a cadmium-cover measurement. However, this measurement was made at a demand of 0.3 so required a small correction (see section 4.4).

The results for the three monitors are completely consistent within the uncertainties quoted in Table 5. A value of 0.4 was obtained for the χ^2/ν defined in eq. (13).

Table 5. Results for 200 kPa SP9, parallel to the beam, no polyethylene moderator.

Monitor	Response $R_{\mathrm{W\text{-}NPL}i}$ to the sub-cadmium fluence in the Westcott convention $n_{th}v_0$ (cm^2)	Response $R_{\mathrm{NPL}i}$ to the true sub-cadmium fluence $n_{th}\overline{v}$ (cm^2)
FC_C	3.020 ± 0.36%	2.534 ± 0.36%
FC_H	3.017 ± 1.1%	2.532 ± 1.1%
Demand	3.032 ± 0.29%	2.544 ± 0.29%
Weighted mean	3.0269 ± 0.22%	2.5399 ± 0.22%

4.7.2 200 kPa SP9, perpendicular to the beam, no polyethylene moderator sphere

Five measurements were performed with the counter bare for this configuration and 4 with it under cadmium. All measurements were made at a demand of 0.3 and appropriate corrections were made for the monitor inconsistency at this demand (see section 4.4). As can be seen from Table 6, there is extremely good agreement between the three monitors with a χ^2/ν value of 0.2.

For this configuration results were also obtained, at a demand level of 0.3, using NPL electronics for the SP9 counter. The values for the responses were 1.0% higher when averaged over the three monitors and the derived uncertainty was 0.61%. The difference is thus within the uncertainties quoted. Furthermore, the measurements were made five days apart, so there may be additional uncertainties, e.g. for variation in the calibration of the monitors with time, which should be added to the values quoted above of 0.61% for the NPL electronics and 0.57% for the AIOSAP electronics.

Table 6. Results for 200 kPa SP9, perpendicular to the beam, no polyethylene moderator.

Monitor	Response $R_{\text{W-NPL}i}$ to the sub-cadmium fluence in the Westcott convention $n_{th}v_0$ (cm^2)	Response $R_{\text{NPL}i}$ to the true sub-cadmium fluence $n_{th}\overline{v}$ (cm^2)
FC_C	3.303 ± 0.82%	2.771 ± 0.82%
FC_H	3.273 ± 1.4%	2.746 ± 1.4%
Demand	3.290 ± 0.95%	2.760 ± 0.95%
Weighted mean	3.293 ± 0.57%	2.763 ± 0.57%

The cadmium ratio for measurements with the bare 200 kPa SP9 counter was about 65 for both parallel and perpendicular orientations of the counter relative to the beam

4.7.3 SP9 20 kPa parallel to the beam no polyethylene moderator sphere

For this configuration measurements of the bare SP9 detector were made at demands of 0.3 and 3.0, and an under-Cd measurement at a demand of 3.0. The data at a demand of 0.3 were corrected as described in section 4.4 and an average taken of all the measurements. The results are given in Table 7. No measurements were made with NPL electronics. This is a data set for which agreement between the results using the three different monitors was relatively poor, with a χ^2/ν value of 1.8. However, the uncertainty in the mean value was taken from the spread of the results so allowance for the spread is made in the quoted uncertainty.

Table 7. Results for 20 kPa SP9, parallel to the beam, no polyethylene moderator.

Monitor	Response $R_{\text{W-NPL}i}$ to the sub-cadmium fluence in the Westcott convention $n_{th}v_0$ (cm^2)	Response $R_{\text{NPL}i}$ to the true sub-cadmium fluence $n_{th}\overline{v}$ (cm^2)
FC_C	0.3662 ± 0.32%	0.3073 ± 0.32%
FC_H	0.3627 ± 1.1%	0.3043 ± 1.1%
Demand	0.3684 ± 0.24%	0.3091 ± 0.24%
Weighted mean	0.3675 ± 0.25%	0.3083 ± 0.25%

4.7.4 SP9 20 kPa perpendicular to the beam no polyethylene moderator sphere

Measurements were performed at demand levels of 0.3 and 3.0, and after correction of the lower demand level data mean values were derived. The results are shown in Table 8. Again the χ^2/ν value was high at 2.1, but allowance has been made for this in the uncertainty quoted for the mean which was derived from the spread of the results.

Table 8. Results for 20 kPa SP9, perpendicular to the beam, no polyethylene moderator.

Monitor	Response $R_{\text{W-NPL}i}$ to the sub-cadmium fluence in the Westcott convention $n_{th}v_0$ (cm^2)	Response $R_{\text{NPL}i}$ to the true sub-cadmium fluence $n_{th}\overline{v}$ (cm^2)
FC_C	0.3918 ± 0.31%	0.3287 ± 0.31%
FC_H	0.3872 ± 1.1%	0.3248 ± 1.1%
Demand	0.3943 ± 0.29%	0.3308 ± 0.29%
Weighted mean	0.3929 ± 0.30%	0.3296 ± 0.30%

Measurements made with NPL electronics, at a demand level of 3.0, gave results which were 0.62% lower. The measured uncertainty in these results was 0.25% and in view of the 0.25% uncertainty in the results with the AIOSAP electronics the two measurements almost agree within the uncertainties. However, the measurements were made on different days, so there will be additional uncertainty components.

The cadmium ratio for measurements with the bare 20 kPa SP9 counter was about 82 for both parallel and perpendicular orientations of the counter relative to the beam.

4.7.5 SP9 200 kPa parallel to the beam with polyethylene moderator sphere

The measurements were performed at a demand level of 0.5 and the results are shown in Table 9. There was remarkable agreement between the values obtained with the three different monitors and the χ^2/ν value was 0.4.

Table 9. Results for 200 kPa SP9, parallel to the beam, with polyethylene moderator.

Monitor	Response $R_{\text{W-NPL}i}$ to the sub-cadmium fluence in the Westcott convention $n_{th}v_0$ (cm^2)	Response $R_{\text{NPL}i}$ to the true sub-cadmium fluence $n_{th}\overline{v}$ (cm^2)
FC_C	1.5429 ± 0.55%	1.2946 ± 0.55%
FC_H	1.528 ± 1.1%	1.282 ± 1.1%
Demand	1.5439 ± 0.43%	1.2955 ± 0.43%
Weighted mean	1.5422 ± 0.32%	1.2940 ± 0.32%

When NPL electronics were used, again at a demand level of 0.5, the results were 0.62% higher with excellent agreement for the three monitors and an overall uncertainty of 0.38%. The difference between the results with NPL electronics and AIOSAP electronics is thus within the uncertainties quoted here.

4.7.6 SP9 200 kPa perpendicular to the beam with polyethylene moderator sphere

For this measurement, as for the previous measurement with the polyethylene sphere, a demand level of 0.5 was used for both the total and under-cadmium measurement, and the results are shown in Table 10. The χ^2/ν value was 0.3. No measurements were made with NPL electronics.

Table 10. Results for 200 kPa SP9, perpendicular to the beam, with polyethylene moderator.

Monitor	Response $R_{\text{W-NPL}i}$ to the sub-cadmium fluence in the Westcott convention $n_{th}v_0$ (cm^2)	Response $R_{\text{NPL}i}$ to the true sub-cadmium fluence $n_{th}\bar{v}$ (cm^2)
FC_C	1.580 ± 0.79%	1.325 ± 0.79%
FC_H	1.562 ± 1.2%	1.310 ± 1.2%
Demand	1.574 ± 0.77%	1.320 ± 0.77%
Weighted mean	1.5741 ± 0.50%	1.3208 ± 0.50%

The cadmium ratio for measurements with the 200 kPa SP9 counter in the moderator was 3.9 for both parallel and perpendicular orientations of the counter relative to the beam.

4.7.7 SP9 20 kPa parallel to the beam with polyethylene moderator sphere

Results for measurements in this configuration are shown in Table 11. Measurements were made with AIOSAP electronics and NPL electronics all at a demand level of 3.0. The χ^2/ν value for the AIOSAP measurements was 1.5, but nevertheless the uncertainty on the final weighted mean, calculated from the spread of the data, was still only 0.30%

Table 11. Results for 20 kPa SP9, parallel to the beam, with polyethylene moderator.

Monitor	Response $R_{\text{W-NPL}i}$ to the sub-cadmium fluence in the Westcott convention $n_{th}v_0$ (cm^2)	Response $R_{\text{NPL}i}$ to the true sub-cadmium fluence $n_{th}\bar{v}$ (cm^2)
FC_C	0.2536 ± 0.38%	0.2128 ± 0.38%
FC_H	0.2530 ± 1.2%	0.2123 ± 1.2%
Demand	0.2558 ± 0.34%	0.2146 ± 0.34%
Weighted mean	0.2547 ± 0.30%	0.2137 ± 0.30%

The results with the NPL electronics were on average 5.2% higher. This is a long way outside the measurement uncertainties and a review of the data revealed no obvious reason for this difference. However, some support for the AIOSAP results, and a reason to suspect those obtained with the NPL electronics, can be derived from a comparison with the results (4.7.8) for the 20 kPa SP9 counter in the moderator sphere with the SP9 counter perpendicular to the beam rather than parallel. The results obtained with the AIOSAP electronics for these two configurations are only 0.8% different. A similar comparison for the 200 kPa counter gave a difference of 1.5% between perpendicular and parallel. Because of the moderation in the sphere these configurations would not be expected to give significantly different results so the similarity of the results with the AIOSAP electronics suggests that there were no problems with these measurements.

4.7.8 SP9 20 kPa perpendicular to the beam with polyethylene moderator sphere

Table 12 shows the results for measurements with this configuration. Measurements were only made with AIOSAP electronics, all at a demand level of 3.0. The χ^2/ν value was 1.3, and the uncertainty on the final weighted mean, calculated from the spread of the data, was 0.29%

Table 12. Results for 20 kPa SP9, perpendicular to the beam, with polyethylene moderator.

Monitor	Response $R_{\text{W-NPL}i}$ to the sub-cadmium fluence in the Westcott convention $n_{th}v_0$ (cm^2)	Response $R_{\text{NPL}i}$ to the true sub-cadmium fluence $n_{th}\overline{v}$ (cm^2)
FC_C	0.2556 ± 0.39%	0.2144 ± 0.39%
FC_H	0.2553 ± 1.2%	0.2142 ± 1.2%
Demand	0.2576 ± 0.34%	0.2162 ± 0.34%
Weighted mean	0.2567 ± 0.29%	0.2154 ± 0.29%

The cadmium ratio for measurements with the 20 kPa SP9 counter in the moderator was 4.3 for both parallel and perpendicular orientations of the counter relative to the beam.

4.8 Summary of the analysis

In general the results obtained using the three different monitors agreed within the uncertainties. The average value of χ^2/ν was almost exactly 1.0 although it might be expected to be slightly lower in view of the correlations introduced by the fact that the SP9 counts were common in all cases.

An inspection of the average values of the differences between the results for a particular monitor and the mean for all three revealed that, for the AIOSAP electronics, the results with FC_H were on average 0.79% below the mean, and in all cases were the lowest result. However, there is a relatively large uncertainty (~1%) in $M_{\Phi i}$ for this monitor, caused by the large, 15%, dead-time correction during the fluence calibration. Overall, the three data sets still agree as well as could be expected in view of the uncertainties. For the other two monitors the results are sometimes larger and sometimes smaller than the mean as would be expected on the basis of statistics. The results for the NPL electronics were more consistent with a χ^2/ν of only 0.4, so the evidence for an error in $M_{\Phi i}$ for monitor FC_H is not conclusive and results for all three monitors were retained.

5 RESULTS

5.1 Correction for the results in a Maxwellian distribution with *kT* = 25.3 meV

No two thermal fields are ever likely to be exactly the same, particularly when, as in the present comparison exercise, they are produced in a variety of different ways. For this reason the organisers of the comparison have requested that: “The participants shall determine the response R_{ref} of the counters for a homogeneous unidirectional irradiation with neutrons with a Maxwellian fluence distribution $\Phi_E^{(\mathrm{ref})}$ characterised by a temperature parameter $kT = 25.3$ meV”. The reference Maxwellian field is described by the expression:

$$\frac{\Phi_E^{(ref)}\,\mathrm{d}E}{\Phi^{(ref)}} = \left(\frac{E}{kT}\right)\exp\left(-\frac{E}{kT}\right)\frac{\mathrm{d}E}{kT} \qquad (16)$$

where:

- $\Phi_E^{(ref)}$ is the fluence at neutron energy E,
- $\Phi^{(ref)}$ is the total fluence in the distribution,
- k is Boltzmann’s constant, and
- T is the temperature of the Maxwellian, $T = 20.4^{\circ}$C for $kT = 25.3$ meV.

The beam from the thermal column is sufficiently plane-parallel to satisfy the requirement of being unidirectional, but the results still need to be corrected to those which would have been obtained in the designated reference spectrum.

The spectrum Φ_E in the NPL thermal column field, in the region below the cadmium cut-off energy, can be expressed[11] as :

$$\frac{\Phi_E \mathrm{d}E}{\Phi} = C_M\left(\frac{E}{kT}\right)\exp\left(-\frac{E}{kT}\right)\frac{\mathrm{d}E}{kT} + C_{1/E}\,\frac{1}{\ln(E_{Cd}/E_{\Delta})}\frac{\mathrm{d}E}{E}\Delta \qquad (17)$$

where:

- C_M is the fraction of the total sub-cadmium fluence in the Maxwellian peak,
- $C_{1/E}$ is the fraction of the total sub-cadmium fluence with a $1/E$ distribution,
- E_{Cd} is the cadmium cut-off energy,
- E_{Δ} is the lower energy limit of the $1/E$ distribution, and
- Δ is a function which is 1 between E_{Δ} and E_{Cd} and 0 outside this region.

Both the expression for the Maxwellian and the $1/E$ distribution are normalised to unity so the fractions of the fluence in the two distributions are given by the factors C_M and $C_{1/E}$. The values of these factors, and of the effective temperature T, were derived from gold foil measurements, and were:

$C_{1/E} = 0.0324$
$C_M = (1 - C_{1/E}) = 0.9676$
$T = 22.6^{\circ}$C above the temperature of the moderator, thus $kT = 27.2$ meV.

Using equations (16) and (17) the correction factor k_1 for the spectral distribution can be calculated for any instrument with response function *r(E)* from:

$$k_1 = \frac{\int_0^\infty \Phi_E^{(ref)} / \Phi^{(ref)} \, r(E) \mathrm{d}E}{\int_0^{E_{Cd}} \Phi_E / \Phi \, r(E) \mathrm{d}E} \tag{18}$$

A FORTRAN program was written to calculate the correction factors for the various configurations using NAG Library routines(12) to perform the integrations. Response functions were provided by the comparison organiser for all four detector configurations used. The results of the calculations are presented in Table 13. No indication was given whether these response functions were calculated for neutron incidence parallel to the stem of the SP9 detector or perpendicular to the stem. In view of the relatively small size of the k_1 corrections this detail is assumed unimportant.

Table 13. Factors k_1 used to correct measured responses to those expected in a pure room-temperature Maxwellian distribution.

Configuration	Response to actual sub-cadmium field	Response in Maxwellian with kT = 25.3 meV	Factor k_1 = Ratio Pure Maxwellian / Actual field
SP9 200 kPa no moderator	0.840	0.868	1.042 ± 0.012 (1.2%)
SP9 20 kPa no moderator	0.834	0.862	1.053 ± 0.016 (1.5%)
SP9 200 kPa with moderator	1.255	1.297	0.955 ± 0.011 (1.1%)
SP9 20 kPa with moderator	1.264	1.307	0.956 ± 0.011 (1.1%)

The uncertainties presented in Table 13 for k_1 were derived by repeating the calculations for this correction factor with the effective temperature of the Maxwellian peak changed by 11°C, which is the estimated uncertainty in this quantity. The correction is also sensitive to the value derived for the fraction, $C_{1/E}$, of the sub-cadmium cut-off fluence with a $1/E$ dependence, and on the value chosen for the parameter, μ, which defines the lower limit, $E_\Delta=\mu kT$, of the $1/E$ component. However, the uncertainty in k_1 due to the uncertainties in $C_{1/E}$ and μ are negligible compared to those due to the uncertainty in the effective temperature.

Figure 9 illustrates the differences in the spectral distributions, and also shows the shapes of the response functions. The different slopes of the response functions for the bare SP9 counters compared to the response functions for the counters within a moderator explain why the values for k_1 are sometimes greater than 1.0 and sometimes less than 1.0. The response function shape for the 20 kPa SP9 counter in the moderator is almost identical to that for the 200 kPa SP9 counter in the moderator and so is not shown.

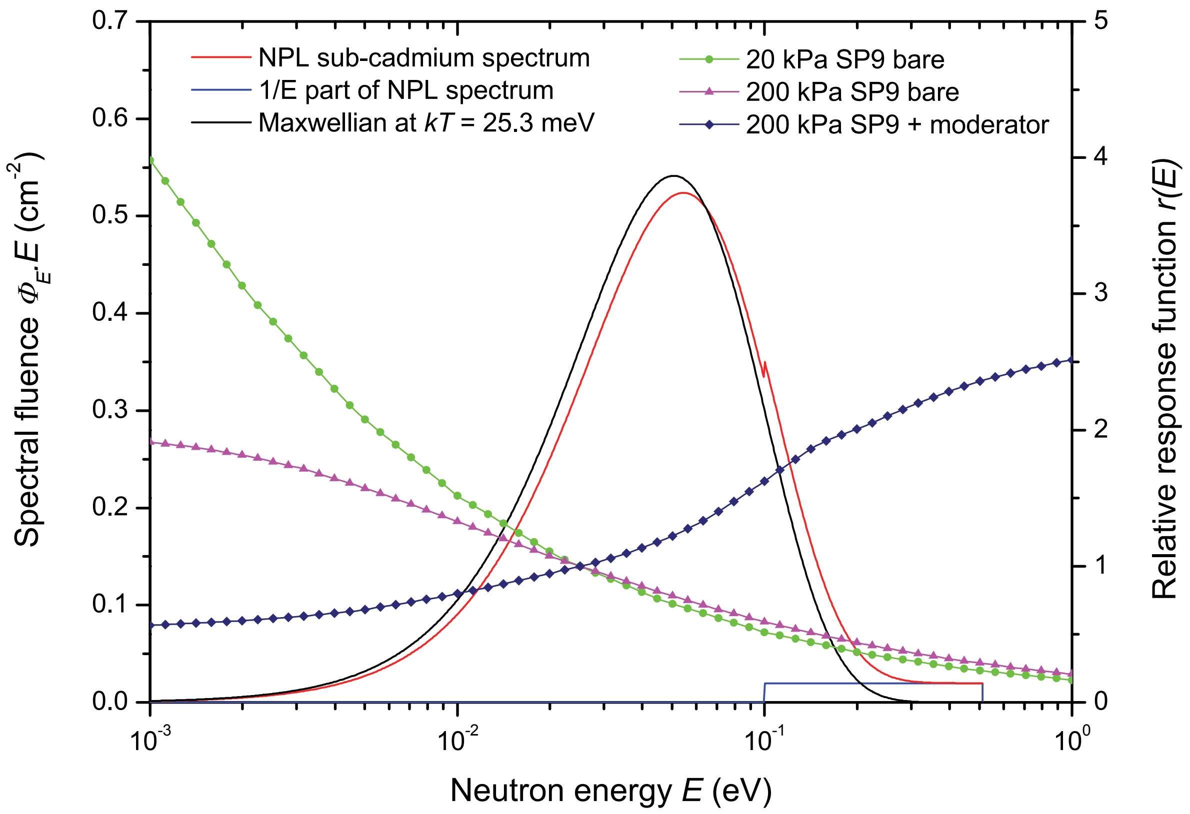

Figure 9. Comparison of the NPL sub-cadmium fluence spectrum with a room-temperature Maxwellian peak. Also illustrated are the response functions used to calculate the correction factors k_1. Note that the response functions have been normalised to unity at 25.3 meV.

5.2 Final results

To obtain the final estimates of the responses in the designated reference field, consisting of a Maxwellian with $kT = 25.3$ meV, the measured responses were multiplied by the relevant k_1 factor from Table 13 to give R_{ref} values.

$$R_{\mathrm{ref}} = k_1 \cdot R_{\mathrm{NPL}} \tag{19}$$

The results are presented in Table 14. Without information from the other participants in the exercise there are only minor comments which can be made about the results. Table 15 compares ratios of R_{NPL} values, for irradiation perpendicular to the beam to those for irradiation parallel to the beam, for the different configurations. The result for the counter perpendicular to the beam is always the larger of the two. For the bare detector this is presumably because of attenuation in the ‘top-hat’ structure on the opposite side of the spherical counter to the stem (see Fig. 1 in the Appendix to the protocol). For the 200 kPa counter the effect is (8.1 ± 0.5)%, and for the 20 kPa counter it is (6.8 ± 0.4)%. The effect is marginally larger for the 200 kPa counter, possibly because of the presence of ^{3}He in the top-hat structure and the higher gas pressure in this counter. The effect when the counters are enclosed in the polyethylene moderator is much smaller. For the 200 kPa counter the effect is (1.5 ± 0.6)%, and for the 20 kPa counter it is (0.8 ± 0.4)%. The reason for the effect is presumably the same although much reduced because of scatter in the moderating sphere.

Table 14. Final results for the responses of the SP9 counters in the eight different configurations measured. The uncertainties are explained in section 5.3**.**

Configuration	Response, R_{NPL}, to the NPL sub-cadmium thermal field $n_{th}\overline{v}_{th}$	Response, R_{ref}, in a Maxwellian with $kT = 25.3$ meV
200 kPa SP9 parallel to the beam no polyethylene moderator	2.540 ± 0.062(2.4%)	2.647 ± 0.072(2.7%)
200 kPa SP9 perpendicular to the beam no polyethylene moderator	2.763 ± 0.067(2.4%)	2.879 ± 0.078(2.7%)
20 kPa SP9 parallel to the beam no polyethylene moderator	0.3083 ± 0.0074(2.4%)	0.3246 ± 0.0092(2.8%)
20 kPa SP9 perpendicular to the beam no polyethylene moderator	0.3296 ± 0.0080(2.4%)	0.3471 ± 0.0099(2.8%)
200 kPa SP9 parallel to the beam with polyethylene moderator	1.294 ± 0.031(2.4%)	1.236 ± 0.033(2.7%)
200 kPa SP9 perpendicular to the beam with polyethylene moderator	1.321 ± 0.032(2.5%)	1.261 ± 0.034(2.7%)
20 kPa SP9 parallel to the beam with polyethylene moderator	0.2137 ± 0.0052(2.4%)	0.2043 ± 0.0054(2.7%)
20 kPa SP9 perpendicular to the beam with polyethylene moderator	0.2154 ± 0.0052(2.4%)	0.2059 ± 0.0054(2.7%)

Table 15. Ratios of count rates, R_{NPL} values, for irradiation perpendicular to the beam to those for irradiation parallel to the beam.

Configuration	Ratio of detector response for irradiation perpendicular to the stem and parallel to the stem
200 kPa SP9 bare	1.0808 ± 0.0055(0.51%)
200 kPa SP9 in polyethylene moderator	1.0154 ± 0.0060(0.59%)
20 kPa SP9 bare	1.0682 ± 0.0043(0.40%)
20 kPa SP9 in polyethylene moderator	1.0077 ± 0.0042(0.42%)

One of the reasons for performing measurements with the SP9 detectors bare and within the polyethylene moderator was to obtain information about the mean energy of the neutron distribution. Data for the NPL measurements are given in Table 16. For both the 200 kPa and the 20 kPa detectors the ratio of the bare response to that in the moderator is about 6% higher for the detector perpendicular to the beam than it is for the detector parallel to the beam. This simple reflects the effect of the top-hat structure which reduces the response by about 6% more when the counter is bare than when it is in the moderator – see Table 15.

Table 16. The ratio of a bare SP9 detector response to that of the corresponding counter in the polyethylene moderating sphere for the responses, R_{NPL}, as determined in the NPL thermal column field.

Configuration	Ratio bare detector response to response in moderator sphere
200 kPa SP9 parallel to the beam	1.963 ± 0.013(0.68%)
200 kPa SP9 perpendicular to the beam	2.089 ± 0.030(1.4%)
20 kPa SP9 parallel to the beam	1.4427 ± 0.059(0.41%)
20 kPa SP9 perpendicular to the beam	1.5293 ± 0.063(0.41%)

5.3 Uncertainties

The model equation linking the measured quantities to the final value for the response can be written, c.f. eqs (11) and (19) as:

$$R_{\mathrm{ref}} = k_1 \cdot k_2 \cdot k_3 \cdot R_{\mathrm{NPL}} = k_1 \cdot k_2 \cdot k_3 \cdot \frac{f(N, M_{Ni(i=1\to 3)}, k^{(\mathrm{Cd})}, N^{(\mathrm{Cd})}, M^{(\mathrm{Cd})}_{Ni(i=1\to 3)}, M_{\Phi i(i=1\to 3)})}{\Phi(th)} \quad (20)$$

The term $f(N, M_{Ni(i=1\to 3)}, k^{(\mathrm{Cd})}, N^{(\mathrm{Cd})}, M^{(\mathrm{Cd})}_{Ni(i=1\to 3)}, M_{\Phi i(i=1\to 3)})$ obviously presents a challenge for uncertainty analysis with the contributions to the uncertainties in the input quantities deriving from statistics and dead-time corrections for several measurements at different counting rates. However, these have been combined in the analysis procedure described in section 4.7 to give the uncertainty estimates presented for R_{NPL} in Table 5 to Table 12. Note that the uncertainties in these tables do not include the uncertainty in the fluence *Φ(th)* derived from gold foil measurements during the monitor calibration.

The various k_i values represent corrections to the original measurements all of which are assigned uncertainties although the actual value of k_i may be 1.0. The factor k_1 relates to the correction of the results to what they would have been in a pure Maxwellian spectrum with $kT = 0.0253$ meV, i.e. the factor converting R_{NPL} to R_{ref}. Values are given in Table 13.

A factor k_2 has been included to allow for variations of the fluence per unit monitor reading between the calibration measurement at high demand and the measurements with the SP9 counters, most of which were at a low demand level. As there was no direct evidence of any difference, the value of k_2 was set to 1.0, but with an uncertainty of 1% was applied derived from a review of the stability of the monitors as a function of demand, c.f. section 4.2.

There is evidence from measurements over the years that the calibration of the monitors varies from day to day. Since only one fluence calibration was performed a factor k_3 is included to allow for day to day variations of the monitor calibrations. The standard deviation of monitor calibration values measured over the period from 1999 to 2007, for a height of 1.6 m in the column, is 1.8%. The variations seen over a period of a few days are expected to be smaller than those seen over periods of years. Also, some of the measurements were performed on the same day as the fluence calibration. A value of 1% has therefore been assigned to the uncertainty in k_3 which, as with k_2, is assigned a value of 1.0.

Since the terms in eq. (20) are combined by either multiplication or division the standard uncertainty in the final response can be derived by adding the components for the different terms in quadrature, and the actual values are presented in Table 17. The assumption is made that the various uncertainty components have a normal distribution.

6 CONCLUSIONS

Measurements have been performed of the thermal responses for the two SP9 proportional counters circulated for CCRI key comparison K8. One detector has a gas filling of 200 kPa of ^{3}He and the other 20 kPa. The responses were measured in a number of configurations; specifically with the stem parallel to the NPL thermal column beam and with it perpendicular to the beam, both for the bare detectors and for these detectors in a 7.62 cm diameter polyethylene moderator. Corrections for epi-thermal neutrons were derived from measurements performed using cadmium covers. The final results have been corrected to the values which would be expected in a pure Maxwellian thermal distribution with $kT = 25.3$ meV. For many of the configurations the results with the AIOSAP electronics provided for use in the exercise were found to agree with results obtained using the type of NIM electronics conventionally used with proportional counters at NPL.

Until the results of the comparison exercise are published no conclusions can be drawn about the accuracy of the results. However, the data as presented in Table 14 show some expected features. For example the results for the bare detectors perpendicular to the beam are always higher than the results for the detectors parallel to the beam as expected because of the feature on the opposite side of the spherical SP9 detector to the stem which attenuates the thermal neutron beam. This effect is very much less evident for the detectors in the moderating sphere because of the numerous thermal neutron scattering events within the polyethylene.

The fact that the response of the 200 kPa detector is only about 8.3 times higher than that of the 20 kPa detector, rather than 10 times, is understandable since the 200 kPa detector is sufficiently efficient that response does not increase linearly with pressure in this pressure region.

The fact that the dead-time of the AIOSAP electronics appeared not to be constant with rate was unexpected, and no reason for this has yet been discovered. It is possible that it was a result of the combination of electronic units used with the AIOSAP to provide input to the scaler system. Fortunately, the effect on the final results is not an issue because the vast majority of the measurements were performed at low count rates where the dead-time correction was small. It is, however, an effect which should be investigated when next the equipment is available.

Acknowledgements
The authors would like to thank Andrew Bennett and Sarb Cheema for running the Van de Graaff during the measurements, and Neil Roberts for calculations of neutron attenuation in cadmium covers. The work was funded by the UK National Measurement System Policy Unit of the Department for Innovation, Universities and Skills.

Table 17. Uncertainty components and combined uncertainties. Note all quoted values are standard uncertainties (σ = 1) providing a confidence level of approximately 67% (k=1).

Uncertainty component	Component value	Uncertainty
Counting statistics in beta counting	-	0.2%
Fluence variations during fluence calibration	-	0.1%
Decay effects during gold foil counting	-	0.1%
Dead-time corrections in beta counting	-	0.1%
Reference beta counting efficiency ε_β	~ 0.4	0.3%
Correction to beta counting efficiency for column neutrons K	~ 1.05	0.4%
Gold capture cross section, σ_0	98.69 b	0.2%
Thermal self-shielding factor G_t	0.9843	0.3%
Departure of gold cross section from $1/v$ dependence g	1.0046	0.1%
Cadmium attenuation correction F	1.01	0.1%
Maxwellian effective temperature T	22.6°C	0.3%
Foil mass	~ 96 mg	0.1%
Height of gold foil and of SP9 detectors	1.6 m	0.3%
Combined uncertainty in the Westcott fluence $n_{th}v_0$		**0.8%**
Effect of uncertainty in T on going from $n_{th}v_0$ to $n_{th}\overline{v}_{th}$	-	1.7%
Relative intensity of epithermal component r	~ 0.02	0.1%
Uncertainty in Westcott cut-off parameter μ	3.681	0.2%
Combined uncertainty in the true fluence $n_{th}\overline{v}_{th}$		**1.9%**
Variation of the fluence with demand k_2	1.0	1.0%
Variation of monitor calibration with time (days) k_3	1.0	1.0%
Combined uncertainty in the response values R_{NPL}*		**2.4%**
Correction to results in a pure Maxwellian spectrum k_1	0.955 - 1053	1.1% - 1.5%
Combined uncertainty in the response values R_{ref} *		**2.6% - 2.8%**

* Note: these uncertainties exclude counting statistics and dead-time for the SP9 counter and monitors, and the uncertainty in $k^{(\mathrm{Cd})}$. These differ for each measured response, varying from 0.2% to 0.5%.

REFERENCES

1 C.H. Westcott, W.H. Walker, and T.K. Alexander, *Effective cross sections and cadmium ratios for the neutron spectra of thermal reactors,* Proceedings of the Second United Nations international conference on the peaceful uses of atomic energy, Vol. 16 Nuclear data and reactor theory, (UN, Geneva, 1958).

2 E.J. Axton, *Absolute measurement of the neutron flux density in the A.E.R.E reactor GLEEP,* J. of Nucl. Energy Parts A/B 17, 125-135, 1963.

3 S.J. Boot, *Calibration of reference thermal and epithermal neutron flux densities from the GLEEP reactor at AERE Harwell,* Nucl. Inst. and Meths. 164, 513-519, 1979.

4 D.J. Thomas and N. Soochak, *Determination of the ^{3}He number density for the proportional counter used in the NPL Bonner sphere system,* NPL Report RS(EXT)104, (NPL, Teddington, July 1988).

5 T.B. Ryves and E.B. Paul, *The Construction and Calibration of a Standard Thermal Neutron Flux Facility at the National Physical Laboratory*, J. Nucl. Energ. 22(12), 759-775, 1968.

6 A.D. Carlson, W.P. Poenitz, G.M. Hale, R.W. Peelle, D.C. Dodder, C.Y. Fu, and W. Mannhart, *The ENDF/B-VI Neutron Cross Section Measurement Standards,* NIST Report NISTIR 5177, National Institute of Standards and Technology, Gaithersburg, MD, USA, 1993.

7 P. Kolkowski and D.J. Thomas, Measurement of the fast neutron component in the beam of the NPL thermal neutron column using a Bonner sphere spectrometer, NPL Report CIRM 28, (NPL, Teddington, May 1999).

8 K.W. Geiger and L. van der Zwan, *Slowing Down Spectrum and Neutron Temperature in a Thermal Neutron Flux Density Standard,* Metrologia, 2, 1-5, 1966.

9 David J. Thomas and Peter Kolkowski, *Thermal fluence and dose equivalent standards at NPL,* NPL Report DQL RN008, March 2005

10 N.J. Roberts, NPL, private communication.

11 D.J. Thomas and N. Soochak, *Determination of the ^{3}He number density for the proportional counter used in the NPL Bonner sphere system*, NPL Report RS(EXT)104, July 1988.

12 http://www.nag.co.uk/

Appendix A: Protocol

CCRI(III)-K8: Key Comparison for Thermal Neutron Fluence Measurements

Comparison Protocol

Introduction

Reference facilities for the fluence of thermal neutrons have been constructed in several ways. Designs based on thermal columns or neutron guides at fission reactors and moderation of fast neutrons produced by accelerators or radionuclide sources have been employed. The details of the phase space density of neutrons at such facilities may differ significantly. In particular, the angular distribution may vary from almost isotropic to unidirectional. Furthermore, the spectral distribution can deviate from a Maxwellian or correspond to a temperature different from that of the moderator. Also the contamination of the thermal beam or field with epithermal neutrons above the cadmium threshold is related to details of the construction of the facility.

To reveal differences in the characteristics of the facilities participating in a comparison of thermal fluence measurements, a transfer instrument, or combination of instruments, is required that is sensitive to the actual spectral distribution. Therefore a comparison is proposed which uses transfer instruments with opposite energy dependency of their response, i.e. one or more instruments for which the response decreases with neutron energy and one or more instruments with increasing response over the thermal region. Basically, the ratio of the responses of two such instruments can be used as an indicator to assess the temperature parameter kT of the spectral distribution.

Transfer Instruments and Ancillary Equipment

The pilot laboratory will provide two spherical proportional counters filled with ^{3}He as transfer instruments.

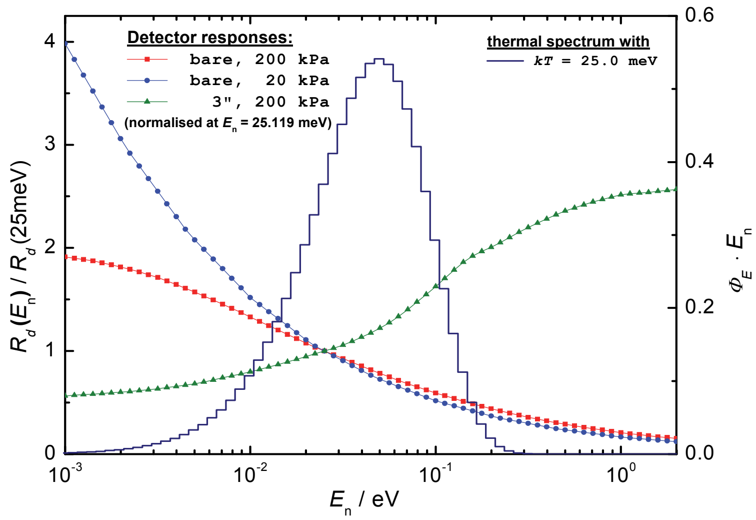

Fig. 1 Relative response $r(E) = R(E)/R(E_{ref})$ for the three transfer instruments as calculated with MCNP (left axis) for $E_{ref} = 25.119$ meV. Also shown is the relative Maxwellian spectral fluence distribution for $kT = 25$ meV (right axis). The responses for the bare counters and the counter in moderator sphere were calculated using MCNP for a parallel beam incident perpendicular and parallel to the symmetry axis, respectively.

The counters are of the CENTRONIC SP9 type and have nominal ^{3}He pressures of 20 kPa and 200 kPa, respectively. In addition, a spherical polyethylene (PE) moderator, 7.62 cm (3") in diameter, is provided to modify the energy dependence of the response of the 200 kPa counter. Therefore three transfer devices are available for the comparison exercise. The selection of the most appropriate bare counter will be made by the participant based on count rate considerations. If possible, all three instruments should be used. The participants are also encouraged to use the 20 kPa counter with the PE moderator if the count rate is sufficient.

The relative response $r(E) = R(E)/R(E_{\mathrm{ref}})$ for $E_{\mathrm{ref}} = 25.3$ meV, as calculated using MCNP [1], is shown in Fig. 1 for the two bare counters and the 200 kPa counter in the 3" PE moderator. The responses $R(E_{\mathrm{ref}})$ for the bare 200 kPa counter, the bare 20 kPa counter and the 200 kPa counter in the 3" PE moderator sphere are about 3 cm^2, 0.4 cm^2 and 1 cm^2, respectively (these numbers are meant for count rate estimates only and can deviate from the result of a Monte Carlo calculation for the actual parameters of the counters by up to 20%!). The relative response of the 20 kPa counter in the moderator sphere has still to be calculated and will be provided by the pilot laboratory at a later time.

The signals provided by the counters are processed by an electronic module (AIOSAP) [2] which comprises a high-voltage supply, a pre-amplifier, a shaping amplifier and two discriminators. This module is also provided by the pilot laboratory. One discriminator (D1) is used to separate events resulting from the ^{3}He(n,p)^{3}H reaction from those due to photons and electronic noise. The number N of the TTL output pulses of D1 have to be counted by the participant to determine the response R in his neutron field or beam. For this purpose, a counting module has to be provided by the participant. The proper setting of D1 has to be checked individually using a Multichannel Analyser (MCA) provided by the participant. The dead time τ introduced by D1 was measured using the pulse interval method. The effective dead time resulting from the interval distribution shown in Fig. 2 is $\tau = (7.2\pm0.9)$ µs. The interval distribution is in compliance with the assumption of a non-extending dead time. More details on the mounting and operation of the detectors and the AIOSAP module can be found in the appendix.

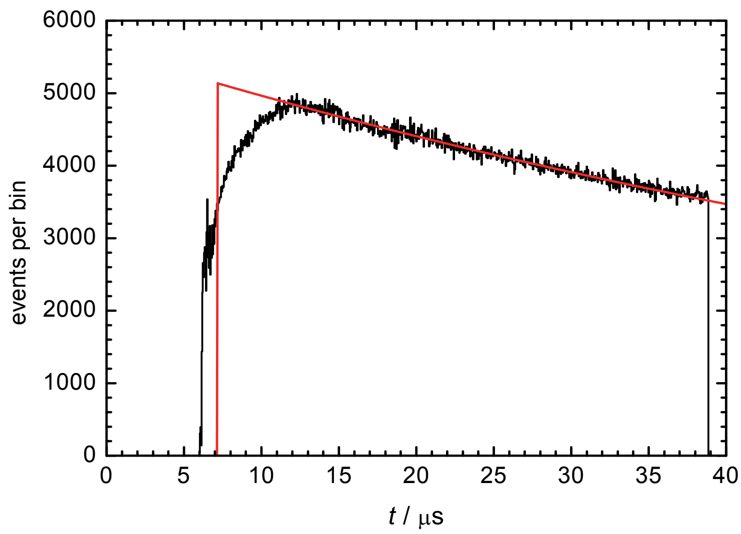

Fig. 2 Distribution of the time intervals between successive output pulses of the discriminator D1 (black histogram). The red solid line shows the fitted interval distribution $N(t) = N_0 \cdot \exp(-\rho(t-\tau_{\mathrm{eff}}))$ with an effective non-extending dead time $\tau_{\mathrm{eff}} = (7.2\pm0.9)$ µs.

Two tight-fitting cylindrical cadmium shields 1 mm in thickness are provided for measuring the effect of epithermal neutrons above the cadmium threshold on the bare counters and the 200 kPa counter inside the 3" PE moderator, respectively.

Determination of the Response

The participants shall determine the response R_{ref} of the counters for a homogeneous unidirectional irradiation with neutrons with a Maxwellian fluence distribution $\Phi_E^{(\mathrm{ref})}$ characterised by a temperature parameter $kT = 25.3$ meV.

$$\frac{\Phi_E^{(\mathrm{ref})}\,\mathrm{d}E}{\Phi^{(\mathrm{ref})}} = \left(\frac{E}{kT}\right)\exp\left(-\frac{E}{kT}\right)\frac{\mathrm{d}E}{kT}$$

This requires that the relative spectral fluence (Φ_E/Φ) and the fluence Φ below the nominal cadmium threshold at 0.68 eV is determined in the neutron field or beam at the same location and under the same conditions as for the measurement with the counter. An appropriate monitoring system may be necessary to relate these two measurements if they cannot be carried out simultaneously. Dead time losses shall be kept below 10% by selecting the most appropriate counter and adjusting the fluence rate, if possible.

Appropriate correction factors have to be determined if the actual irradiation conditions deviate from the reference conditions. Most important, the spectral distribution of the actual neutron field can deviate from a Maxwellian with the reference temperature parameter. The relative responses shown in Fig. 1 are provided in numerical form for the calculation of correction factors. The correction factor k_1 for the spectral distribution is given by

$$k_1 = \frac{\int_0^{\infty}\left(\Phi_E^{(\mathrm{ref})}/\Phi^{(\mathrm{ref})}\right) r(E)\,\mathrm{d}E}{\int_0^{E_{\mathrm{Cd}}}\left(\Phi_E/\Phi\right) r(E)\,\mathrm{d}E}$$

where the integration over the relative spectral fluence (Φ_E/Φ) of the neutron field or beam is extended up to the nominal cadmium threshold energy E_{Cd} at 0.68 eV [3]. Also dead time losses have to be corrected for. The dead time correction k_2 is

$$k_2 = \frac{1}{1-\tau\,(\mathrm{d}N/\mathrm{d}t)}$$

for a non-extending dead time.

Other correction factors can arise, for example, from the inhomogeneous fluence distribution over the sensitive area of the counter. This effect can either be corrected experimentally by using a scanning procedure or calculated using the Monte Carlo method. Also the angular distribution of the spectral fluence may require corrections if fields are used which are not unidirectional. An MCNP model of the detector for the calculation of correction factors can be made available by the pilot laboratory on request. Correction factors are also required if the fluence is not measured at the same position as the counter or, in case of inhomogeneous fields, the sensitive area of the instrument used for the fluence measurement is different from that of the counter.

With these correction factors k_i and the number of monitor counts M_Φ , M_N and $M_N^{(\mathrm{Cd})}$ for the measurement with the instrument used for the fluence measurement, the counter without cadmium cover and with cadmium cover, the response is given by

$$R_{\mathrm{ref}} = \prod_{i=1}^{n} k_i \cdot \frac{\left(N / M_N - k^{(\mathrm{Cd})} N^{(\mathrm{Cd})} / M_N^{(\mathrm{Cd})}\right)}{\left(\Phi / M_\Phi\right)}$$

Here $n \geq 2$ denotes the number of correction factors k_i. The correction factor $k^{(\mathrm{Cd})}$ accounts for the absorption of epithermal neutrons in the Cd shield (1 mm Cd + 1 mm Al) and has to be calculated by the participants if this correction cannot be neglected.

Report

The report to be delivered for the evaluation of the results has to include the following details:

- A brief description of the calibration facility and the methods used for characterising the neutron field or beam.
- Specification of the spectral neutron fluence (Φ_E/Φ) and the total fluence Φ (below the nominal cadmium threshold at 0.68 eV) and a documentation of the traceability to primary national standards.
- Description of the measurements carried out with the transfer instruments including readings N and $N^{(\mathrm{Cd})}$ of the transfer instruments in the neutron fields or beams, monitors readings M and $M^{(\mathrm{Cd})}$, measurement times and pulse-height spectra of the detectors measured in coincidence with the discriminator signal.
- Evaluation of the response R_{ref} under reference conditions including the values of all corrections factors k_i as well as a description of how these values were calculated.
- Evaluation of an uncertainty budget for R_{ref}. All uncertainties have to be specified as standard measurement uncertainties for a coverage factor $k = 1$. The recommendations of the *Guide to the Expression of Uncertainty in Measurement* [4] should be followed.

Evaluation and Publication of the Results

The results reported by the participants will be evaluated by the pilot laboratory. The key comparison reference values (KCRV) [5] will be calculated for each of the three transfer instruments as the weighted mean of the results reported by the participants. Reciprocals of the uncertainties reported by the participants will be used to calculate the weights. From the KCRV and the specified uncertainties, the degree of equivalence (DoE) will be calculated. After discussion and approval of the evaluation report by all participants, the results of the comparison will be published on part C of the Key Comparison Data Base of the BIPM (type B final report) and in Metrologia (short summary and results).

Because the pilot laboratory will also participate in the comparison exercise, all reports will have to be filed at the BIPM. The BIPM will forward the reports to the pilot laboratory after the pilot laboratory has filed its report.

Transport Arrangements

The pilot laboratory will perform a stability test with the two counters after each return from a participant. In case of any changes, the last participant will be notified and appropriate action will be taken. The pilot laboratory will cover the expenses for shipping the equipment to the participants while the participants have to cover the cost of the return shipments.

Time Table

Laboratory	**Date of receipt**	**Date of return**
AIST	Nov. 2006	Jan. 2007
NPL	Feb. 2007	Apr. 2007
CIAE	May 2007	Jul. 2007
PTB (pilot lab.)	Nov. 2007	Jan. 2008
NIST	Mar. 2008	May 2008
IRSN	Nov. 2008	Jan. 2009

The indicated dates refer to the beginning of a month

References

[1] X-5 Monte Carlo Team, *MCNP – A General Monte Carlo N-Particle Transport Code, Version 5*, Report LA-UR-03-1987, Los Alamos National Laboratory, April 24, 2003

[2] A.V. Alevra, *All-in-one Spectrometry Analogue Processor AIOSAP-01, Manual*, Braunschweig 2006

[3] K.H. Beckurtz and K. Wirtz, *Neutron Physics*, paragraph 12.2.2., Springer-Verlag Berlin, Göttingen, Heidelberg, New York, 1964

[4] *Guide to the Expression of Uncertainty in Measurement*. International Organisation for Standardisation, Geneva, Switzerland, 1995. ISBN 92-67-10188-9, Second Edition

[5] M.G. Cox, *The Evaluation of Key Comparison Data: An Introduction*, Metrologia **39** (2002) 587-588 and
M.G. Cox, *The Evaluation of Key Comparison Data*, Metrologia **39** (2002) 589-595

Appendix: Instruction for use of the equipment provided by the pilot laboratory

General Remarks

Two spherical ^{3}He detectors of the CENTRONIC SP9 type were chosen for the key comparison for thermal neutron fluence measurements. The two bare detectors have nominal ^{3}He pressures of 200 kPa (SP9/20) and 20 kPa (SP9/200). To modify the fluence response of the two detectors a spherical polyethylene (PE) moderator 7.62 cm (3″) in diameter is provided. For the determination of the fluence of epithermal neutrons, two cadmium shields are provided, one for the bare counter and one for the counter inside the moderator. The thickness of the cadmium layer is 1 mm. An electronic module (AIOSAP) is provided which comprises a high voltage supply and the analogue pulse processing and discrimination units. The participants have only to set the appropriate pulse-height threshold and count the number of events above this threshold using a counting module for standard TTL pulses.

Operation of the ^{3}He Proportional Counters

The bare counter and the high-voltage cable connecting the counter to the AIOSAP module are shown in Fig. 1. As can be seen from this figure, the bare SP9 has a nose and a stem with a special (PET) socket (15) on the opposite side of the spherical sensitive volume. The serial numbers of the SP9/20 and the SP9/200 counters are 9313-111 and 8916-104, respectively. They are indicated on the stem together with the nominal pressure and the appropriate voltage.

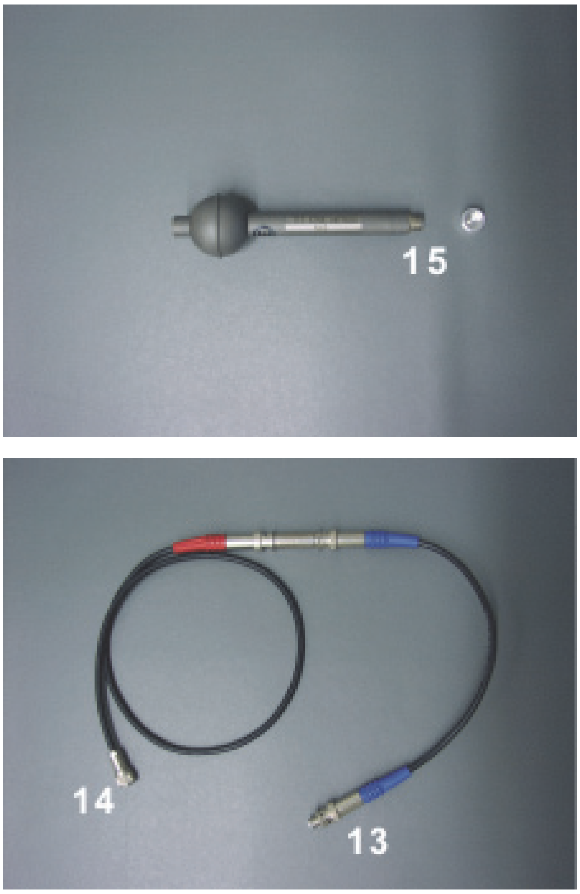

Fig. 1 SP9 counter (upper panel) and the high-voltage cable connecting the counter to the AIOSAP module (lower panel)

A short cable interfacing this special socket to a standard SHV socket is provided. The high-voltage cable connecting the detector with the AIOSAP module should be as short as possible for optimal pulse processing.
Fig. 2 shows the mounting of the bare counter in the cadmium shield. The counter is connected to the socket on the inner side of the lid and then inserted into the cylindrical shield. The shield for the bare counter has a ring at the bottom with accepts the nose of the counter and fixes its position.
The sequence of steps for assembling the moderator sphere with the counter inside and for inserting the sphere in its cadmium shield is shown in Fig. 3. The diameter of the cylindrical shield for the counter inside the spherical moderator is only slightly larger than the diameter of the moderator sphere. This defines the position of the counter inside the shield. When mounting the detectors inside the shields, any excessive force has to be avoided to prevent damage to the counters! The outer dimensions of the shields are shown in Fig. 4.

For the bare counter, the point of reference is marked by the rims of the spherical sensitive volumes. The positions of points of reference of the counters inside the shields are marked on the outside of the shields.

For the bare counter, the symmetry axis must be oriented perpendicular to the neutron beam direction. If the counter is operated inside the moderator, the beam direction must be parallel to the symmetry axis of the counter with the beam incident on the nose. The same applies for the measurements with the cadmium shields.

Operation of the AIOSAP module

The front panel of the AIOSAP module is shown in Fig. 5. A detailed manual is provided with the module. If necessary, the unit can be operated with the internal set of batteries instead of using the external power supply shown in Fig. 6. The settings when <u>not</u> in operation are indicated in Table 1. The controls secured by the red plastic caps should not be changed by the participants.

Table 1 Settings for the AIOSAP module when <u>not</u> in operation. The labels refer to Fig. 5.

1. Switch (1) ITG : OFF
2. Switch (2) Shaping : 1µs
3. Switch (3) Power : OFF
4. Switch (4) HV: OFF
5. Switch (5) COARSE GAIN: x2
6. Switch (6) Pulser: P
7. Switch (7) Display: HV
8. High-voltage control (8): 0

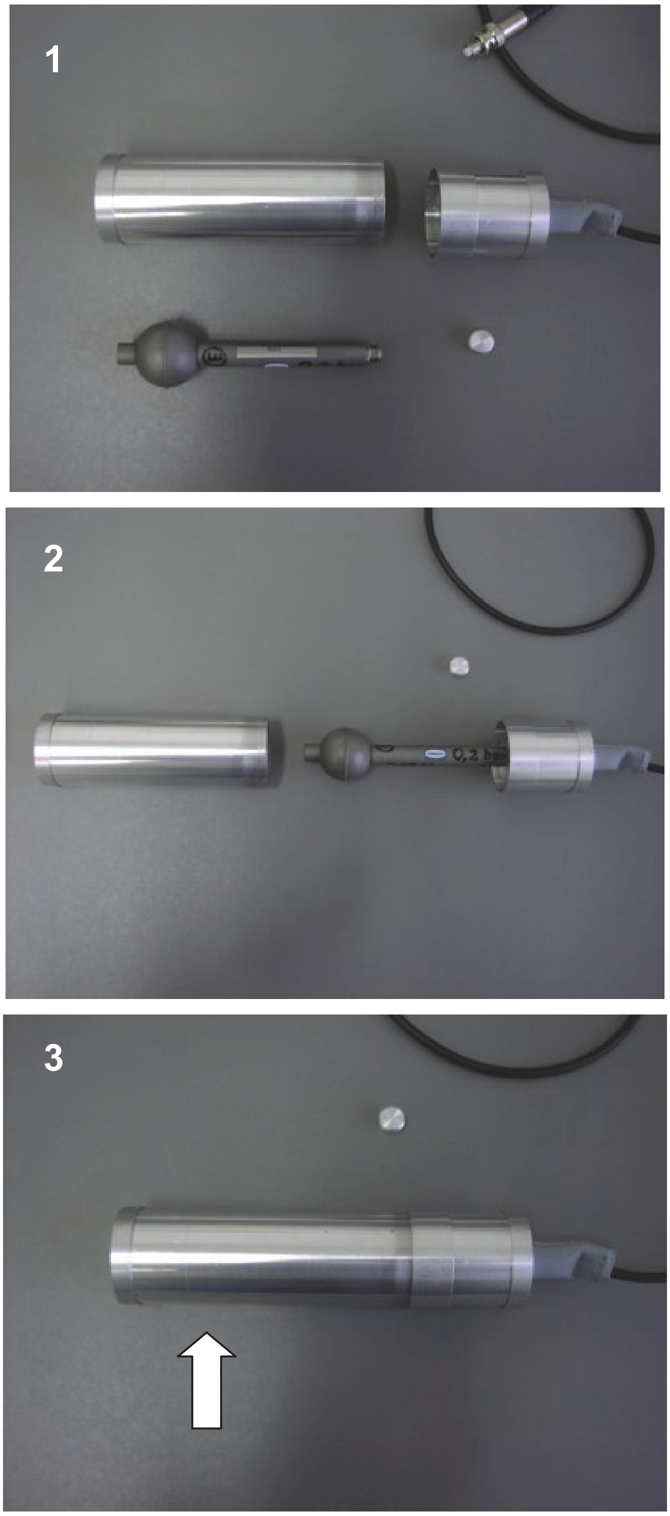

Fig. 2 Insertion of the bare counter into the cadmium shield. The beam has to be incident perpendicular to the stem of the counter.

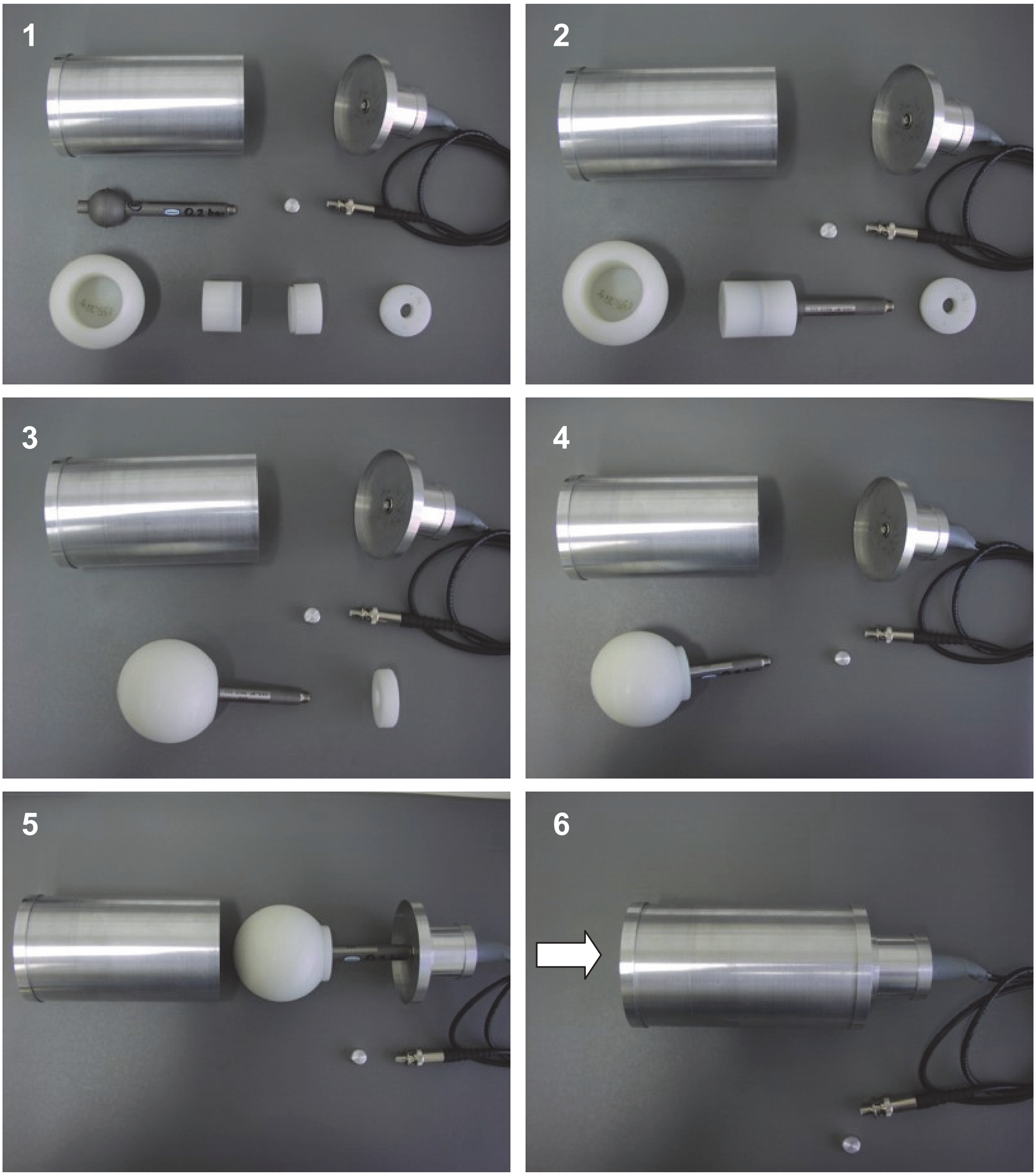

Fig. 3 Mounting of the moderator sphere with the counter inside and insertion into the cylindrical cadmium shield. The beam has to be incident parallel to the detector stem.

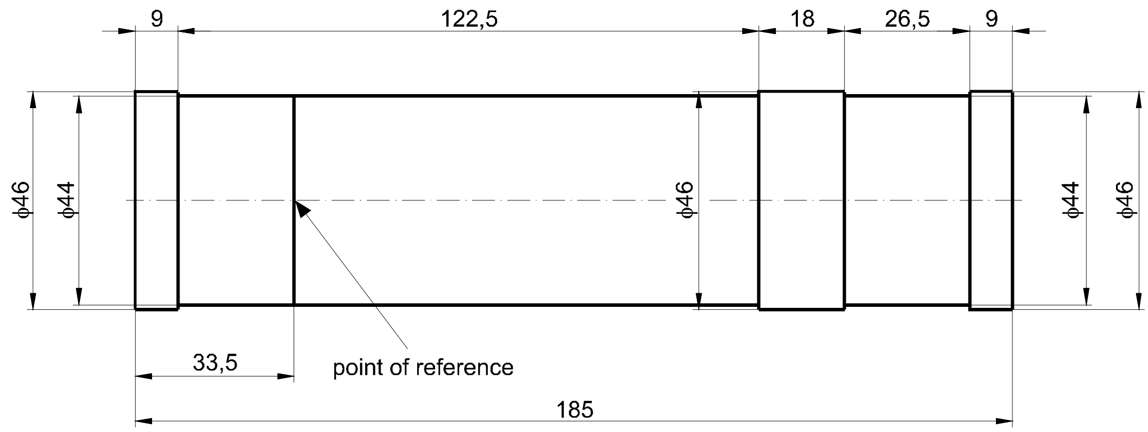

shield for bare SP 9 counter

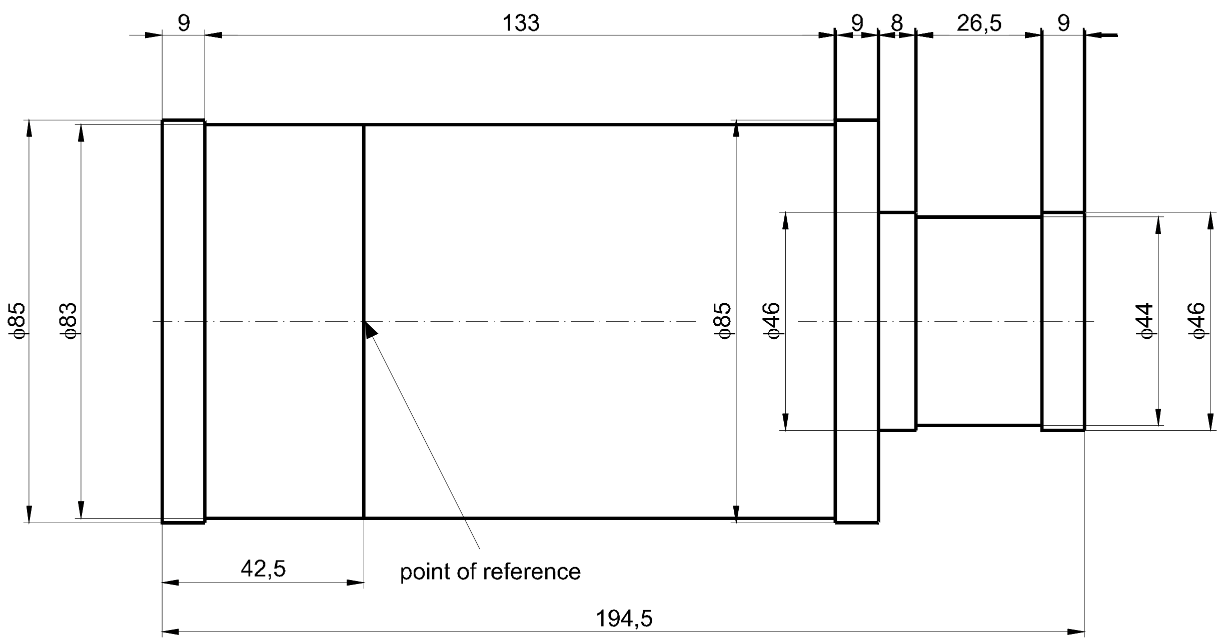

shield for 3" sphere with SP 9 counter

Fig. 4 Outer dimensions of the shields for the bare SP9 counter and the 3" moderator sphere. The walls of the shields consist of 1 mm AlMg3 on the outside and an inner layer of 1 mm cadmium. The point of reference is on the axis of the cylinders at the distances from the end caps indicated on the drawing. These positions are marked by lines engraved in the housings.

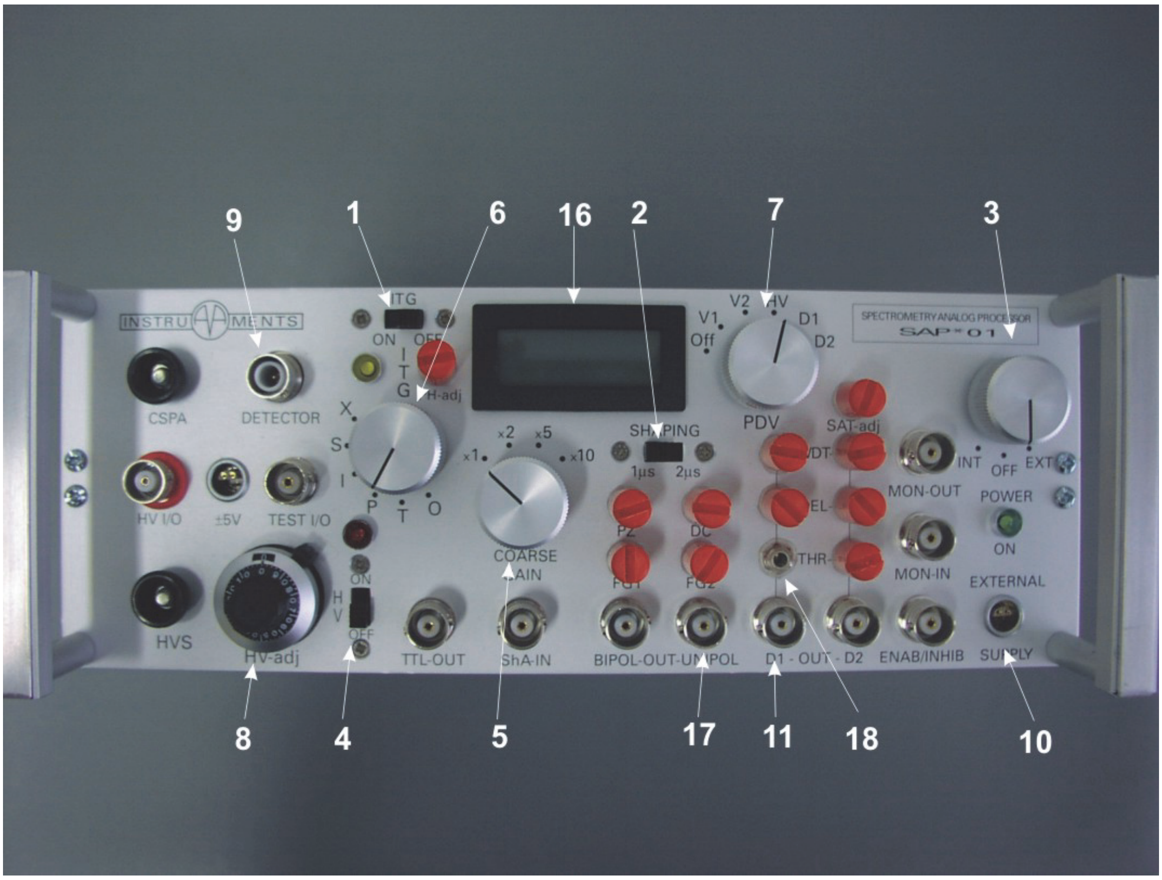

Fig. 5 Front panel of the AIOSAP module. The labels of the controls, displays and connectors are explained in the text and Table 1.

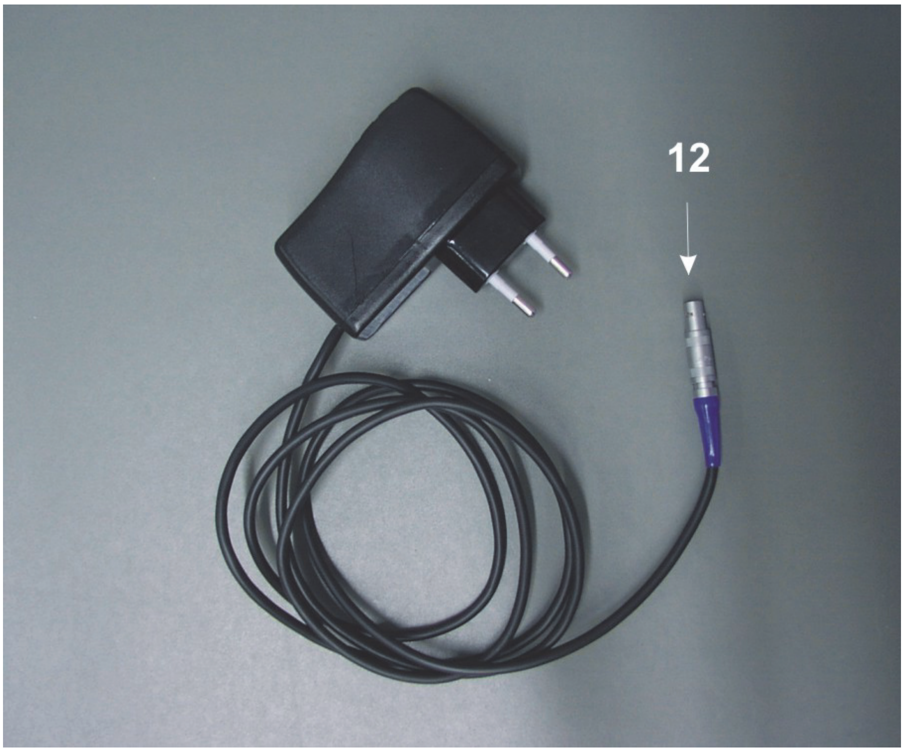

Fig. 6 External power supply for the AIOSAP module. The power supply operates on 110 V - 230 V AC. The switch on the power supply has to be set to 6 V.

The start-up procedure for the AIOSAP module is as follows:

1. Connect plug (12) of external power supply to socket (10).
2. Connect plug (13) of high-voltage cable to socket (9).
3. Connect plug (14) of high-voltage cable to socket (15).
4. Connect discriminator out (11) to the counting module supplied by the participant by a 50 Ω BNC cable.
5. Set switch (3) to EXT.
6. Set switch (4) to ON.
7. Set the high-voltage control (8) slowly to the appropriate value. The voltage applied to the counter is shown on the display (16).
   Counter SP9/200: 795 V
   Counter SP9/20: 755 V

Reminder: set the voltage control (8) to zero before connecting or disconnecting a counter!

The discriminator D1 is used to separate events induced by photons or electronic noise from events caused by $^{3}He(n,p)^{3}H$ reactions. The discriminator output signal from the BNC socket (11) is fed to a counting module which has to be supplied by the participant. The TTL pulses from the discriminator D1 have an amplitude of 5 V and a duration of 6 µs (see Fig. 7). The dead time introduced by the discriminator was measured to be (7.2±0.9) µs.

To check the proper setting of the discriminator, a pulse-height spectrum has to be measured. For this purpose, the unipolar signal available at BNC socket (17) should be used. The data acquisition system has to be provided by the participant. It has to be triggered or operated in coincidence mode using the discriminator signal available at BNC socket (11). The width of this signal is adjusted to 6 µs (see Fig. 7). The discriminator threshold was set to about 15% of the pulse height of the main peak (see Fig. 8) to effectively discriminate against electronic noise and photon-induced events. The setting of the discriminator D1can be changed by the participant using potentiometer (18) if this turns out to be necessary.

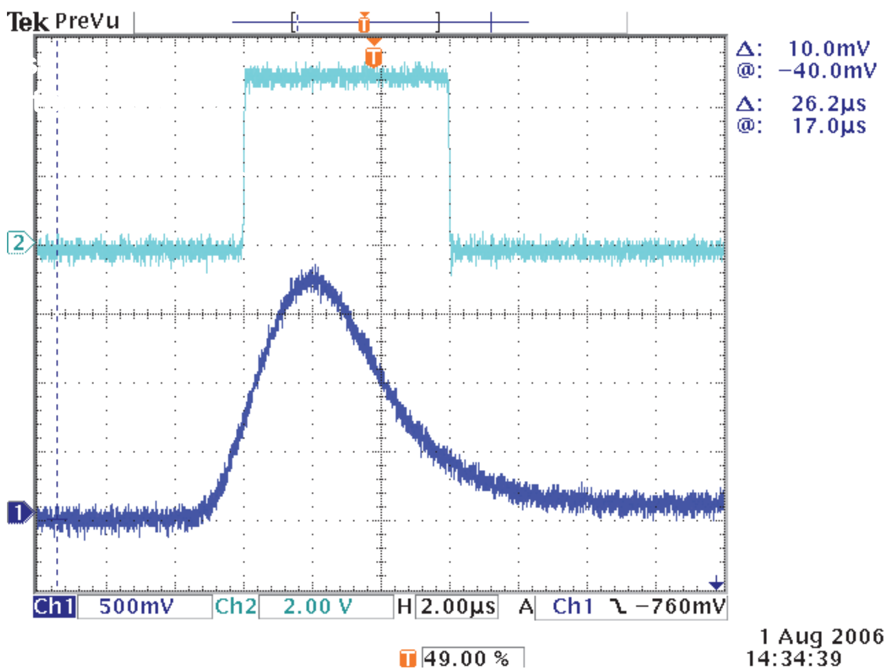

Fig. 7 Timing diagram of the unipolar analogue signal (lower trace) and the TTL discriminator signal (upper trace)

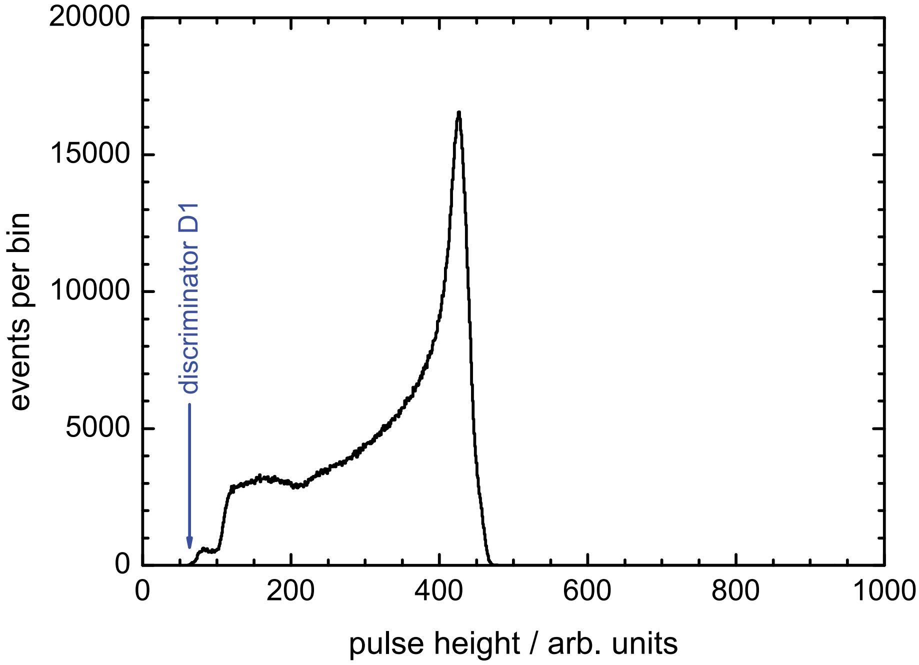

Fig. 8 Pulse-height spectrum of the bare SP9/200 counter measured using a thermal neutron field.

Measurements with the cadmium shield showed that the additional photon background resulting from neutron capture in the cadmium is negligible and shows up only at in the pulse-height region below the threshold.

Appendix B: Printout of Westcott fluence analysis

Output from the Fortran program, Westcott, which is used to calculate the fluences from the gold foil saturated disintegration rates

```
PROGRAM WESTCOTT  -  Version 1.2 compiled    June 2005
THERMAL AND EPITHERMAL FLUENCES CALCULATED FROM FOIL ACTIVATION

Run date: 13-02-2009                Run time: 18:26:29

Au 109 bare + Au 900 in Cd, NPL col 1.6m posn. Evac. Small foils.

  D0(bare)     D0(Cd)    Eff Temp K    FC rate
 5.0537E+00  6.3350E-01  3.1510E+02  4.5792E+03


     FCd      At Wt        G(th)      W-cott g    Sigma(0)
 1.0100E+00  1.9697E+02  9.8430E-01  1.0046E+00  9.8690E+01


   G(res)       S(0)     Res Attn f       W       W-cott K       mu
 3.6700E-01  1.7300E+01  9.9000E-01  2.7000E-02  1.9939E+00  3.6810E+00


 CALCULATED RATIOS AND FLUENCES  (kT = 0.0272 eV)

    R(Cd)      r(T/T0)        r        R(1/v)
 7.9774E+00  2.0715E-02  1.9996E-02  9.6253E+01


  n(th)v(0)     nv(0)     n(M)v(0)   n(1/E)v(0)    n(1/E)/n(M)
 1.4794E+04  1.4949E+04  1.4597E+04  3.5160E+02    2.4087E-02


  For the KT and mu values used:
  E(Cd) =  5.1227E-01   El =   9.9949E-02
  epithermal fraction [4*r/sqrt(Pi*mu)] =   2.3520E-02

  For the Maxwellian distn. v(bar)/v(0) =   1.1690E+00
  n(M)v(bar) =   1.7064E+04
  n(1/E)v(bar) per unit lethargy =   3.4942E+02
  n(1/E)v(bar) between El and E(Cd) =   5.7102E+02
  ( 3.346 % of n(M)v(bar)  3.238 % of n(th)v(bar))

  For sub-Cd neutrons:
  n(th)v(bar) =   1.7635E+04
  v(bar)/v(0) =   1.1921E+00

  For the epi. fluence El to E(Cd) v(bar)/v(0) =   2.9090E+00
  and thus v(bar) for this region =   6.3998E+05 cm/sec
  n(M)  =   6.6351E-02
  n(th) =   6.7244E-02
  n(1/E) between El and E(Cd) =   8.9225E-04
  ( 1.345 % of n(M)  1.327 % of n(th))


  Fluences divided by the fission chamber count rate

  n(th)v(0)     nv(0)     n(M)v(0)   n(th)v(bar)   n(M)v(bar)
 3.2306E+00  3.2645E+00  3.1877E+00  3.8511E+00  3.7264E+00
```

CCRI(III)-K8: Key Comparison for Thermal Neutron Fluence Measurements

Report on the determination of the fluence response of spherical ^{3}He detectors at the PTB thermal neutron reference field at GeNF

Reinhard Böttger and Stefan Löb
Physikalisch-Technische Bundesanstalt
Bundesallee 100, 38116 Braunschweig, Germany

Facility

The calibration facility for the determination of the fluence response of the transfer instruments used for this intercomparison is installed at one neutron beam line of the FRG-1 research reactor at GeNF [1]. This thermal neutron reference field [2] has been used in recent years for calibration or testing of radiation protection instruments or various other applications. Thus, the field properties together with the reproducibility have been studied in detail in various measurement periods.

A combination of two diaphragms defines a nearly unidirectional thermal neutron beam with a quadratic cross section of at most 30 x 30 mm^2 at the reference position. The beam intensity may be varied by changing the cross section of the first aperture (max. 3 x 3 mm^2) remote-controlled, while a set of smaller apertures may be placed at the position of the second diaphragm. For every configuration of apertures the fluence rate and the neutron energy distribution has to be determined individually.

An (almost black) ^{6}Li glass scintillation detector for the determination of the absolute neutron current is installed at the reference position. Time-of-flight measurements are carried out to determine the spectral distribution of the thermal neutron beam by means of the start signal from a chopper wheel near the first aperture and the stop signal from the ^{6}Li glass scintillation detector. The flight path length of 6.61 m is identical to the distance between the first diaphragm and the reference position. A beam stop is installed about 60 cm further downstream. The ^{6}Li glass detector was employed to calibrate a ^{3}He beam monitor used in transmission being installed directly behind the second diaphragm. As the beam spot size is generally smaller as the object to be irradiated, a scanner [3] (here: device, which moves objects in a plane perpendicular to the beam direction in a defined pattern of movement) is an essential part of the irradiation facility to obtain larger, homogeneous field sizes, with the drawback of lowering the fluence rates. Further details about the thermal neutron reference facility are given in [2].

General field properties

The spectral fluence distribution of the thermal neutron beam at GeNF can be described by a Maxwellian distribution with a temperature parameter of 21 meV to 24 meV being close to the reference thermal neutron distribution with $kT = 25.3$ meV.

Furthermore, the beam is nearly free from photon contamination and epithermal neutrons, as the Cadmium-ratio is about $3.3 \cdot 10^4$.

With a standard set of apertures, a fluence rate of $8 \cdot 10^4$ cm^{-2} s^{-1} is achieved in the direct beam, while with the scanner in operation (standard field size 30 x 30 cm^2 for larger objects) only fluence rates of about 10^3 cm^{-2} s^{-1} can be obtained.

Measurements with transfer instruments

Before starting with the response determination of the SP9 detectors, the transmission monitor was calibrated with the ^{6}Li glass scintillation detector at the reference position and with a strongly reduced beam intensity to keep dead time corrections small. Time-of-flight experiments were performed afterwards with various sizes of the second aperture.

The measurements aiming to determine the fluence response of the spherical ^{3}He proportional detectors were performed between November 15 and 22, 2007.

Irradiations were carried out with both detectors, exposed to the beam at the reference position with and without the 3" moderator sphere.

Thus all four transfer instruments were investigated, further denoted as SP9/200, SP9/20, SP9/200mod and SP9/20mod.

Due to the high cadmium-ratio of the beam, a contribution from epithermal neutrons was not observed behind a Cd-shielding. Therefore, measurements with the specially designed Cd-shield were not performed.

For the signal processing and high voltage supply the provided AIOSAP module was utilized.

The proportional counters were operated with the high voltage as required in the appendix of the comparison protocol, which is 795 V for the SP9/200 and 755 V for the SP9/20.

The orientation of the stem of the detector with and without moderator was also set according to the protocol instruction.

All irradiations were performed with the scanner in operation. The size of the second aperture was chosen as 10 x 10 mm^2. Thus, at the reference position, the size was 13 x 13 mm^2. With this geometry, the cross section of the thermal neutron beam is much smaller than the dimensions of the detectors and the scanner field size. The scanner was operated only in the spot scanning mode [3] with a step width of 10 mm in both dimensions. Data were taken only when the detector was in the rest position of the respective point of irradiation. In this way, dead time corrections could be carried out for each position individually.

To keep dead time corrections low, at least for three transfer instruments the beam intensity had to be reduced by lowering the cross section of the first diaphragm due to the high efficiency of the applied ^{3}He detectors for thermal neutrons. Time-of-flight experiments showed that the spectral fluence does not change when lowering the beam intensity.

Table 1 shows the relative beam intensity applied for the irradiation of the transfer instruments.

Detector	**Relative intensity in %**
SP9/200	14
SP9/200mod	22
SP9/20	41
SP9/20mod	100

Table 1: Reduction of the beam intensity for the set of ^{3}He detectors investigated.

Results

The neutron field

The spectral fluence distribution for the field with the 10 x 10 mm^2 aperture used throughout these irradiations was derived from the experimentally determined time-of-flight spectrum at full beam intensity. The mean energy is 46 meV, while the best fit is obtained with a Maxwellian distribution with a temperature parameter of $kT = 23$ meV. Both spectra are displayed in Fig. 1.

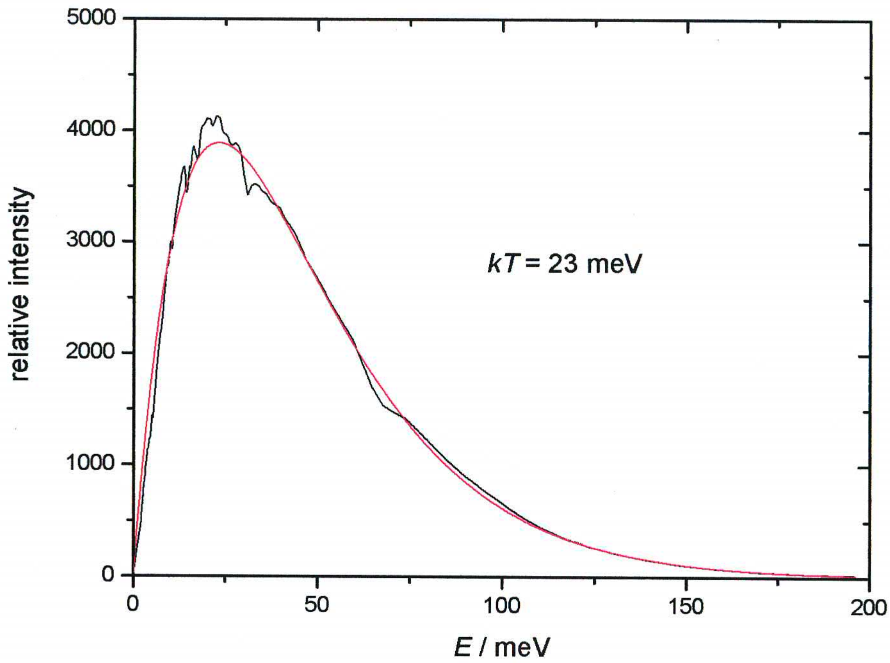

Fig. 1: Neutron spectral fluence measured in November 2007 together with a Maxwellian fit of $kT = 23$ meV (red).

For the determination of the fluence response R_{ref} of the transfer instruments, the number of counts from the monitor detector is to be multiplied by the monitor calibration factor f to obtain the neutron rate at the reference position. For this field geometry used for all SP9 irradiations, it amounts to: $f = 386.5 \pm 7.8$. The evaluation of the standard measurement uncertainty was performed according to the *Guide to the Expression of Uncertainty in Measurement* [4]. Appendix A includes the uncertainty budget for the fluence measurement based on the ^{6}Li glass scintillation detector.

Apart from measuring the thermal neutron current directly by means of a quasi black detector system, the irradiation of a thin gold foil (thickness 20 µm) at the reference position can also be used to determine the average neutron current during an extended period of irradiation (nearly 72 h), however, with a circular geometry of the second aperture. With the data from the transmission monitor, both methods can be directly compared.

By these activation measurements as part of the quality assurance, the traceability of the neutron flux to the primary national activity standard of the PTB could be realized. A comprehensive description of the measurement procedure and the data analysis can be found in ref. [2].

As in previous measurement campaigns, the results from ^{6}Li glass/monitor neutron current determination and gold foil activation on the other hand show excellent agreement, as can be seen in Table 2.

Method	Thermal neutron current/s^{-1}
^{6}Li glass scintillator/monitor	(7.020 ± 0.150) E04
Gold foil activation	(7.024 ± 0.140) E04

Table 2: Results from different methods of neutron current determination.

Fluence response of the detectors

To obtain pulse height spectra for the inspection of the correct setting of the threshold, the set of counters was exposed to the direct neutron beam strongly reduced by the first diaphragm. As an example, Fig. 2 shows the pulse height spectrum of the SP9/20 without moderator. The threshold is set at a position of about 10 % of the peak position.

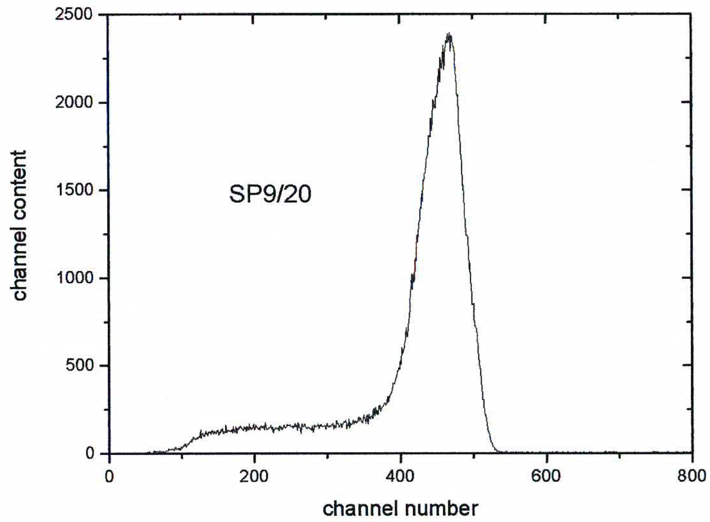

Fig. 2: Pulse height spectrum of the low pressure spherical ^{3}He proportional counter SP9/20.

For the calculation of the fluence response R_{ref} of the transfer instruments at the reference energy 25.3 meV, only the correction factors k_1 and k_2 as defined in the comparison protocol have to be considered due to the field properties allowing to omit measurements with the provided cadmium shielding.

Correction factor k_1

The correction factors are calculated by folding the normalized spectral distributions with the relative response of the detectors. The results for k_1 are tabulated in Table 3.

Detector	k_1
SP9/200	0.979 ± 0.003
SP9/20	0.976 ± 0.003
SP9/200mod	1.024 ± 0.003
SP9/20mod	1.023 ± 0.003

Table 3: Spectral correction factor k_1 for the set of ^{3}He detectors investigated.

The stated uncertainties for k_1 are due to the experimentally determined spectral fluence, as an uncertainty of 1 cm is assumed for the flight path length, while no uncertainties are assigned to the calculated relative responses.

Due to the opposite energy dependence of their responses, the correction factors for the bare counters are smaller than unity, while they are larger for the spheres with 3" moderator, as expected.

Correction factor k_2

A non-extended dead time of $\tau = (7.2 \pm 0.9)\ \mu s$ is assumed according to the protocol to calculate the dead time correction factor k_2. No measurements were performed to verify this value during the November 2007 campaign.

In the scanning procedure, the number of counts of every data point is corrected for dead time losses individually. Thus k_2 is defined here (different from the definition in the protocol) as

$$k_2 = \frac{\sum_{i=1}^{n} N_i \cdot \tau_{i,corr}}{\sum_{i=1}^{n} N_i}$$

with n = number of positions in the spot scan mode

N_i = Number of counts for the individual measuring position

$\tau_{i,corr}$ = dead time correction for the number of counts of the individual measuring position

As count rates of up to 15 kHz for only few scanner positions may occur for the direct exposure of the SP9/200 even at a reduced beam current, it is essential to follow this procedure of point-wise dead time correction in the scanning mode as used here. The dead time correction is, however, much smaller for the measurements with the moderator sphere (max. count rates about 1 kHz), as can be seen from Table 4.

Detector	k_2
SP9/200	1.080 ± 0.010
SP9/20	1.019 ± 0.002
SP9/200mod	1.005 ± 0.001
SP9/20mod	1.005 ± 0.001

Table 4: Overall dead time correction factors for the set of ^{3}He detectors investigated.

To estimate the uncertainty of the scan field area, various measurements to determine SP9-detector responses were performed with different combinations of beam intensity, primary field size and specially scan field size. From these data, a 2 % upper limit for the uncertainty of the scan field size used for these irradiations could be derived.

Thus, with the fluence determined and the number of corrected counts from the transfer instruments, the fluence response for the reference energy 25.3 meV can be calculated.

The results are given in Table 5; with a coverage factor 1.0 for the uncertainty.

Detector	Response R_{ref}/cm^2
SP9/200	3.129 ± 0.094
SP9/20	0.375 ± 0.012
SP9/200mod	1.322 ± 0.038
SP9/20mod	0.217 ± 0.006

Table 5: Fluence response R_{ref} for the transfer instruments.

The appendixes B to E show the uncertainty budgets calculated according to GUM [4].

Acknowledgement

The assistance and cooperation of the staff of the PTB and the GeNF working group is gratefully acknowledged.

References

[1] *Internet*: http://genf.gkss.de

[2] R. Böttger, H. Friedrich, H. Janßen:
The PTB Thermal Neutron Reference Field at GeNF
PTB-Bericht PTB-N-47, August 2004, ISBN 3-86509-199-7

[3] C. Birattari, G. Manfredi and M. Silari:
Scanning procedures for calibration of radiation detectors
Rev. Sci. Instrum. **66** (8), August 1995

[4] *Guide to the Expression of Uncertainty in Measurement*. International Organisation for Standardisation, Geneva, Switzerland, 1995, ISBN 92-67-10188-9, 2nd Edition

Appendix

A: Uncertainty budget for the determination of the monitor calibration factor.

B: Uncertainty budget for the fluence response of SP9/200.

C: Uncertainty budget for the fluence response of SP9/20.

D: Uncertainty budget for the fluence response of SP9/200mod.

E: Uncertainty budget for the fluence response of SP9/20mod.

Appendix A:Determination of the monitor calibration factor (field size $10x10mm^{2,}$ November 2007)

Model Equation:

$L_1=L_0/(1-(\tau*L_0*0.01));$

$f=Li_{korr}*L_1/Mon$

List of Quantities:

Quantity	Unit	Definition
L_1		L_0 , dead time corrected
L_0		Number of pulses from LiGl scintillation detector within 100 s
τ		Dead time
f		Monitor calibration factor (field size $10x10mm^{2,}$ November 2007)
Li_{korr}		Absorption correction for LiGl
Mon		Number of pulses from the ^{3}He-transmission monitor within 100s

L_1: Temporary

L_0: Type B rectangular distribution
Value: 4146740
Halfwidth of Limits: 3500

τ: Type B rectangular distribution
Value: $3.6\cdot10^{-6}$
Halfwidth of Limits: $0.6\cdot10^{-6}$

f: Result

Li_{korr}: Type B rectangular distribution
Value: 1.045
Halfwidth of Limits: 0.012

Mon: Type B rectangular distribution
Value: 13180
Halfwidth of Limits: 200

Uncertainty Budget:

Quantity	Value	Standard Uncertainty	Degrees of Freedom	Sensitivity Coefficient	Uncertainty Contribution	Index
L_1	$4.8744 \cdot 10^6$	82400				
L_0	$4.14674 \cdot 10^6$	2020	infinity	$110 \cdot 10^{-6}$	0.22	0.1 %
τ	$3.600 \cdot 10^{-6}$	$346 \cdot 10^{-9}$	infinity	$19 \cdot 10^6$	6.5	70.2 %
Li_{korr}	1.04500	$6.93 \cdot 10^{-3}$	infinity	370	2.6	10.8 %
Mon	13180	115	infinity	-0.029	-3.4	18.9 %
f	386.5	7.79	infinity			

Result: Quantity: f
Value: 386.5
Expanded Uncertainty: ±7.8
Coverage Factor: 1.0
Coverage: manual

Appendix B:Determination of the response of SP9/200 detector

The response of spherical, 3He filled detectors was determined at the thermal neutron reference field of the PTB at GKSS.

Model Equation:

$R=k_1*k_2*SP9*F/(Mon*f)$

List of Quantities:

Quantity	Unit	Definition
R	cm^2	Response SP9/200
k_1		Correction to reference spectrum E = 25.3 meV
k_2		Dead time correction
SP9		Number of pulses from SP9 detector
F	cm^2	Scan area
Mon		Number of pulses from monitor detector
f		Monitor calibration factor for the field in November 2007, aperture size 10x10 mm2

R: Result

k_1: Type B normal distribution
Value: 0.979
Expanded Uncertainty: 0.003
Coverage Factor: 1

k_2: Type B normal distribution
Value: 1.08
Expanded Uncertainty: 0.01
Coverage Factor: 1

SP9: Type B normal distribution
Value: 529901
Expanded Uncertainty: 728
Coverage Factor: 1

F: Type B normal distribution
Value: 256 cm^2
Expanded Uncertainty: 5 cm^2
Coverage Factor: 1

Mon: Type B normal distribution
Value: 118609
Expanded Uncertainty: 344
Coverage Factor: 1

f: Import
Filename: Mon-Kalibrierfaktor 10x10 Nov07.SMU
Symbol: f

Uncertainty Budget:

Quantity	Value	Standard Uncertainty	Degrees of Freedom	Sensitivity Coefficient	Uncertainty Contribution	Index
k_1	0.97900	$3.00 \cdot 10^{-3}$	50	3.2	$9.6 \cdot 10^{-3}$ cm^2	1.0 %
k_2	1.0800	0.0100	50	2.9	0.029 cm^2	9.6 %
SP9	$529.901 \cdot 10^3$	728	50	$5.9 \cdot 10^{-6}$	$4.3 \cdot 10^{-3}$ cm^2	0.2 %
F	256.00 cm^2	5.00 cm^2	50	0.012	0.061 cm^2	42.6 %
Mon	$118.609 \cdot 10^3$	344	50	$-26 \cdot 10^{-6}$	$-9.1 \cdot 10^{-3}$ cm^2	0.9 %
f	386.5	7.80	infinity	$-8.1 \cdot 10^{-3}$	-0.063 cm^2	45.6 %
R	3.129 cm^2	0.0936 cm^2	260			

Result: Quantity: R
Value: 3.129 cm^2
Expanded Uncertainty: ±0.094 cm^2
Coverage Factor: 1.0
Coverage: manual

Appendix C: Determination of the response of SP9/20 detector

The response of spherical, 3He filled detectors was determined at the thermal neutron reference field of the PTB at GKSS.

Model Equation:

$R=k_1*k_2*SP9*F/(Mon*f)$

List of Quantities:

Quantity	Unit	Definition
R	cm^2	Response SP9/20
k_1		Correction to reference spectrum E = 25.3 meV
k_2		Dead time correction
SP9		Number of pulses from SP9 detector
F	cm^2	Scan area
Mon		Number of pulses from monitor detector
f		Monitor calibration factor for the field in November 2007, aperture size 10x10 mm2

R: Result

k_1: Type B normal distribution
Value: 0.976
Expanded Uncertainty: 0.003
Coverage Factor: 1

k_2: Type B normal distribution
Value: 1.019
Expanded Uncertainty: 0.002
Coverage Factor: 1

SP9: Type B normal distribution
Value: 125529
Expanded Uncertainty: 354
Coverage Factor: 1

F: Type B normal distribution
Value: 121 cm^2
Expanded Uncertainty: 3 cm^2
Coverage Factor: 1

Mon: Type B normal distribution
Value: 104097
Expanded Uncertainty: 323
Coverage Factor: 1

f: Import
Filename: Mon-Kalibrierfaktor 10x10 Nov07.SMU
Symbol: f

Uncertainty Budget:

Quantity	Value	Standard Uncertainty	Degrees of Freedom	Sensitivity Coefficient	Uncertainty Contribution	Index
k_1	0.97600	$3.00 \cdot 10^{-3}$	50	0.38	$1.2 \cdot 10^{-3}$ cm^2	0.9 %
k_2	1.01900	$2.00 \cdot 10^{-3}$	50	0.37	$740 \cdot 10^{-6}$ cm^2	0.4 %
SP9	$125.529 \cdot 10^3$	354	50	$3.0 \cdot 10^{-6}$	$1.1 \cdot 10^{-3}$ cm^2	0.8 %
F	121.00 cm^2	3.00 cm^2	50	$3.1 \cdot 10^{-3}$	$9.3 \cdot 10^{-3}$ cm^2	58.4 %
Mon	$104.097 \cdot 10^3$	323	50	$-3.6 \cdot 10^{-6}$	$-1.2 \cdot 10^{-3}$ cm^2	0.9 %
f	386.5	7.80	infinity	$-970 \cdot 10^{-6}$	$-7.6 \cdot 10^{-3}$ cm^2	38.7 %
R	0.375 cm^2	0.0122 cm^2	150			

Result: Quantity: R
Value: 0.375 cm^2
Expanded Uncertainty: ±0.012 cm^2
Coverage Factor: 1.0
Coverage: manual

Appendix D: Determination of the response of SP9/200 detector with 3" moderator

The response of spherical, 3He filled detectors was determined at the thermal neutron reference field of the PTB at GKSS.

Model Equation:

$$R=k_1*k_2*SP9*F/(Mon*f)$$

List of Quantities:

Quantity	Unit	Definition
R	cm^2	Response SP9/200 mod
k_1		Correction to reference spectrum E = 25.3 meV
k_2		Dead time correction
SP9		Number of pulses from SP9 detector
F	cm^2	Scan area
Mon		Number of pulses from monitor detector
f		Monitor calibration factor for the field in November 2007, aperture size 10x10 mm2

R: Result

k_1: Type B normal distribution
Value: 1.024
Expanded Uncertainty: 0.003
Coverage Factor: 1

k_2: Type B normal distribution
Value: 1.005
Expanded Uncertainty: 0.001
Coverage Factor: 1

SP9: Type B normal distribution
Value: 149771
Expanded Uncertainty: 387
Coverage Factor: 1

F: Type B normal distribution
Value: 256 cm^2
Expanded Uncertainty: 5 cm^2
Coverage Factor: 1

Mon: Type B normal distribution
Value: 77237
Expanded Uncertainty: 278
Coverage Factor: 1

f: Import
Filename: Mon-Kalibrierfaktor 10x10 Nov07.SMU
Symbol: f

Uncertainty Budget:

Quantity	Value	Standard Uncertainty	Degrees of Freedom	Sensitivity Coefficient	Uncertainty Contribution	Index
k_1	1.02400	$3.00 \cdot 10^{-3}$	50	1.3	$3.9 \cdot 10^{-3}$ cm^2	1.0 %
k_2	1.00500	$1.00 \cdot 10^{-3}$	50	1.3	$1.3 \cdot 10^{-3}$ cm^2	0.1 %
SP9	$149.771 \cdot 10^3$	387	50	$8.8 \cdot 10^{-6}$	$3.4 \cdot 10^{-3}$ cm^2	0.8 %
F	256.00 cm^2	5.00 cm^2	50	$5.2 \cdot 10^{-3}$	0.026 cm^2	46.6 %
Mon	77237	278	50	$-17 \cdot 10^{-6}$	$-4.8 \cdot 10^{-3}$ cm^2	1.6 %
f	386.5	7.80	infinity	$-3.4 \cdot 10^{-3}$	-0.027 cm^2	49.8 %
R	1.322 cm^2	0.0378 cm^2	230			

Result: Quantity: R
Value: 1.322 cm^2
Expanded Uncertainty: ±0.038 cm^2
Coverage Factor: 1.0
Coverage: manual

Appendix E: Determination of the response of a SP9/20 detector with 3" moderator

The response of spherical, 3He filled detectors was determined at the thermal neutron reference field of the PTB at GeNF.

Model Equation:

$R=k_1*k_2*SP9*F/(Mon*f)$

List of Quantities:

Quantity	Unit	Definition
R	cm^2	Response SP9/20 mod
k_1		Correction to reference spectrum E = 25.3 meV
k_2		Dead time correction
SP9		Number of pulses from SP9 detector
F	cm^2	Scan area
Mon		Number of pulses from monitor detector
f		Monitor calibration factor for the field in November 2007, aperture size 10x10 mm2

R: Result

k_1: Type B normal distribution
Value: 1.023
Expanded Uncertainty: 0.003
Coverage Factor: 1

k_2: Type B normal distribution
Value: 1.005
Expanded Uncertainty: 0.001
Coverage Factor: 1

SP9: Type B normal distribution
Value: 343620
Expanded Uncertainty: 586
Coverage Factor: 1

F: Type B normal distribution
Value: 256 cm^2
Expanded Uncertainty: 5 cm^2
Coverage Factor: 1

Mon: Type B normal distribution
Value: 1080233
Expanded Uncertainty: 1039
Coverage Factor: 1

f: Import
Filename: Mon-Kalibrierfaktor 10x10 Nov07.SMU
Symbol: f

Uncertainty Budget:

Quantity	Value	Standard Uncertainty	Degrees of Freedom	Sensitivity Coefficient	Uncertainty Contribution	Index
k_1	1.02300	$3.00 \cdot 10^{-3}$	50	0.21	$640 \cdot 10^{-6}$ cm^2	1.1 %
k_2	1.00500	$1.00 \cdot 10^{-3}$	50	0.22	$220 \cdot 10^{-6}$ cm^2	0.1 %
SP9	$343.620 \cdot 10^{3}$	586	50	$630 \cdot 10^{-9}$	$370 \cdot 10^{-6}$ cm^2	0.4 %
F	256.00 cm^2	5.00 cm^2	50	$850 \cdot 10^{-6}$	$4.2 \cdot 10^{-3}$ cm^2	47.5 %
Mon	$1.08023 \cdot 10^{6}$	1040	50	$-200 \cdot 10^{-9}$	$-210 \cdot 10^{-6}$ cm^2	0.1 %
f	386.5	7.80	infinity	$-560 \cdot 10^{-6}$	$-4.4 \cdot 10^{-3}$ cm^2	50.8 %
R	0.2166 cm^2	$6.14 \cdot 10^{-3}$ cm^2	220			

Result: Quantity: R
Value: 0.2166 cm^2
Expanded Uncertainty: $\pm 6.1 \cdot 10^{-3}$ cm^2
Coverage Factor: 1.0
Coverage: manual